Louisiana Tech University
Louisiana Tech Digital Commons

Doctoral Dissertations | Graduate School

Winter 2007

Structural behavior of PVC pipe liners subjected to seasonal groundwater loading

Qing Cai
Louisiana Tech University

Follow this and additional works at: https://digitalcommons.latech.edu/dissertations

Part of the Mechanical Engineering Commons

Recommended Citation
Cai, Qing, "" (2007). *Dissertation*. 546.
https://digitalcommons.latech.edu/dissertations/546

This Dissertation is brought to you for free and open access by the Graduate School at Louisiana Tech Digital Commons. It has been accepted for inclusion in Doctoral Dissertations by an authorized administrator of Louisiana Tech Digital Commons. For more information, please contact digitalcommons@latech.edu.

STRUCTURAL BEHAVIOR OF PVC PIPE LINERS SUBJECTED TO SEASONAL GROUNDWATER LOADING

By

Qing Cai, B.S.

A Dissertation Presented in Partial Fulfillment
Of the Requirement for the Degree
Doctor of Philosophy

COLLEGE OF ENGINEERING AND SCIENCE
LOUISIANA TECH UNIVERSITY

MARCH, 2007

Reproduced with permission of the copyright owner. Further reproduction prohibited without permission.

UMI Number: 3264693

INFORMATION TO USERS

The quality of this reproduction is dependent upon the quality of the copy submitted. Broken or indistinct print, colored or poor quality illustrations and photographs, print bleed-through, substandard margins, and improper alignment can adversely affect reproduction.

In the unlikely event that the author did not send a complete manuscript and there are missing pages, these will be noted. Also, if unauthorized copyright material had to be removed, a note will indicate the deletion.

UMI®

UMI Microform 3264693

Copyright 2007 by ProQuest Information and Learning Company.

All rights reserved. This microform edition is protected against unauthorized copying under Title 17, United States Code.

ProQuest Information and Learning Company
300 North Zeeb Road
P.O. Box 1346
Ann Arbor, MI 48106-1346

Reproduced with permission of the copyright owner. Further reproduction prohibited without permission.

LOUISIANA TECH UNIVERSITY

THE GRADUATE SCHOOL

January 12, 2007
Date

We hereby recommend that the dissertation prepared under our supervision by Qing Cai entitled STRUCTURE BEHAVIOR OF PVC PIPE LINERS SUBJECTED TO SEASONAL GROUNDWATER LOADING be accepted in partial fulfillment of the requirements for the Degree of Doctor of Philosophy

Supervisor of Dissertation Research

Head of Department
Mechanical Engineering
Department

Recommendation concurred in:

Advisory Committee

Approved:
Director of Graduate Studies

Approved:
Dean of the Graduate School

Dean of the College

GS Form 13
(5/03)

Reproduced with permission of the copyright owner. Further reproduction prohibited without permission.

ABSTRACT

Thin-walled polymeric liners are routinely used to rehabilitate deteriorated underground pipe lines that are structurally sound but have lost their hydraulic integrity. These host pipes are said to be "partially deteriorated" since they can support soil and surface loading. For this case, the pipe liners must only be designed to withstand the pressure of the groundwater that seeps through openings in the host pipe and migrates through the small annular gap between the liner and the host pipe. This external pressure will cause the polymeric liner to slowly deform inward toward the center of the pipe, and the compressive hoop stresses in the pipe wall may cause sudden collapse or buckling when the liner deflections or stresses reach critical values. A significant body of research exists that details the structural response and design of these pipe liners assuming constant groundwater pressure. This dissertation focuses on the influence of varying groundwater pressure on the response and design of pipe liners. The work involves material characterization of two PVC liner materials, finite element simulation of liner response under varying groundwater loading, and development of a correction factor that effectively accounts for water level variations on 50-year liner design.

Material characterization testing of 16 specimens cut from higher compliance and higher stiffness PVC liner materials was conducted continuously over one year. The specimens were subjected to three-point bending to understand the accumulation of creep deformation and the recovery of this deformation due to partial unloading of the

Reproduced with permission of the copyright owner. Further reproduction prohibited without permission.

specimens. Two loading and two partial unloading cycles were applied to the specimens to model seasonal groundwater variations. A five-unit generalized Kelvin Model was employed to fit the creep and recovery data resulting from the material characterization data. The 12 retardation constants resulting from this initial fitting were converted to relaxation constants suitable for use with the viscoelastic material models available in the ABAQUS© finite element software.

A two-dimensional finite element model was constructed for a pipe liner having 5% ovality, 0.4% annular gap and a diameter to thickness ratio of 32.5. A trapezoidal groundwater loading pattern was adopted to simulate seasonal groundwater variation. The results indicate that liners designed for a 50-year life can withstand higher peak pressures when groundwater levels vary seasonally due to recovery of deformation during the partial unloading period. The results also show that pipe liners have a longer life when they are subjected to more frequent recovery periods. A correction factor was derived and directly applied to the ASTM F1216 design equation for the partially deteriorated case. The correction factor allows a designer to quantitatively estimate the influence of variable groundwater loading on liner design; example calculations show significant reductions in the required liner thickness when large drops in water level occur during the dry season or when the dry season is longer than the wet season.

Reproduced with permission of the copyright owner. Further reproduction prohibited without permission.

APPROVAL FOR SCHOLARLY DISSEMINATION

The author grants to the Prescott Memorial Library of Louisiana Tech University the right to reproduce, by appropriate methods, upon request, any or all portions of this Dissertation. It is understood that "proper request" consists of the agreement, on the part of the requesting party, that said reproduction is for his personal use and that subsequent reproduction will not occur without written approval of the author of this Dissertation. Further, any portions of the Dissertation used in books, papers, and other works must be appropriately referenced to this Dissertation.

Finally, the author of this Dissertation reserves the right to publish freely, in the literature, at any time, any or all portions of this Dissertation.

Author Qing Cai

Date 03.01.2007

GS Form 14
(5/03)

Reproduced with permission of the copyright owner. Further reproduction prohibited without permission.

TABLE OF CONTENTS

ABSTRACT iii

TABLE OF CONTENTS vi

LIST OF TABLES ix

LIST OF FIGURES xii

ACKNOWLEDGMENTS xvi

CHAPTER ONE INTRODUCTION 1
1.1 Background and Research Need 2
1.2 Objectives and Scope 4

CHAPTER TWO LITERATURE REVIEW 6
2.1 Introduction 6
2.2 Time-Dependent Behavior of Polymers 6
2.2.1 Creep in Polymers 7
2.2.2 Recovery in Polymers 10
2.3 Creep-Buckling of CIPP Liners 14
2.3.1 Liner Buckling Tests 14
2.3.2 Liner Buckling Models 15
2.4 Variation in Groundwater 18
2.4.1 Occurrence of Groundwater 18
2.4.2 Groundwater Level Fluctuations 20
2.5 Summary 23

CHAPTER THREE LINEAR VISCOELASTICITY MODELS 25
3.1 Introduction 25
3.2 Kelvin Model 26
3.3 Maxwell Model 28
3.4 Four-Parameter Model 30
3.5 Generalized Maxwell and Kelvin Models 32
3.5.1 Generalized Maxwell Model 32
3.5.2 Generalized Kelvin Model 34
3.6 Summary 36

CHAPTER FOUR MATERIAL CHARACTERIZATION TESTING 38
4.1 Introduction 38
4.2 Material Testing Assumptions and Methods 38
4.3 Test Specimens 39
4.3.1 Specimen Preparation 40
4.3.2 Conditioning 41

Reproduced with permission of the copyright owner. Further reproduction prohibited without permission.

4.4 Testing Apparatus 42
4.4.1 Bending Table 42
4.4.2 Stirrups 43
4.4.3 Dial Indicator 44
4.4.4 Loading System 46
4.5 Determination of Specimen Loading 47
4.6 Testing Procedure 52
4.6.1 Testing Procedure for Loading (Creep) 52
4.6.2 Testing Procedure for Partial Unloading (Strain Recovery) 53
4.6.3 Testing Procedure for Reloading 53
4.6.4 Testing Procedure for Reunloading 53
4.7 Summary 54

CHAPTER FIVE ANALYSIS OF MATERIAL TESTING RESULTS 55
5.1 Introduction 55
5.2 Fitting of Experimental Data 55
5.2.1 Fitting Function 56
5.2.2 Retardation Times 58
5.2.3 Multiple Linear Regression Model 60
5.2.4 Determination of Retardation Constants 61
5.3 Numerical Interconversion 66
5.4 Single Element Model Verification 72
5.5 Summary 74

CHAPTER SIX FINITE ELEMENT MODELING 75
6.1 Introduction 75
6.2 Assumptions 76
6.3 Finite Element Model 76
6.3.1 Basic Liner Geometrical Parameters 77
6.3.2 Model Setup 78
6.3.3 Nonlinear Features 80
6.3.4 Loading Conditions 81
6.3.5 Viscoelastic Modeling 82
6.3.6 Simulation of Groundwater Level Variation 82
6.4 Model Verification 84
6.4.1 Mesh Refinement 84
6.4.2 Verification with Glock's Model 86
6.5 Summary 87

CHAPTER SEVEN STRUCTURAL BEHAVIOR OF PVC PIPE LINERS 88
7.1 Introduction 88
7.2 Essential Factors 88
7.2.1 The 50-Year Pressure 89
7.2.2 Variations in Groundwater Level 90
7.3 Effects of Groundwater Variation 91
7.3.1 Effects on 50-Year Pressure 91
7.3.2 Effects on Liner Deformation 93
7.3.3 Effects on Liner Design 100
7.3.4 Liner Design Examples 105
7.4 Summary 109

CHAPTER EIGHT CONCLUSIONS AND RECOMMENDATIONS 110
8.1 Conclusions 110

Reproduced with permission of the copyright owner. Further reproduction prohibited without permission.

8.1.1 Material Characterization Testing 110
8.1.2 Material Modeling 110
8.1.3 Finite Element Modeling 111
8.1.4 Modified ASTM Liner Design Approach 113
8.2 Recommendations 114

APPENDIX A MATERIAL CHARACTERIZATION DATA 116

APPENDIX B INTERCONVERSION BETWEEN MATERIAL MODELS 134

APPENDIX C TYPICAL ABAQUS© INPUT FILES 142

APPENDIX D DETERMINATION OF 50-YEAR PRESSURES 151

REFERENCES 155

Reproduced with permission of the copyright owner. Further reproduction prohibited without permission.

LIST OF TABLES

Table 4.1 Extra force exerted by the dial indicators 45

Table 4.2 Loading table for creep and recovery testing..... 51

Table 5.1 Compliance constants for generalized Voigt model 62

Table 5.2 Relaxation modulus for generalized Kelvin model 70

Table 5.3 Relaxation modulus for generalized Kelvin Model in terms of g_n and ρ_n 71

Table 6.1 Geometric parameters for the 2-D models..... 78

Table 6.2 Boundary conditions for the two-lobe buckling model 79

Table 6.3 Mesh refinement for the higher compliance PVC 85

Table 6.4 Mesh refinement for the higher stiffness PVC 86

Table 7.1 Buckling time for PVC-HC under the variation: TVR=0.33 and DVR=0.75 .. 92

Table 7.2 Buckling time for PVC-HS under the variation: TVR=0.33 and DVR=0.75... 93

Table 7.3 Correction factors for HC PVC, 3-month cycle 101

Table 7.4 Correction factors for HS PVC, 3-month cycle..... 101

Table 7.5 Correction factors for HC PVC, 6-month cycle 101

Table 7.6 Correction factors for HS PVC, 6-month cycle..... 102

Table A.1 Experimental data for higher compliance PVC specimen - HC01 117

Table A.2 Experimental data for higher compliance PVC specimen - HC02 118

Table A.3 Experimental data for higher compliance PVC specimen - HC03 119

Reproduced with permission of the copyright owner. Further reproduction prohibited without permission.

Table A.4 Experimental data for higher compliance PVC specimen - HC04 120

Table A.5 Experimental data for higher compliance PVC specimen - HC05 121

Table A.6 Experimental data for higher compliance PVC specimen - HC06 122

Table A.7 Experimental data for higher compliance PVC specimen - HC08 123

Table A.8 Experimental data for higher stiffness PVC specimen - HS01 124

Table A.9 Experimental data for higher stiffness PVC specimen - HS02 125

Table A.10 Experimental data for higher stiffness PVC specimen - HS03 126

Table A.11 Experimental data for higher stiffness PVC specimen - HS04 127

Table A.12 Experimental data for higher stiffness PVC specimen - HS05 128

Table A.13 Experimental data for higher stiffness PVC specimen - HS06 129

Table A.14 Experimental data for higher stiffness PVC specimen - HS07 130

Table A.15 Experimental data for higher stiffness PVC specimen - HS08 131

Table D.1 Buckling time for PVC-HC for TVR=0.33 (load cycle: 3 months) 152

Table D.2 Buckling time for PVC-HC for TVR=1 (load cycle: 3 months) 152

Table D.3 Buckling time for PVC-HC for TVR=3 (load cycle: 3 months) 152

Table D.4 Buckling time for PVC-HS for TVR=0.33 (load cycle: 3 months) 152

Table D.5 Buckling time for PVC-HS for TVR=1 (load cycle: 3 months) 153

Table D.6 Buckling time for PVC-HS for TVR=3 (load cycle: 3 months) 153

Table D.7 Buckling time for PVC-HC for TVR=0.33 (load cycle: 6 months) 153

Table D.8 Buckling time for PVC-HC for TVR=1 (load cycle: 6 months) 153

Table D.9 Buckling time for PVC-HC for TVR=3 (load cycle: 6 months) 154

Table D.10 Buckling time for PVC-HS for TVR=0.33 (load cycle: 6 months) 154

Table D.11 Buckling time for PVC-HS for TVR=1 (load cycle: 6 months) 154

Reproduced with permission of the copyright owner. Further reproduction prohibited without permission.

Table D.12 Buckling time for PVC-HS for TVR=3 (load cycle: 6 months) 154

Reproduced with permission of the copyright owner. Further reproduction prohibited without permission.

LIST OF FIGURES

Fig. 2.1 Phenomenological description of creep 7

Fig. 2.2 Tensile creep elongation and recovery of plasticized PVC material at different temperatures [3] 8

Fig. 2.3 Creep and recovery of metals and plastics [5] 11

Fig. 2.4 Final recovery of PVC following creep [12] 13

Fig. 2.5 Groundwater and water table [33] 19

Fig. 2.6 Hydrological cycle [34] 20

Fig. 2.7 Groundwater fluctuation in monitoring well versus rainfall [36] 21

Fig. 2.8 Water-level fluctuations in observation well FA-01 located in Thana Faridpur, southwest of Dhaka [42] 23

Fig. 3.1 Kelvin Model 26

Fig. 3.2 Kelvin Model response 28

Fig. 3.3 Maxwell Model 28

Fig. 3.4 Maxwell Model response 29

Fig. 3.5 Standard Linear Liquid Model 30

Fig. 3.6 Standard Linear Liquid Model response 31

Fig. 3.7 Generalized Maxwell Model describing rheodictic behavior 32

Fig. 3.8 Generalized Maxwell Model describing arrheodictic behavior 33

Fig. 3.9 Generalized Kelvin Model describing rheodictic behavior 35

Fig. 3.10 Generalized Kelvin Model describing arrheodictic behavior 36

Reproduced with permission of the copyright owner. Further reproduction prohibited without permission.

Fig. 4.1 Higher compliance (left) and higher stiffness (right) PVC pipe liner 40

Fig. 4.2 Specimen for bending creep test 41

Fig. 4.3 Bending table for three-point bending tests 42

Fig. 4.4 Stirrup on specimen with cable and dial indicator 43

Fig. 4.5 Dial indicators 44

Fig. 4.6 Loading system 47

Fig. 4.7 Flexural stress vs. groundwater table 48

Fig. 4.8 Creep test on PVC pipe liner materials 52

Fig. 5.1 Loading history on material test specimens 57

Fig. 5.2 Generalized Kelvin Model (5 Kelvin units) 60

Fig. 5.3 Strain vs. time for HC-PVC under stress level 1 (205 psi), curve fit generated using constants from table 5.1 63

Fig. 5.4 Strain vs. time for HC-PVC under stress level 2 (410 psi), curve fit generated using constants from table 5.1 63

Fig. 5.5 Strain vs. time for HS-PVC under stress level 1 (250 psi), curve fit generated using constants from table 5.1 64

Fig. 5.6 Strain vs. time for HS-PVC under stress level 2 (500 psi), curve fit generated using constants from table 5.1 64

Fig. 5.7 Strain vs. time for HC-PVC under stress level 1 (205 psi) and stress level 2 (410psi), curve fit generated using constants from table 5.1 65

Fig. 5.8 Single element model used for verification 72

Fig. 5.9 Time dependent loading applied to the single element model 73

Fig 5.10 Plot of axial strain from single element FEA model for HC PVC material constants from table 5.2 were used 73

Fig. 6.1 Schematic of the two-lobe model with even gap 77

Fig. 6.2 Two-lobe finite element model (External pressure is applied to the liner in the gap between the liner and the host pipe) 80

Reproduced with permission of the copyright owner. Further reproduction prohibited without permission.

Fig. 6.3 Step variation of groundwater pressure [27] 83

Fig. 6.4 Sinusoidal variation simulating variations
in groundwater pressure [27] 84

Fig. 6.5 Trapezoidal groundwater loading pattern adopted for this research 84

Fig. 7.1 Fifty-year pressure for higher compliance PVC material 89

Fig. 7.2 Fifty-year pressure for higher stiffness PVC material 90

Fig. 7.3 Schematic of a pipe liner experiencing the two-lobe deformation pattern 94

Fig. 7.4 Displacement vs. time for the PVC HC liner
(3-month cycle, load= P_{50v}, TVR=1/3, DVR=3/4) 95

Fig. 7.5 Displacement vs. time for the PVC HC liner
(3-month cycle, load= P_{50v}, TVR=1/3, DVR=1/2) 96

Fig. 7.6 Displacement vs. time for the PVC HC liner
(3-month cycle, load= P_{50v}, TVR=1/3, DVR=1/4) 96

Fig. 7.7 Comparison with liner response for constant groundwater loading and
variable groundwater loading at short times (3-month cycle, load= P_{50}) 97

Fig. 7.8 Displacement vs. time for the PVC HC liner
(3-month cycle, load= P_{50v}, TVR=1, DVR=3/4) 98

Fig. 7.9 Displacement vs. time for the PVC HC liner
(3-month cycle, load= P_{50v}, TVR=3, DVR=3/4) 98

Fig. 7.10 Comparison with liner response for constant groundwater loading and
variable groundwater loading at short times (3-month cycle, load= P_{50}) 99

Fig. 7.11 Effect of time variation frequency for a liner subjected to loading
of 50-year pressure with TVR=1/3 and DVR=3/4 100

Fig. 7.12 Correction factor curves (HC, 3-month cycle) 102

Fig. 7.13 Correction factor curves (HS, 3-month cycle) 103

Fig. 7.14 Correction factor curves (HC, 6-month cycle) 103

Reproduced with permission of the copyright owner. Further reproduction prohibited without permission.

Fig. 7.15 Correction factor curves (HS, 6-month cycle)..... 104

Fig. 7.16 Groundwater level from 1998-2002 for a well in Dalton Holme, UK [62]..... 107

Fig. 7.17 Liner thickness change (%) versus correction factors..... 108

Fig. A.1 Average experimental strain vs. time for higher compliance PVC specimens. 132

Fig. A.2 Average experimental strain vs. time for higher stiffness PVC specimens..... 133

Reproduced with permission of the copyright owner. Further reproduction prohibited without permission.

ACKNOWLEDGMENTS

I wish to express my sincere gratitude and appreciation to my advisor Dr. David Hall for his invaluable guidance, encouragement and generous support throughout my graduate studies. I would like to thank Dr. Raymond Sterling for his long-term support and understanding in all the years I have been at Louisiana Tech University. I would also like to thank Dr. Jay Wang for his support, encouragement, and service on my advisory committee. Sincere acknowledgement is also extended to Dr. Michael Baumert and Dr. Weizhong Dai for their kindness of serving as advisory committee members. I would also like to show my appreciation to Dr. Wei Zhao for helping me carry out the testing and for providing me guidance and assistance in the preparation of this dissertation.

I also want to show my appreciation to all my friends, on and off campus; their help made this work easier and more enjoyable. Finally, I would like to thank my parents, my brother, my sister-in-law, and my girlfriend, without their love and support this dissertation would not have been completed.

Reproduced with permission of the copyright owner. Further reproduction prohibited without permission.

CHAPTER ONE

INTRODUCTION

For sewer-pipe systems that have undergone significant deterioration, the repair and rehabilitation of the system is often required to maintain system viability. Trenchless rehabilitation technologies have become increasing popular over the past 20 years by allowing the replacement or repair of pipelines with little or no soil excavation. Trenchless techniques reduce damage to existing services and structures and minimize damage to the environment. Trenchless methods are especially attractive for installing or rehabilitation infrastructure in congested areas by reducing the impact on nearby businesses and on traffic flow.

Fold-and-Form Pipe (FFP), Deformed-Reform Pipe (DRP), and Cured-In-Place Pipe (CIPP) are very popular pipeline rehabilitation technologies whereby a tight-fitting plastic liner is installed in deteriorated underground pipelines to reduce water infiltration and stabilize the soil around the host pipe. The FFP and DRP method utilize thermoplastic pipe liners (typically PVC or HDPE) which are folded or deformed to reduce the cross-sectional area so that they can be pulled into place inside the host pipe. Once in place, the liner is typically exposed to internal pressure and heat, causing the liner to expand and conform to the internal shape of the host pipe. The practice of CIPP method is to invert a polymer-saturated fabric tube into the damaged host pipe and then

Reproduced with permission of the copyright owner. Further reproduction prohibited without permission.

pass hot water or steam inside the liner so that it can expand and cure in place and take the shape of the host pipe.

Liners installed to rehabilitate deteriorated pipe are usually expected to extend the lifetime of the existing structure by at least 50 years. Since these liners are often installed in pipes that lie below the water table, the external surface of the liners is exposed to water pressure that can lead to slow inward deformations which may eventually cause the liner to collapse or buckle. An understanding of the long-term deformation characteristics of the liner material and the varying nature of the groundwater loading are important issues that are the focus of this research.

1.1 Background and Research Need

The actual loading condition applied to the pipe liners may be divided into two kinds of external loadings. One is soil and traffic loading which acts on the host pipe through the interaction with the soil. The other is the loading due to external water pressure. However, previous research and field applications have suggested that the host pipe is usually strong enough to carry soil and traffic loads and the only significant loading on the liners is the external pressure resulting from the ground water. The job of the liner is often to reduce the infiltration of water, which can stabilize the host pipe/liner system by stopping erosion of soil into the pipe.

Most plastic materials will continue to deform over time even when the loading applied to the material is constant. This time-dependent deformation is called creep. When a pipe liner is exposed to external pressure, the compressive hoop stress that is induced may lead to buckling of the pipe wall. For constrained tubes such as a pipe liner, collapse is typically manifested as large inward radial deflections at a single location (or

Reproduced with permission of the copyright owner. Further reproduction prohibited without permission.

lobe). Therefore, it is essential to consider the creep behavior of the plastic pipe liner when evaluating the stability of the liner subjected to long-term external groundwater loading.

When plastic materials are exposed to tensile loading over a period of time, the material stretches in the direction of the applied loading as creep deformation accumulates. Removing some or all of the loading usually causes some of the tensile strain to disappear over time as the material attempts to return to its initial shape. This time-dependent reduction in strain is called recovery. During recovery, the amount of the recoverable strain may be a large portion of the original time-dependent creep strain. Since the groundwater levels which lead to loading of liners may vary during the wet and dry seasons, some recovery may be experienced by pipe liners during the dry season when the depth of the water table drops, since a lower water table results in less external pressure loading. Recovery of previous creep deformation and internal deflections experienced by a pipe liner may result in the extension of the life of the liner.

It can be noted that most of the long-term buckling tests have been performed on liners at relatively high stress levels so that a buckling event can be experienced within the duration of the research project, which is almost always 10,000 hours or less. This elevated loading condition results in stresses that are much higher than expected for liners that are installed in field applications where a 50 year life is expected. Thus, when exploring the long-term performance of a liner material, it is important to study the material at stress levels that are as close as possible to those expected in the field.

Reproduced with permission of the copyright owner. Further reproduction prohibited without permission.

1.2 Objectives and Scope

The primary objective of this research is to observe the creep and strain recovery of PVC liners subjected to varying pressure caused by seasonal groundwater changes. The ABAQUS© finite element software is used here to construct a 2-D model to simulate the response of a pipe liner exposed to varying external pressure. The material properties embedded into the finite element code require extensive creep-deformation testing which was also completed as part of this work. This research program includes the following activities:

- Conduct a literature review on creep and strain recovery of plastic and PVC liners.
- Conduct strain recovery tests (up to 8,640 hours) on two kinds of PVC liner materials (higher compliance PVC and higher stiffness PVC) in accordance with American Society for Testing and Materials (ASTM) D2990-01 [1] using eight specimens for each material. Two stress levels, 5% and 10% of the yield strength, were applied to obtain the material properties at stress levels similar to those expected under field conditions. Creep tests were first carried out over a period of 2,160 hours, which is equivalent to three months or one season. Then, 50% of the loading was removed from all of the specimens, and the material was allowed to recover for 2,160 hours. The specimens were then reloaded for 2,160 hours by reapplying 50% of the loading that was initially removed. Finally, 50% of the loading was again removed for 2,160 hours to complete the annual load/unload cycle associated with seasonal groundwater variations.

Reproduced with permission of the copyright owner. Further reproduction prohibited without permission.

- Establish a suitable mathematical viscoelastic model to fit the experimental data and obtain the material constants.
- Construct a finite element model to simulate the liner-pipe contact and the long-term liner buckling. The material properties obtained from the tests were used in the model using the features available in ABAQUS©.
- The end result of this research is a new liner buckling model that effectively accounts for seasonal groundwater changes on pipe liner design.

Reproduced with permission of the copyright owner. Further reproduction prohibited without permission.

CHAPTER TWO

LITERATURE REVIEW

2.1 Introduction

Plastic pipe liners that are used in trenchless rehabilitation technologies are flexible and have similar design considerations as thin-walled metal pipes. However, due to the viscoelastic nature of plastic materials (typically for thermosetting and thermoplastic materials), the time-dependent behavior should be considered when studying the long-term behavior of the liners. Since the only significant loading acting on the liner is the groundwater pressure that changes seasonally due to natural and human factors, the primary concerns of the present research are focused on the creep and creep recovery behaviors of encased plastic liners subjected to seasonal groundwater pressures. An overview of the creep and creep recovery phenomenon in plastic materials is given in this chapter followed by several relevant liner buckling models. The chapter concludes with an overview of seasonal groundwater variations.

2.2 Time-Dependent Behavior of Polymers

Polymers are typically materials consisting of long chain-like molecules in a tangled and coiled arrangement. The major difference between the deformational behavior of polymeric materials and metals is that the strain response of polymeric materials depends not only on the magnitude of the load but also on the time (time-

Reproduced with permission of the copyright owner. Further reproduction prohibited without permission.

dependent behavior). Creep and creep recovery are the two main types of time-dependent behaviors of polymers.

2.2.1 Creep in Polymers

Creep is a slow continued extension of a plastic material under constant load (Findley, 1976). A load placed on a polymer material will result in an initial deformation, but since the load is continuously applied over time, additional deformation will occur.

The concept of creep can be phenomenologically illustrated by Fig. 2.1. A typical creep strain development curve is usually divided into three stages [2]. Initially, the strain rate slows with increasing strain. This is known as primary creep. The strain rate eventually reaches a minimum and becomes near-constant. This is known as secondary or steady-state creep. The creep strain rate remains at this steady-state rate for most of the life of a structure. The stress dependence of this rate depends on the creep mechanism. In tertiary creep, the strain-rate exponentially increases with the accumulation of additional strain. The division is rather arbitrary and constant strain rates are rarely found in real test data.

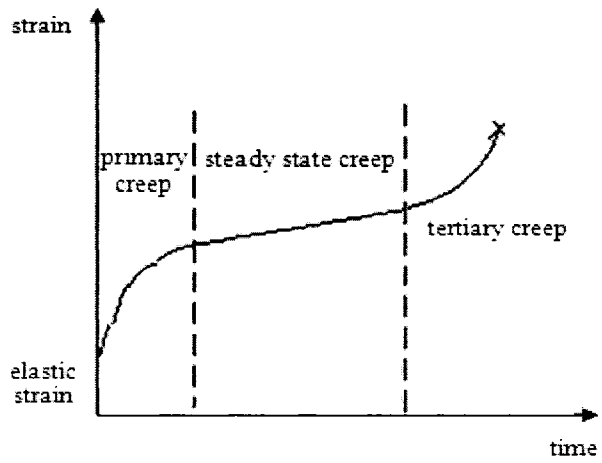

Fig. 2.1 Phenomenological description of creep

Reproduced with permission of the copyright owner. Further reproduction prohibited without permission.

Creep in polymeric materials is quite different from the creep in metals. It occurs by chains untangling and slipping relative to one another and may be affected by many factors. In a tensile test, the amount of specimen elongation will depend on the magnitude of the loading, but the exact shape of the deformation-time curve will depend not only on the material composition but on the temperature at which the test is run [3], as shown in Fig. 2.2. For plasticized PVC, at the temperature between the rigid and rubbery, the deformation curve required relatively longer time to slow down and the creep curve almost becomes horizontal after several months.

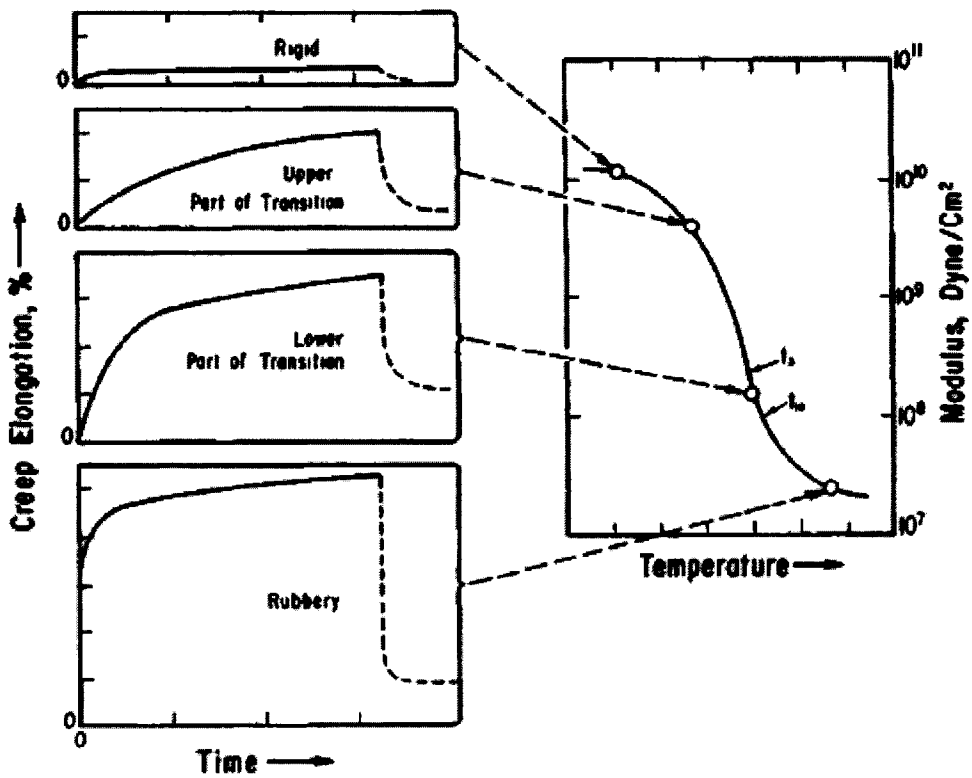

Fig. 2.2 Tensile creep elongation and recovery of plasticized PVC material at different temperatures [3]

Because polymers consist of long chain-like molecules, when a stress is applied, the entropy of the material system may change from high to low as the chains elongate

Reproduced with permission of the copyright owner. Further reproduction prohibited without permission.

and become more aligned (more ordered). When the elongation becomes higher, creep can occur by the molecular chains sliding past each other resulting in inelastic flow of the polymer. Below the glass transition temperature, a polymer material has to overcome two types of resistance before inelastic flow may occur [4]: intermolecular resistance to segment rotation and back stresses caused by entropy change.

The irregularity of the random molecular structure of polymers makes the creep process more complex. So, it is difficult to employ only a single equation to describe the creep behavior of all polymers. Based on material experiments, many empirical equations have been created to represent the creep curves of plastics. If we assume that creep of linear viscoelastic materials (materials where the strain rate scales linearly with stress) can be described by using a mechanical model consisting of elastic elements (springs) and linear viscous elements (dash pots), then a useful empirical equation, which has been utilized by a number of investigators to represent creep of linear viscoelastic materials, can be written as:

$$\varepsilon = \varepsilon_0 + \sum_i A_i(1 - e^{-c \cdot t}) + B \cdot t \tag{2.1}$$

where ε_0, A_i and B are the material constants related to the applied stress and c is independent of stress [5]. It can be noticed that the second term in Eq. 2.1 will approach to zero when time is large enough, which indicates that the creep rate for linear viscoelastic materials will become a constant after a transition period time.

Another empirical function, called the power function of time, was also used to predict creep of many different rigid plastics and can yield a good match to the experimental data over a wide span of test times ([6], [7], and [8]). The function may be written as:

Reproduced with permission of the copyright owner. Further reproduction prohibited without permission.

$$\varepsilon^{CR} = \varepsilon^{0} + \varepsilon^{+} t^{n} \tag{2.2}$$

where ε^{0}, ε^{+} are functions of stress and n is independent of stress.

For nonlinear viscoelastic materials or various soft materials such as rubber, power functions of stress [9] have been widely used to fit the stress-strain-time curve. The function may be written as:

$$\varepsilon^{CR} = k\sigma^{p} t^{n} \tag{2.3}$$

where ε^{CR} is the creep strain, σ is stress, and k, p and n are the material constants.

2.2.2 Recovery in Polymers

Recovery, also called delayed elasticity, is a procedure of the time-dependent disappearance of creep strain. When some or all of the applied stress is released before creep rupture occurs, the polymer will immediately regain a portion of its initial shape as an elastic material would, then follows a slow recovery where the material returns closer to its initial shape as time passes. Some plastics may show full recovery if the recovery time is sufficient while others may have limited recovery with a significant portion of permanent inelastic deformation remaining (never to be recovered). Compared with the recovery of metals, the recovery of polymers from creep strain can be a larger portion of the accumulated strain [5] as shown Fig. 2.3.

Reproduced with permission of the copyright owner. Further reproduction prohibited without permission.

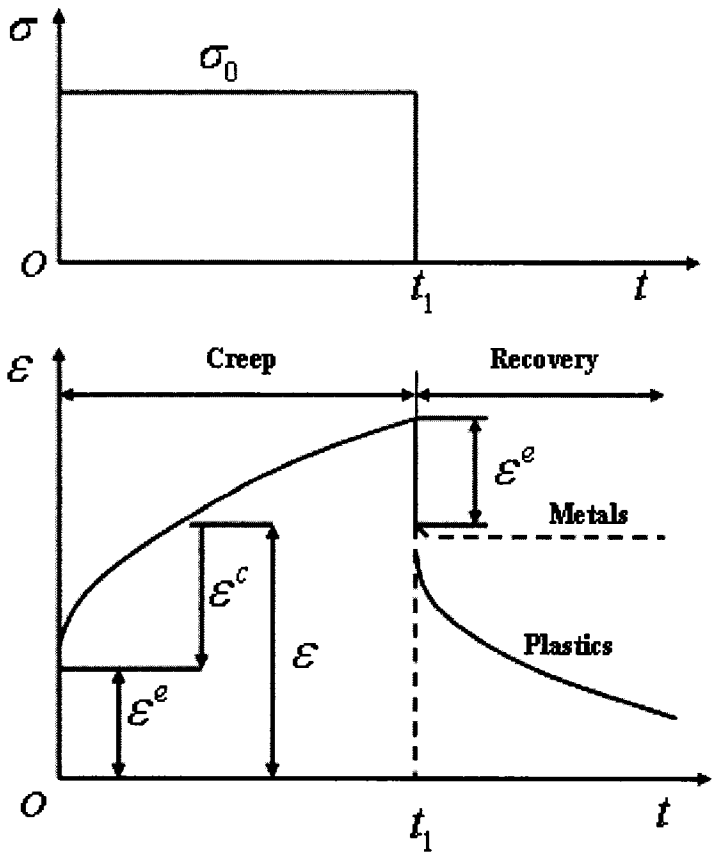

Fig. 2.3 Creep and recovery of metals and plastics [5]

Blage [10] studied the deformation responses of amorphous polymeric materials under small stresses and suggested that delayed elasticity occurs at temperatures above T_g and under a loading with slower rates. On the molecular level, delayed elasticity is caused by changes in the conformation of molecules.

Kung [11] studied recovery processes of some amorphous polymers such as polymethyl methacrylate (PMMA) and polycarbonate (PC), and proposed that there are probably two recovery processes in amorphous polymers: one occurs at the temperatures below T_g releasing stored energy and recovering volume and the other occurs at the temperature above T_g releasing stored energy but recovering dimension.

Reproduced with permission of the copyright owner. Further reproduction prohibited without permission.

Maseeh [4] studied the creep recovery of polyimide thin films and found that the configurational entropy of the material changed when the molecular alignment occurs. And during recovery, the reorientation of polymer chains may dissipate some energy, so energy loss may occur after shape recovery.

Similar to creep, many empirical equations are proposed to represent the recovery curves of plastics. Generally, when the response of a polymer is in the linear viscoelastic regime, the simplest description of creep recovery is the Boltzmann linear superposition principle which describes the response of a polymer material to different loading histories: the strain response of a specimen is proportional to the applied stress and all deformations are additive, as shown in Eq. 2.4:

$$\varepsilon(t) = \sum_{n} (\sigma_n - \sigma_{n-1}) \cdot D(t - t_n) \tag{2.4}$$

where σ is the applied stress and $D(t)$ is the compliance function. The Boltzmann principle can also be written in continuous form, as shown in Eq 2.5.

$$\varepsilon(t) = \int_{-\infty} D(t - \tau) d\sigma(t) \tag{2.5}$$

Findley [12] reported the 26-year (230,000 hours) creep and recovery experiments on two thermoplastics (polyvinyl chloride and polyethylene) at constant values of tensile stress, temperature and relative humidity. The first period of creep was predicted by the following equation,

$$\varepsilon = \varepsilon^0 + \varepsilon^+ \cdot t^n \tag{2.6}$$

where ε^0 is time independent strain due to stress change, ε^+ is a coefficient of the time dependent term, t is initial time period, and n is time exponent.

Reproduced with permission of the copyright owner. Further reproduction prohibited without permission.

The strain during recovery at zero stress can be predicted using the superposition principle together with Eq (2.6),

$$\varepsilon = \varepsilon^0 + \varepsilon^+ \cdot t^n - [\varepsilon^0 + \varepsilon^+ \cdot (t - t_1)^n], \quad t > t_1 \tag{2.7}$$

where t_1 is the time at which stress was removed. The recovery at zero stress can be well predicted as shown in Fig. 2.4.

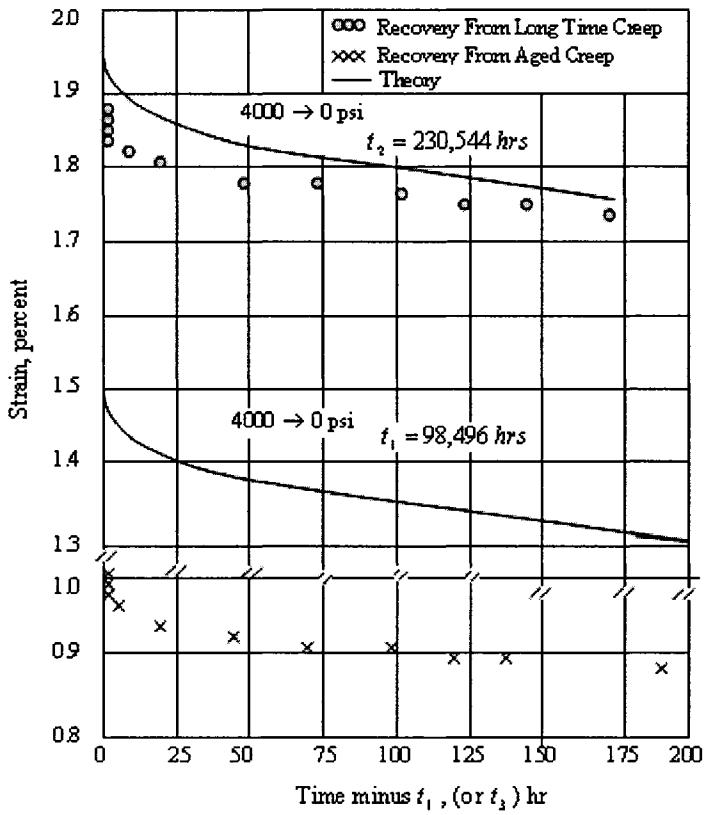

Fig. 2.4 Final recovery of PVC following creep [12]

Although the Boltzmann principle can be used to predict recovery behavior of linear viscoelastic materials, it is not applicable when the response of polymer is in the nonlinear viscoelastic regime. Ward and Onat [13] tested a multiple-integral approach on oriented polypropylene fibers and found that it can successfully describe the recovery of polypropylene; however, it is not true for all other polymers. Neis and Sackman [14]

Reproduced with permission of the copyright owner. Further reproduction prohibited without permission.

performed tensile and compressive multiple loading tests on low density polythelene and found that multiple-integral approach can not well predict unloading behavior. Lockett and Turner [15] pointed out that the factor that the multiple-integral approach fails to describe the recovery behavior is probably due to the fact that the kernel function derived from loading experiments may not be the same as the function derived from unloading experiments [16].

2.3 Creep-Buckling of CIPP Liners

2.3.1 Liner Buckling Tests

Since creep-buckling is an important factor related to stiffness and stability of the liner under external hydrostatic pressure, several material characterization tests including short-term and long-term tests have been carried out to study the structural behavior of CIPP liners.

In an attempt to provide better knowledge of constrained buckling, liner short-term tests were conducted at the Trenchless Technology Center (TTC) at Louisiana Tech University [17] on the Insituform Enhanced liners. It was found that a liner typically deflected in a two-lobe mode but collapsed into a one-lobe model with one domain lobe snapping through and the other being released partially. Boot and Welch [18] conducted short-term buckling test on liners encased in steel pipe and found that liners with little or no imperfections had higher buckling pressure than liners with high imperfections.

Welch [19] was the first to study the time-dependent behavior of polymeric materials for liner life prediction. Similar tests for the Insituform polymer material under tension, compression and bending conditions were conducted by Lin [20] and continued by Mahalingam [21].

Reproduced with permission of the copyright owner. Further reproduction prohibited without permission.

Straughan, Guice and Mal-Duraipandian [22] conducted tests on CIPP and FFP liners to determine the critical buckling pressure and the long-term modulus, and based on their pressure acceleration testing, they also concluded that the behavior of polymers is nonlinear viscoelastic over broad ranges of stresses.

Welch [19] investigated the effect of host pipe ovality on liner resistance and found that the effect was significant. Chunduru, Barber, and Bakeer [23] tested circular and oval encased HDPE liners and further pointed out that liner thickness and imperfections may affect the critical buckling pressures as well as ovality.

In addition to the short-term buckling tests, a series of 10,000 hour buckling tests have been carried out to analyze the long-term buckling of CIPP liners at the TTC ([22], [24], [25], and [26]). Kini [27] conducted a recovery analysis of a CIPP-lined oval pipe subjected to varied groundwater pressure. A sinusoidal variation was used to simulate groundwater variations in a finite element model, and the results indicated that the displacement predicted by a recovery model is lower than that predicted by a non-recovery model.

2.3.2 Liner Buckling Models

Experimentation and direct observation have shown that buckling is the primary mode of failure on pipe structures. So, the instability criterion should be emphasized in pipe design. Based on the buckling concept defined by Timoshenko [28], a lot of research work has been carried out to develop equations governing the liner buckling process.

The basic liner design equation for buckling of an unrestrained pipe is given as following,

$$P_{cr} = \frac{2 \cdot E \cdot t^3}{(1-v^2) \cdot D_m^3} \tag{2.8}$$

Reproduced with permission of the copyright owner. Further reproduction prohibited without permission.

where

P_{cr} = Groundwater load, psi

E = Modulus of elasticity of the pipe, psi

t = Pipe wall thickness, inches

ν = Poisson's ration (0.3, average)

D_m = Mean pipe diameter, inches

The current CIPP design equation for partially deteriorated pipes is taken from ASTM Designation F1216-05 Appendix X1 [29], by adding some empirical factors such as safety factors, ovality, and the effect of long-term creep to the basic equation. The ASTM model is only valid for buckling for ovalities of the host pipe of up to 10 percent. Where the host pipe is more than 10 percent out-of-round, special considerations are required [30]. The ASTM buckling equation is

$$P_{cr} = \frac{2 \cdot K \cdot E_L}{1-\nu^2} \times \frac{1}{(SDR-1)^3} \times \frac{C}{N} \tag{2.9}$$

where

$$C = \text{ovality reduction factor} = \left[\frac{(1-\frac{q}{100})}{(1+\frac{q}{100})^2} \right]^3$$

P_{cr} = groundwater load, psi

K = enhancement factor of the soil and existing pipe adjacent to the new pipe (typically, K=7)

ν = Poisson's ration (0.3, average)

Reproduced with permission of the copyright owner. Further reproduction prohibited without permission.

SDR = standard dimension ration of CIPP = OD/t = outside liner diameter / average liner thickness

q = percent ovality of original pipe

$$= \frac{[MaximumInsideDiameter - MeanInsideDiameter] \times 100}{MeanInsideDiameter}$$

N = factor of safety

E_L = long-term (time corrected) modulus of elasticity for CIPP, psi

The ASTM F1216 model is based on the buckling theory of free rings, while, in reality, the liners are encased in a rigid host pipe. Therefore, the ASTM model is sometimes considered to be too conservative because of the inappropriate mathematical model. In reality, setting the value of K = 7 is more conservative for thinner liners since they receive more support from the host pipe and may have effective K values higher than 7.

Glock analyzed the stability problem of a circular thin ring encased in rigid boundaries under the effect of external hydrostatic pressure as well as thermal load. Glock's model assumes that there is no friction between the ring and the rigid cavity, and used the nonlinear-deformation theory to develop his model. Glock's model is given as

$$P_{cr} = (\frac{1}{SDR-1})^{2.2} \frac{E}{1-\nu^2} \tag{2.16}$$

where P_{cr} = critical buckling pressure

E = flexural modulus of elasticity

SDR = Standard Dimension Ratio

= outside diameter / mean pipe wall thickness

t = mean liner thickness

Reproduced with permission of the copyright owner. Further reproduction prohibited without permission.

ν = Poisson's ration (0.3 average)

A number of improved buckling models for liners have been developed using Glock's model as a starting point. Omara [31] developed a modified Glock's model by considering an ovality reduction factor. Lu [32] further modified Omara's model by accounting for the effect of gap on the prediction of critical buckling pressure.

2.4 Variation in Groundwater

Groundwater is the only significant loading acting on a liner installed in a structurally sound host-pipe. To simplify the problem, most of the researchers who have investigated the creep behavior of CIPP liners have assumed that the liner is subjected only to a time constant hydrostatic pressure built up by infiltration through the cracks in the deteriorated host pipe. This approach has been adopted to take a conservative stance on liner design, since a higher groundwater table leads to higher pressures and requires thicker liners for a 50-year life. However, the groundwater table is certainly not constant in field conditions since seasonal changes can result in large swings in the water table.

2.4.1 Occurrence of Groundwater

When rain and snow reach the surface of the earth, a portion of the precipitation is carried away into surface streams, lakes or oceans. Another portion of the precipitation will directly infiltrate into the ground and slowly move down through the unsaturated zone (gaps between soil particles are filled with both air and water), eventually reaching a saturated zone (gaps between soil particles are filled with water) and becoming groundwater. The water table is the boundary between these two zones, as shown in Fig. 2.5.

Reproduced with permission of the copyright owner. Further reproduction prohibited without permission.

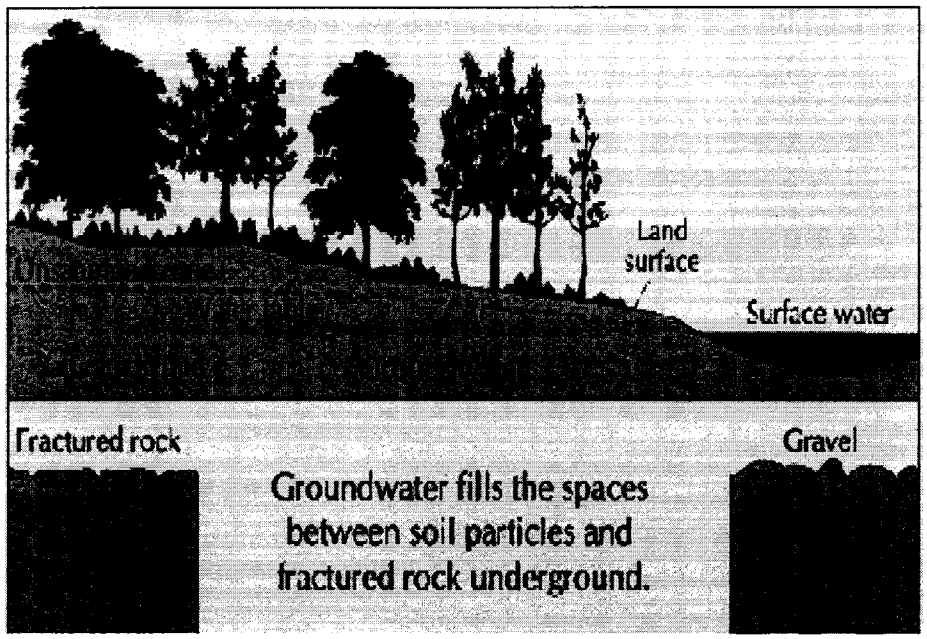

Fig. 2.5 Groundwater and water table [33]

Even after becoming groundwater, the water still flows downwards and then travels laterally when it is stopped by an impermeable layer. Under the influence of gravity, the groundwater returns to the surface by seeping into the beds of lakes, rivers and oceans. By evaporation from water and ground surfaces, the surface water is continually returned to the atmosphere and forms clouds which will result in rain or snowfall [34], as shown in Fig. 2.6. The ceaseless procedure is called the "hydrological cycle", and this cycle will cause the annual water table variation.

Reproduced with permission of the copyright owner. Further reproduction prohibited without permission.

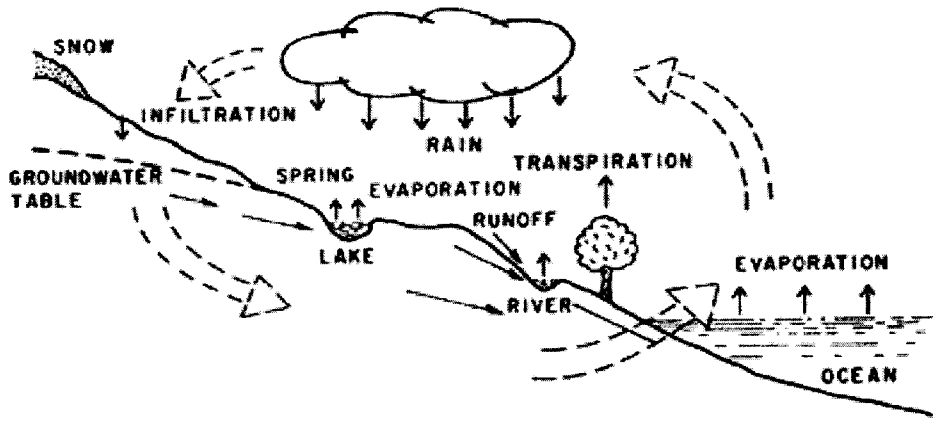

Fig. 2.6 Hydrological cycle [34]

2.4.2 Groundwater Level Fluctuations

The actual groundwater level is not constant. It will change throughout the year in response to natural and human-caused factors such as rainfall, irrigation, pumping, and other land activities. The balance between ground water recharge and discharge reflect the groundwater level changes: when the recharge to an aquifer exceeds discharge, ground-water levels rise; and when discharge exceeds recharge, ground-water levels decline.

Seasonal rainfall is the main natural reason that causes the seasonal fluctuation of the groundwater. During a wet season, especially in the winter or early spring, the groundwater table will probably be at its highest since it will be recharged due to frequent rains (or snowmelt) and low evaporation. During a dry season, especially in the summer, the water table will be at its lowest since there is no rain falling and there is a corresponding high level of evaporation due to the increased temperature. The groundwater will be discharged into streams and rivers to keep them flowing throughout the year.

Reproduced with permission of the copyright owner. Further reproduction prohibited without permission.

Butterworth [35] used long-term rainfall records collected in south-east Zimbabwe to evaluate the effects of variations in rainfall on groundwater. The results suggested that long-term trends in groundwater levels are apparent and reflect the effect of cycles in rainfall. A similar tendency of groundwater fluctuation with rainfall was reported at the Berkeley Lab in Berkeley, California[36]. The Berkeley Lab groundwater monitoring program collected water samples and monitored groundwater levels using a series of 174 wells, where Moraga Formation volcanic rocks, Orinda Formation sediments, and Great Valley Group sediments constitute the major rock units at the site and principally control the movement of groundwater in this area. Fluctuations in measured groundwater levels in wells generally show a good correlation with rainfall (Fig. 2.7). And, generally, the response of water levels after rainfall occurs is rapid in most site wells. Fluctuations may reach as great as 4.2 meters (14 feet) in some wells.

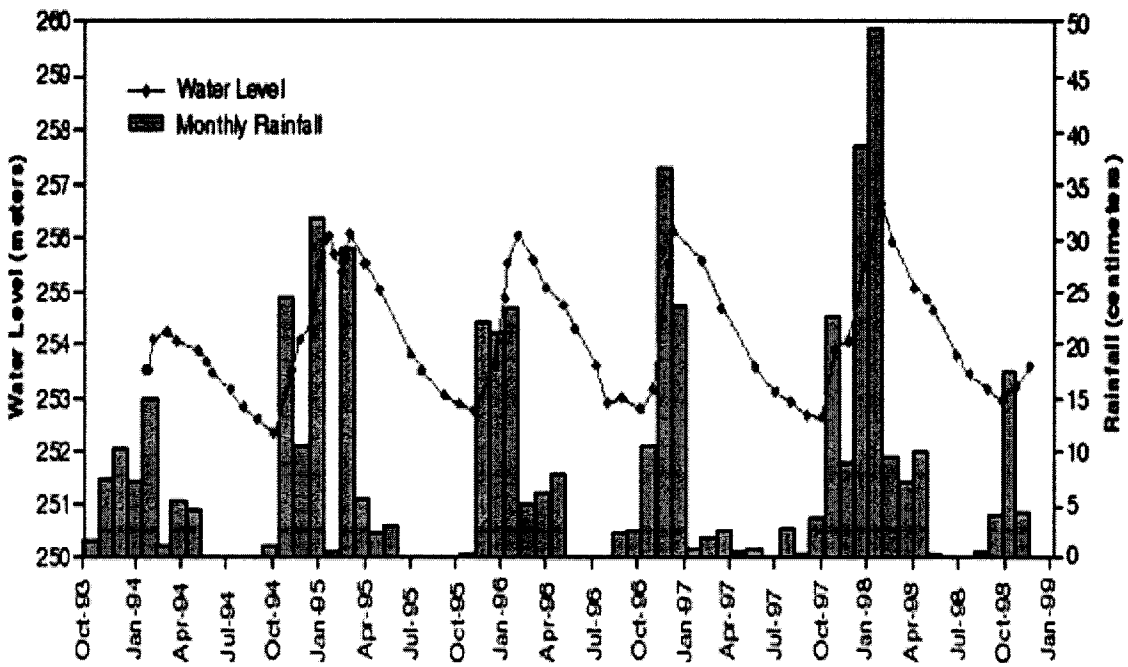

Fig. 2.7 Groundwater fluctuation in monitoring well versus rainfall [36]

Reproduced with permission of the copyright owner. Further reproduction prohibited without permission.

As stated earlier, when rain and snow reach the surface of the earth, water infiltrates into the soil and downward to groundwater. Movement of water through soils varies in the different soil types: some fields may drain immediately after rainfall whereas others remain flooded for weeks at a time. A report on the on water and the soil, presented by Cornell University [37], reported that the type of soil in a field, ranging from dense and impermeable clays to loose and gravelly sands, is a factor that relates how much water will percolate through the surface layer to become groundwater.

Ocean tides are also known as a natural factor that can affect the groundwater fluctuation in coastal regions. In most coastal areas, groundwater and seawater interact because of tidal fluctuations. These tide-induced water table fluctuations have been studied numerically by a number of researchers ([38], [39], and [40]).

Irrigation and pumping are the main significant human activities that affect the groundwater levels change. Lovelace [41] investigated water resources used for rice irrigation in southwestern Louisiana and found that seasonal pumping for rice irrigation, which typically occurs from February through June, causes the water-level declines, and water levels generally recover after pumping during the rice-growing season, typically during July through January. Pradeep [42] studied long-term records of water level fluctuation in Bangladesh and concluded that there were five meters of seasonal fluctuation in groundwater level between 1967 and 1997, as shown in Fig. 2.8, before and after the advent of irrigation. In 1989, a study of perimeter wells in a citrus grove in South Florida evaluated the effectiveness of the surface water management system; the study showed groundwater level variations ranging from 0.09 to 2.9 meters (0.3 to 9.7 feet) [43]. Another study of the central Willamette Basin in Oregon revealed that the

Reproduced with permission of the copyright owner. Further reproduction prohibited without permission.

seasonal groundwater fluctuations coupled with summer pumping increased the variation to as much as 55 feet [44].

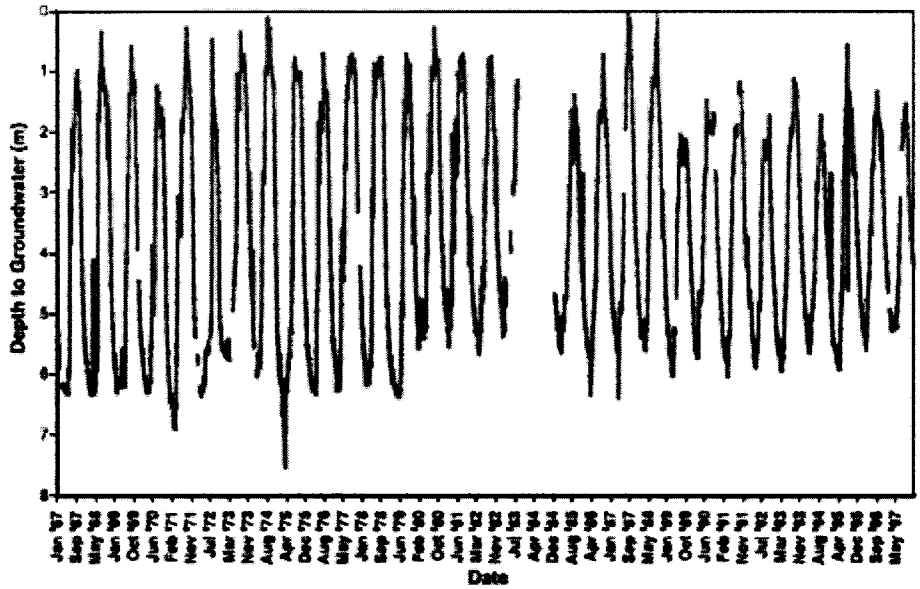

Fig. 2.8 Water-level fluctuations in observation well FA-01 located in Thana Faridpur, southwest of Dhaka [42]

2.5 Summary

Creep deformation occurs over a period of time when a material is subjected to constant stress at constant temperature. In metals, creep usually occurs at elevated temperatures. But, in plastic materials, creep occurs at room temperature. Recovery is a time-dependent decrease in strain after the removal of stress. The recovery in plastics is much greater than that observed in metals. The degree of the recovery in plastics depends on the microstructural changes that occur in the material, under constant stress, over a period of time. Creep and recovery are time-dependent behaviors that often are associated with pipe liners; both should be incorporated in the constitutive model used to predict the long-term behavior of the liner material. And, it can be found that the superposition

Reproduced with permission of the copyright owner. Further reproduction prohibited without permission.

principle (adding elastic and inelastic strain components) with some modifications can be used to predict the creep on loading and recovery after unloading.

Most researchers have assumed that the external pressure applied on the liner is constant for the entire liner lifetime. However, this assumption usually is not accurate as there will be some seasonal fluctuations in the groundwater level due to natural and human causes. The variation in the groundwater level may lead to strain recovery in the liner which plays an important role in the evolution of the stresses, strains, and deflections in the liner.

Reproduced with permission of the copyright owner. Further reproduction prohibited without permission.

CHAPTER THREE

LINEAR VISCOELASTICITY MODELS

3.1 Introduction

The response of the viscoelastic materials may vary significantly with time even though the applied loads are constant. Viscoelastic behavior can be represented by rheological models consisting of a combination of springs and dashpots arranged in series and parallel. These models provide some insight into the microstructural response of a viscoelastic material to an applied load; for example, a spring can be directly related to the stretching of atomic bonds, and a dashpot provides a mechanical analogy for the viscous sliding of chain molecules past one another during creep deformation. While these models do not describe all of the relevant details of the microstructural deformation process, they do provide a framework for effectively modeling the bulk response of the material response under creep and recovery conditions.

While most polymers show linear or nearly linear viscoelastic behavior at small stresses (stresses much lower than the yield limit), these same materials may become significantly nonlinear at elevated stresses [5]. When selecting a material model to predict the long-term response of a structure such as a liner, it is important to utilize a model that accurately reflects the behavior of the material under the conditions expected in field applications. The stress levels acting on a liner subjected to external pressure varies around the circumference of the liner, and the stresses are highest at the regions of

Reproduced with permission of the copyright owner. Further reproduction prohibited without permission.

maximum inward radial deflection (the deflection lobes). Since the groundwater pressure in field conditions is generally less than 20% of the instantaneous buckling pressure, P_{cr}, the peak stresses at all points in the liner, including the lobes, can be considered to be "small" compared to the yield strength of the material [27]. Thus, a linear viscoelastic model is employed throughout this work.

3.2 Kelvin Model

The Kelvin Model is a two-element model consisting of a simple spring and a dashpot. The components are combined together in parallel as shown in Fig. 3.1. The total strain response of this model is the same as the strain in each element, and the total stresses are equal to the sum of the stresses in the elements.

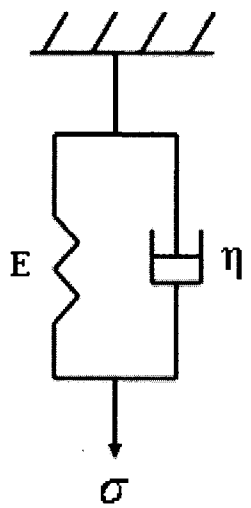

Fig. 3.1 Kelvin Model

For a step input of stress σ_0, the strain function is given as:

$$\varepsilon(t) = \sigma_0 \cdot D\left[1 - \exp(-\frac{t}{\tau_v})\right] \tag{3.1}$$

Reproduced with permission of the copyright owner. Further reproduction prohibited without permission.

where, σ_0 is the applied stress

τ_v is the retardation time for a Voigt unit, $\tau_v = \eta/E$

η is the coefficient of viscosity

E is Young's modulus

D is the retardation modulus

The response of the Kelvin element to a constant load σ_0 is shown in Fig. 3.2. When the load is applied, the immediate deformation may be constrained by the dashpot (the strain is retarded). The dashpot initially elongates at an instantaneous rate σ_0/η. However, as time continues, the rate of elongation of the dashpot decreases with the load being increasingly generated in the spring. Eventually the dashpot stops elongation when the entire load is generated in the spring. The spring has a limiting deformation of σ_0/E. When the load is removed from the element, the potential energy stored in the spring will be released and generate a restored force to pull the dashpot back to its initial position.

Reproduced with permission of the copyright owner. Further reproduction prohibited without permission.

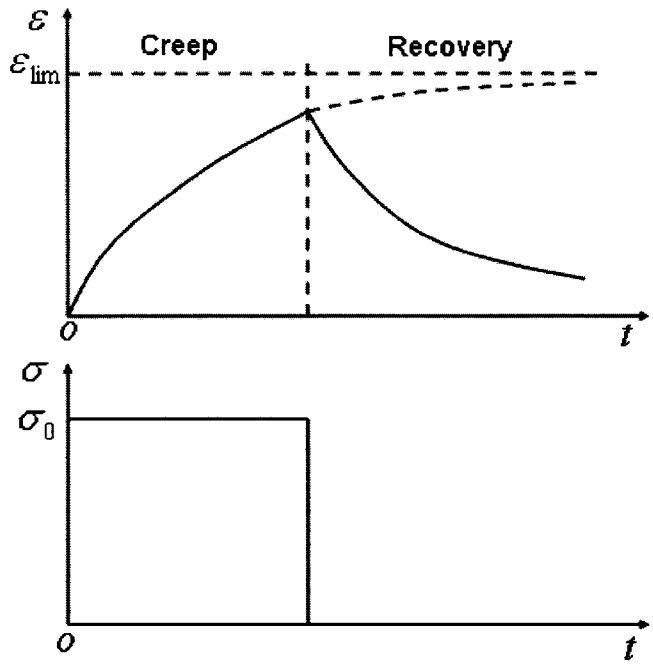

Fig. 3.2 Kelvin Model response

3.3 Maxwell Model

The Maxwell Model is also a two-element model where a spring element and a viscous dashpot element are connected in series as shown in Fig. 3.3. In a series model, the stresses in all elements are the same, and the strains in the elements are additive.

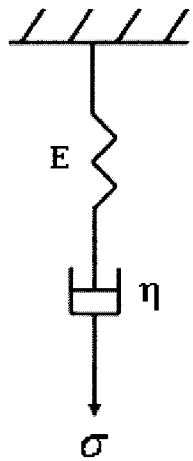

Fig. 3.3 Maxwell Model

Reproduced with permission of the copyright owner. Further reproduction prohibited without permission.

The strain function for a step input of stress σ_0 is given as:

$$\varepsilon(t) = \frac{\sigma_0}{E} + \frac{\sigma_0}{\eta} t \tag{3.2}$$

where, σ_0 is the applied stress

η is the coefficient of viscosity

E is Young's modulus

The response of the Maxwell element to a constant load σ_0 is shown in Fig. 3.4. When the load is applied, the model behaves as a simple spring at very short time by gaining an instantaneous deformation of σ_0 / E. As time passes, the dashpot (a viscous component) deforms at a constant velocity σ_0 / η, and the position of the dashpot at any time is equal to the velocity multiplied by time. When the load is removed, the Maxwell element does not return to its initial position. This residual strain is permanent creep deformation.

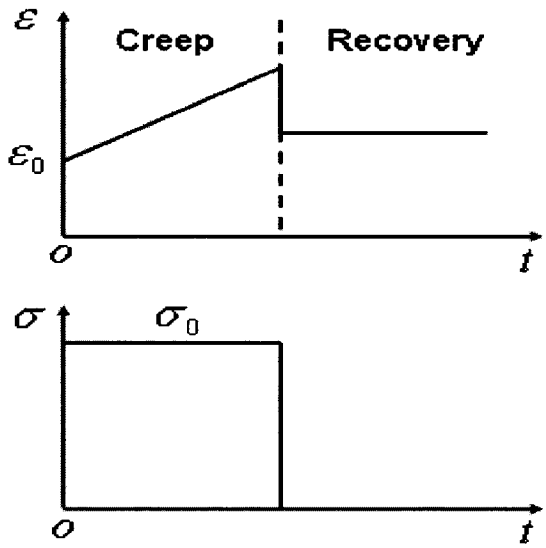

Fig. 3.4 Maxwell Model response

Reproduced with permission of the copyright owner. Further reproduction prohibited without permission.

3.4 Four-Parameter Model

The Kelvin and Maxwell Model described in Sections 3.2 and 3.3 can be thought of as units instead of stand-alone material models [45]. Because their structural elements (springs and dashpots) constrain the model, they can not fully represent viscoelastic behavior. Therefore, the Standard Linear Liquid Model or Burger's Model is developed to represent the essential coexistence of creep and relaxation using a minimum number of elements. The Standard Linear Liquid Model is shown in Fig. 3.5.

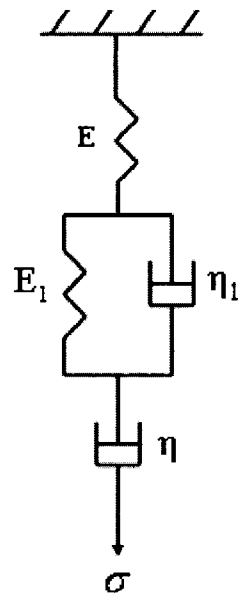

Fig. 3.5 Standard Linear Liquid Model

The presence of the isolated dashpot allows the model to be strained in the steady-state flow once the springs are fully extended. The total strain at time t will be the sum of the strain in the Maxwell unit and that in the Kelvin unit.

The strain function for a step input of stress σ_0 is given as:

$$\varepsilon(t) = \sigma_0 \left\{ D_g + D\left[1 - \exp(-\frac{t}{\tau})\right] \right\} + \frac{t}{\eta} \tag{3.3}$$

Reproduced with permission of the copyright owner. Further reproduction prohibited without permission.

where, σ_0 is the stress applied

D_g is the glassy compliance at time t=0

D is the retardation compliance

$1/\eta$ is the steady state creep constant.

The response of the Standard Linear Liquid Model to a constant load σ_0 is shown in Fig.3.6.

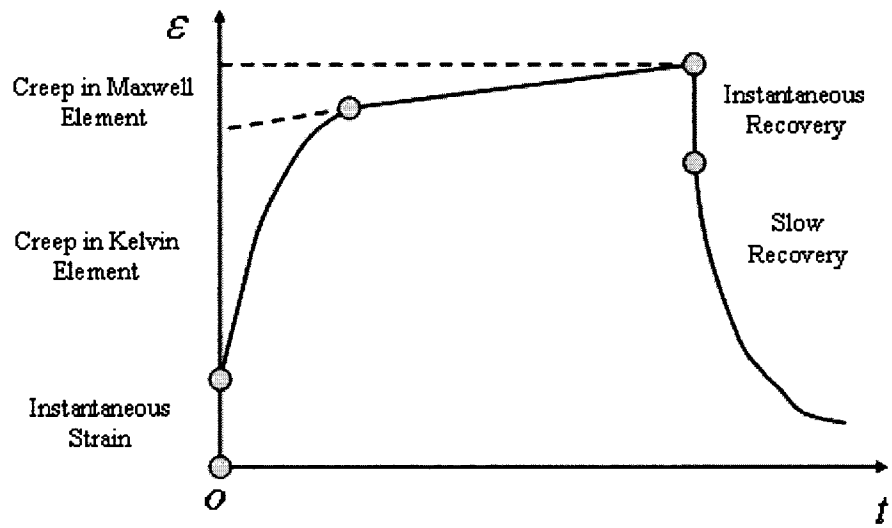

Fig. 3.6 Standard Linear Liquid Model response

When the stress σ_0 is applied, the initial response is identical to that of the Maxwell element, with an instantaneous deformation equal to σ_0 / E_0. The Kelvin element initially has zero deformation. Further, the Kelvin element responds with an exponential time-dependent deformation with a maximum value of σ_0 / E_1. When the Kelvin element has achieved maximum elongation, the Maxwell dashpot continues to

Reproduced with permission of the copyright owner. Further reproduction prohibited without permission.

extend. For long time deformation, the element exhibits viscous flow with the slope simply as σ_0 / η. This is the steady-state creep rate.

3.5 Generalized Maxwell and Kelvin Models

Although the standard four-parameter models may describe the observed material behavior with reasonably good approximation, models with a larger number of mechanical elements are generally required to represent the behavior of most viscoelastic materials [45]. Depending on the strain/stress excitation, the generalized series-parallel models have two forms: the generalized Maxwell Models and the generalized Kelvin Models.

3.5.1 Generalized Maxwell Model

By adding future Maxwell units, in parallel, to the standard four-parameter Maxwell Model, we obtain the generalized Maxwell Model (Fig. 3.7).

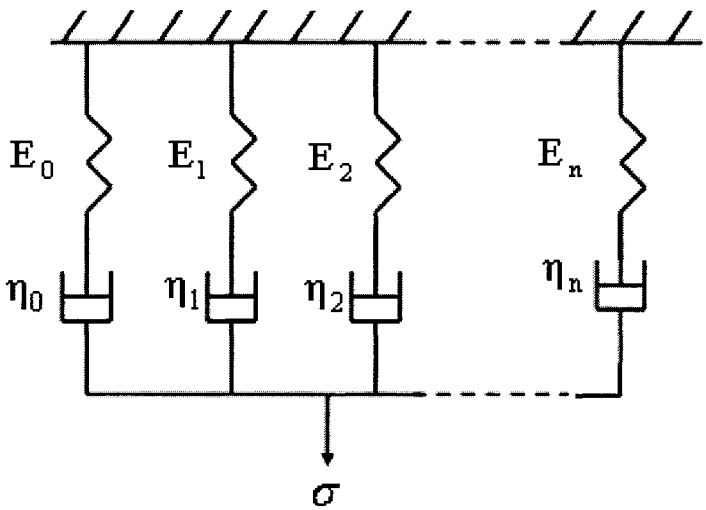

Fig. 3.7 Generalized Maxwell Model describing rheodictic behavior

Reproduced with permission of the copyright owner. Further reproduction prohibited without permission.

This model represents rheodictic behavior, which has no equilibrium modulus. The relaxation modulus for this model is given:

$$E(t) = \sum_n E_n \exp(-\frac{t}{\tau_n}) \tag{3.4}$$

where the summation index n runs from 0 to n. The special case of n = 1 corresponds to the standard four-parameter model. Function $E(t)$ represents a superposition of exponentials, and such a series is known in mathematics as a PRONY series or a Dirichlet series.

When an extra isolated spring has to be added in parallel as shown in Fig. 3.8, the new model can be used to represent arrheodictic behavior.

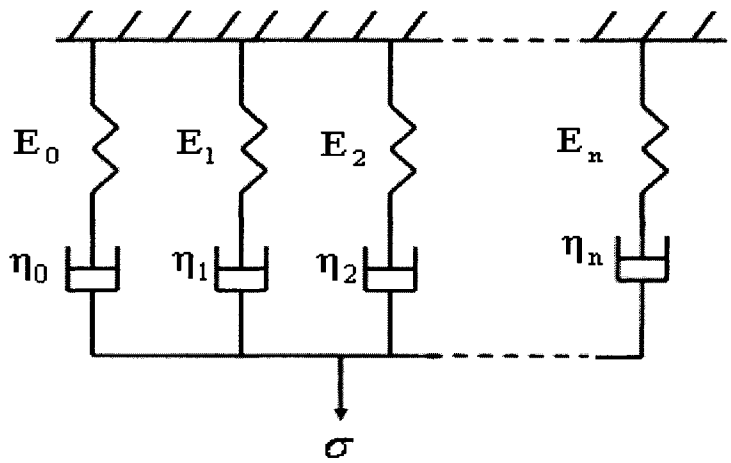

Fig. 3.8 Generalized Maxwell Model describing arrheodictic behavior

The relaxation modulus for the generalized Maxwell Model in terms of the relaxation model is given by

$$E(t) = \{E_e\} + \sum_n E_n \exp(-\frac{t}{\tau_n}) \tag{3.5}$$

where the summation index n runs from 1 to n.

Reproduced with permission of the copyright owner. Further reproduction prohibited without permission.

3.5.2 Generalized Kelvin Model

For the series-parallel models, by proper choice of the numerical values of their parameters, pairs of Maxwell and Kelvin models can respond identically to the same excitation. The models that satisfy this requirement are called conjugate models.

The general rules, also known as Alfrey's rules, for the construction of the conjugate model from a given primitive may be stated as follows [45]:

1. *"The number of elements of each kind (springs and dashpots) must be the same in the conjugate model.*
2. *A parallel combination of two elements of different kinds is replaced by a series combination and vice versa.*
3. *The absence (presence) of an isolated element of one kind requires the presence (or absence) of an isolated element of the other kind in the conjugate model."*

By applying Alfrey's rules to generalized Maxwell Models, their conjugates can be obtained as shown in Figs. 3.9 and 3.10, which are always called as generalized Kelvin models.

Reproduced with permission of the copyright owner. Further reproduction prohibited without permission.

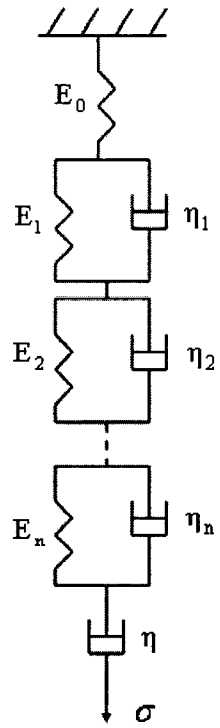

Fig. 3.9 Generalized Kelvin Model describing rheodictic behavior

The retardation compliance of generalized Kelvin Model describing rheodictic is given by:

$$D(t) = D_g + \sum_n D_n\left[1 - \exp(-\frac{t}{\tau_n})\right] + \left\{\frac{t}{\eta}\right\} \qquad (3.6)$$

where the summation index runs from 1 to n.

Reproduced with permission of the copyright owner. Further reproduction prohibited without permission.

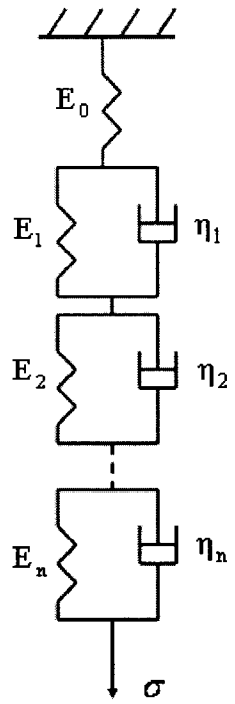

Fig. 3.10 Generalized Kelvin Model describing arrheodictic behavior

The retardation compliance of a generalized Kelvin Model describing arrheodictic is given by:

$$D(t) = D_g + \sum_n D_n \left[1 - \exp(-\frac{t}{\tau_n})\right] \tag{3.7}$$

When the behavior is rheodictic, the sum of the viscosities is then the steady-flow viscosity. When the behavior is arrheodictic, the sum of the viscosities does not represent the steady-flow viscosity.

3.6 Summary

Mechanical models that can be used to represent linear viscoelastic behavior were discussed in this chapter, and the response of these models under both creep and stress relaxation conditions were analyzed. Models which extend the four-parameter series

Reproduced with permission of the copyright owner. Further reproduction prohibited without permission.

parallel model by including a larger number of simple Maxwell and Kelvin units can effectively describe the creep and stress relaxation behavior of polymeric materials.

Reproduced with permission of the copyright owner. Further reproduction prohibited without permission.

CHAPTER FOUR

MATERIAL CHARACTERIZATION TESTING

4.1 Introduction

The major complicating factor that must be considered when evaluating the long-term performance of pipe liners is the time-dependent deformation that accumulates in response to groundwater loading. To estimate this time-dependent behavior and make predictions for future performance, specimens cut from liner materials should be evaluated through laboratory testing. The specimens, apparatus, and the test procedure used for the required material characterization tests are discussed in this chapter. The specimens were tested in flexure based on ASTM D2990-01[1], and procedures for loading and unloading were conducted to simulate seasonal fluctuations in the groundwater.

4.2 Material Testing Assumptions and Methods

Creep testing, including tensile, compressive and flexural testing, is frequently utilized to estimate the long-term properties of polymeric materials. In this study, three-point bending testing was performed on material samples to study the long-term material properties to two PVC materials.

The stresses induced at different points around the circumference of a liner vary from point to point and also vary with time as the contact conditions between the wall of

Reproduced with permission of the copyright owner. Further reproduction prohibited without permission.

the liner and the host pipe evolve. Pipe liners generally deform such that two opposite lobes form, and the radial deflections and stresses in the liner have the largest magnitude at the center of the lobes. At this critical point, the stress is tensile on the inner surface of the liner and compressive at the outer surface of the liner (almost a state of pure flexural stress). The stresses in regions where the liner contacts the host pipe are nearly uniform compression due to compressive hoop stress. It is the flexural stresses associated with the lobes that are most dominant ([26] and [46]). It is important to test a material using a loading configuration that effectively mimics the stresses that lead to structural failure in the field. Thus, flexural testing is used to evaluate the creep-deformation response of the PVC liner materials studied here.

4.3 Test Specimens

The material tested in this research was Polyvinyl Chloride (PVC). Two different 8-inch diameter folded PVC liner materials were provided by the manufacturer: the blue liner in Fig. 4.1 (on the left) with higher compliance, and the white liner with higher stiffness. According to ASTM D790 [47], test specimens for flexural creep measurements shall be rectangular bars. Bars were cut from the PVC liners in the circumferential direction since this direction corresponds to the direction of the flexural stresses induced by groundwater loading in field applications.

Reproduced with permission of the copyright owner. Further reproduction prohibited without permission.

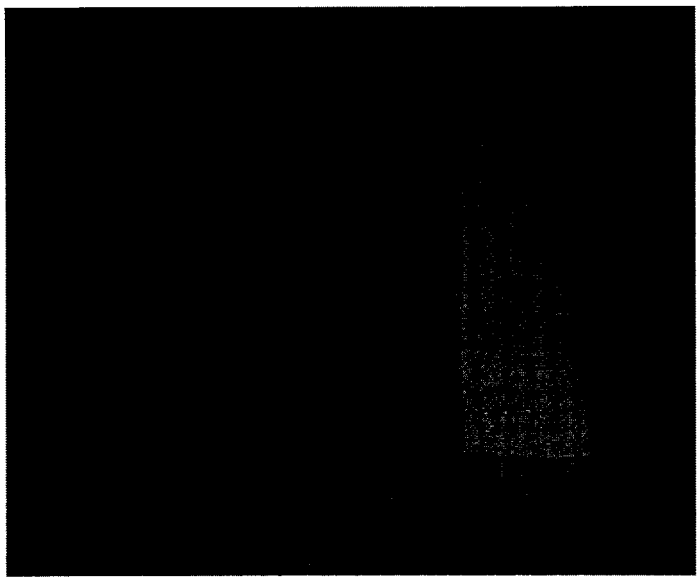

Fig. 4.1 Higher compliance (left) and higher stiffness (right) PVC pipe liner

4.3.1 Specimen Preparation

Before the test began, the pipe liner sample was cut into rectangular pieces approximately 12 inches by 10 inches (longitudinal by circumferential). Since the material was slightly curved, samples were flattened by placing them concave-side down on a steel plate slightly larger than the sample. Another steel plate was placed on top of the sample along with a 20 lb. weight. The assembly was placed in an oven at a temperature 15°C higher than the glass transition temperature of the material. T_H for the higher compliance pipe liner was 100°C (212°F), and T_H for the higher stiffness pipe liner was 105°C (221°F). After the heating, the oven was turned off to allow the samples to cool; the samples were removed from the oven after 24 after hours.

Individual specimens for creep testing were cut from two larger rectangular samples based on the dimensions given in ASTM D790 [47]. The width b was four times of the depth d of specimens, and the support span L for specimens was 16 times of the depth of the specimens, as shown in Fig. 4.2. Ten specimens were cut (along the

Reproduced with permission of the copyright owner. Further reproduction prohibited without permission.

circumferential direction) from the flattened, rectangular sample using a band saw. The specimens were then placed in a jig between parallel steel plates, and the edges of the specimen were cut to their final dimensions using a trim bit on a router. The router-cut edges were smooth and uniform.

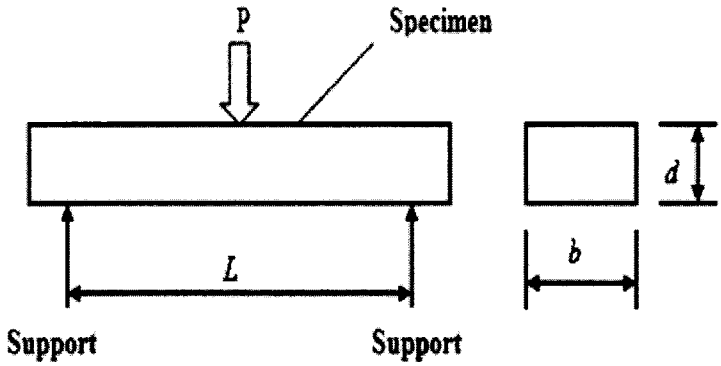

Fig. 4.2 Specimen for bending creep test

4.3.2 Conditioning

The creep compliance of viscoelastic materials is a function of both time and temperature. At a fixed time, a viscoelastic material will display large differences in properties as the temperature changes. To simplify the problem, the varying modulus of elasticity was investigated here by keeping the temperature constant. Also, to reduce the effect of moisture content, the humidity was controlled at a constant level. All of the test specimens were conditioned in an environmental chamber at a temperature of $71 \pm 2^{0}F$ and a relative humidity of 50% for a week prior to testing in accordance with ASTM D2990-01 [1].

Reproduced with permission of the copyright owner. Further reproduction prohibited without permission.

4.4 Testing Apparatus

The testing apparatus utilized to conduct the three-point flexural testing consisted of a bending table, loading stirrups, stainless-steel cable, plastic containers for applying loading, and dial indicator. Two different loading levels were applied to the materials. Since the deflections under very low loads were much smaller than the deflections under the higher loads, dial indicators with two different resolutions were utilized, 0.0001 inches and 0.001 inches, respectively.

4.4.1 Bending Table

As shown in Fig. 4.3, a bending table 88.2 inches long, 24 inches wide, and 36 inches high was used in the creep bending tests. This bending table provides space for testing 20 samples simultaneously. Each specimen was simply supported at both ends on fixed steel rods 0.5 inches in diameter. The span between the rods was set equal to four times the width b of the specimens.

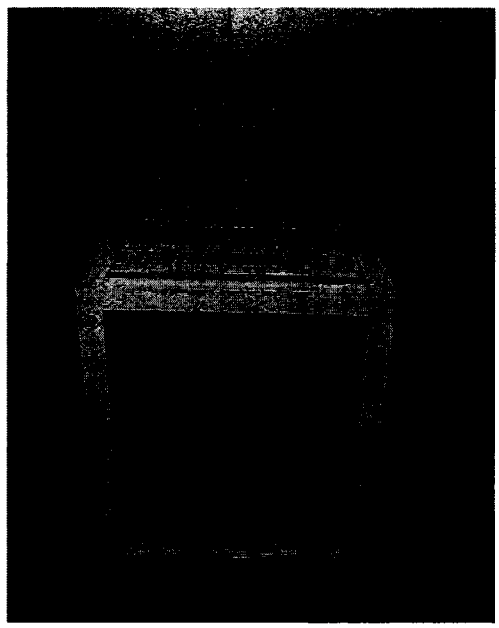

Fig. 4.3 Bending table for three-point bending tests

Reproduced with permission of the copyright owner. Further reproduction prohibited without permission.

4.4.2 Stirrups

Stainless steel stirrups (Fig. 4.4) were fabricated to transfer the load to the specimen from a weighted cable. The stirrups were aligned at the center of the specimens with the axis of the stirrup perpendicular to the axis of the specimen. The diameter of the stirrup was set to 0.375 inches to avoid indentations to the specimen caused by loading (as specified by ASTM D2990-01 [1]. Also to prevent any imbalance in specimen loading (that is, to avoid twisting of the sample about its axis), slots were cut at both ends of the stirrups to provide an opening for the cable to pass through. The stirrup was also specially designed to facilitate the measurement: the top of the stirrup was machined to provide a flat region for the needle of the dial indicator to ride on, thereby reducing the error in reading compared to a round dial indicator/stirrup interface.

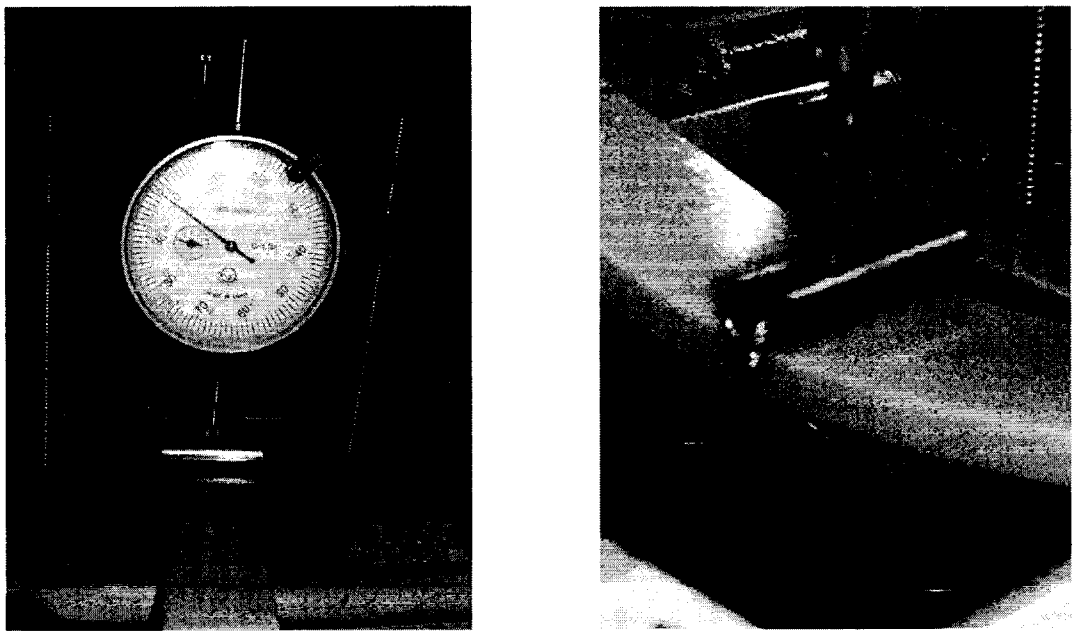

(A) (B)

Fig. 4.4 Stirrup on specimen with cable and dial indicator

Reproduced with permission of the copyright owner. Further reproduction prohibited without permission.

4.4.3 Dial Indicator

Dial indicators with resolutions of 0.001 and 0.0001 inches were utilized to measure the deflection of the specimens at mid-span. The return action of the indicators is forced by a tension spring, allowing the indicator tip to remain in firm contact with the surface to be measured. However, for the three-point flexural testing conducted here, the contact force between the indicator tip and the stirrup would exert a significant amount of "extra" load on the specimen, with the magnitude of this load varying as the plunger extends during specimen deformation (decrease in specimen loading = spring constant * deflection). Consequently, the dial indicator had to be modified by removing the springs, as shown in Fig. 4.5. The force of gravity caused the plunger to remain in contact with the stirrup during testing, eliminating the need for the spring.

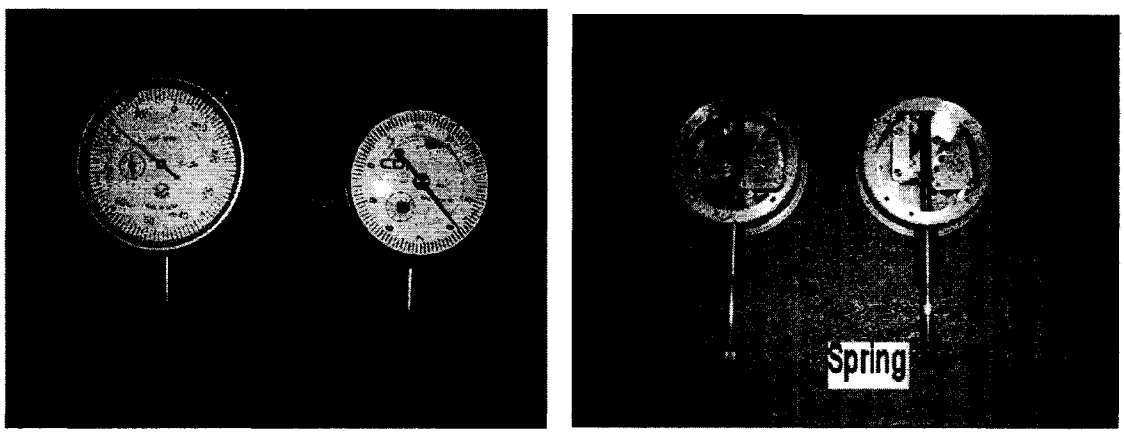

(A) (B)

Fig. 4.5 Dial indicators

After removing the springs from the dial indicators, we found that the dial indicator without the main return spring still exerted an extra force on the specimen due to the gravitational force of the plunger and other built-in spring(s). Since this force also

Reproduced with permission of the copyright owner. Further reproduction prohibited without permission.

affected the creep behavior of the specimens, the magnitude of the force was quantified using a digital balance. Three dial indicators were chosen randomly from each of the two resolutions; five observations were taken for each of the dial indicators with 0.001-inch graduations, and ten observations were taken for each of the dial indicators with 0.0001-inch graduations. The results are listed in Table 4.1. The average extra force exerted on the specimens was 0.047 lb for the dial indicator with 0.001-inch graduations and 0.127 lb for the dial indicator with 0.0001-inch graduations. The weight of the stirrup and cable (0.015 lb) was also considered as a part of the total force in this research.

Table 4.1 Extra force exerted by the dial indicators

0.001 inches graduations	Dial Indicator 1	Dial Indicator 2	Dial Indicator 3
Measurement 1 (Unit: lb)	0.06	0.055	0.055
Measurement 2 (Unit: lb)	0.05	0.04	0.05
Measurement 3 (Unit: lb)	0.05	0.03	0.045
Measurement 4 (Unit: lb)	0.05	0.055	0.045
Measurement 5 (Unit: lb)	0.05	0.025	0.045
Average (Unit: lb)	**0.052**	**0.041**	**0.048**
0.0001 inches graduations	Dial Indicator 1	Dial Indicator 2	Dial Indicator 3
Measurement 1 (Unit: lb)	0.071	0.135	0.125
Measurement 2 (Unit: lb)	0.085	0.17	0.07
Measurement 3 (Unit: lb)	0.06	0.17	0.1
Measurement 4 (Unit: lb)	0.1	0.16	0.14
Measurement 5 (Unit: lb)	0.075	0.135	0.15
Measurement 6 (Unit: lb)	0.01	0.195	0.135
Measurement 7 (Unit: lb)	0.0125	0.17	0.135
Measurement 8 (Unit: lb)	0.09	0.15	0.125
Measurement 9 (Unit: lb)	0.16	0.15	0.075
Measurement 10 (Unit: lb)	0.105	0.245	0.115
Average (Unit: lb)	**0.097**	**0.168**	**0.117**

Reproduced with permission of the copyright owner. Further reproduction prohibited without permission.

4.4.4 Loading System

To study the effect of groundwater level variation on the strain recovery, both loading and unloading procedures were required for the testing. After conditioning, constant loading was applied to each specimen for a period of 2,160 hours, which is roughly equivalent to three months or one season. Next, 50% of the loading applied to the samples was removed to allow the specimens to recover a portion of the accumulated deformation, and specimen deformation was observed for the next 2,160 hours. Then, the loading removed in the previous recovery loading cycle was reapplied to the specimen for another 2,160 hour period. Finally, 50% of the loading was again removed for 2,160 hours to complete the annual load-unload-load-unload cycle associated with seasonal changes in groundwater levels.

To allow for rapid and smooth load changes, two cylindrical plastic containers containing lead weights were connected together with an s-hook, as shown in Fig. 4.6. The total load applied to the specimens was computed by considering the weight of the dial indicator plunger (and springs), the weight of the stirrup, the weight of the cable and connecting hardware, the weight of the plastic containers, and the weight of the lead in the containers. The weight to be removed in the recovery test was placed in the second cylinder and attached to the bottom of the first cylinder as shown. This configuration allowed the second cylinder to be easily unhooked and re-hooked during the recovery and reload testing.

Reproduced with permission of the copyright owner. Further reproduction prohibited without permission.

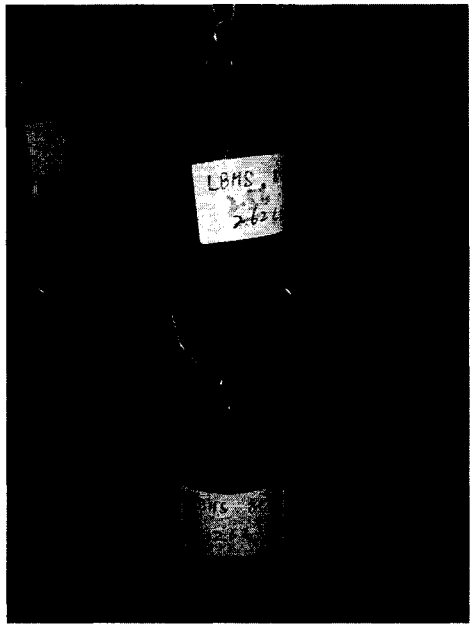

Fig. 4.6 Loading system

4.5 Determination of Specimen Loading

At the center of the lobe on a deflected pipe liner, the stress is tensile on the inner surface of the liner and compressive at the outer surface of the liner. When the flexural stress exceeds the flexural strength or when radial deflections lead to elastic instability, the liner will become unstable and buckle. For a material characterization specimen loaded using a three-point bending configuration, the maximum flexural stress occurs at the midpoint of the specimen at the outer surface (tensile at the bottom). The loading that was applied to each of the specimens was set so that the peak stress at the crown of a pipe liner was roughly equal to the peak stress in a material test specimen.

A two-dimensional, short-term, finite element buckling model of a liner installed in a host pipe with 5% ovality and 0.4% gap was completed to determine the flexural stress at the crown of the higher compliance PVC material. The material properties were selected according to the report provided by the manufacturer: 145,000 psi as the flexural

Reproduced with permission of the copyright owner. Further reproduction prohibited without permission.

modulus for the higher compliance PVC material and 4,100 psi as the flexural strength. Based on the short-term buckling analysis, the critical buckling pressure (P_{cr}) was 65.99 psi for the higher compliance PVC which corresponds to a 152.30-foot water table (far beyond what would be seen in the field). The relationship between the groundwater table and maximum flexural stress for the higher compliance pipe liner is shown in Fig. 4.8. A similar plot was developed for the higher stiffness liner pipe.

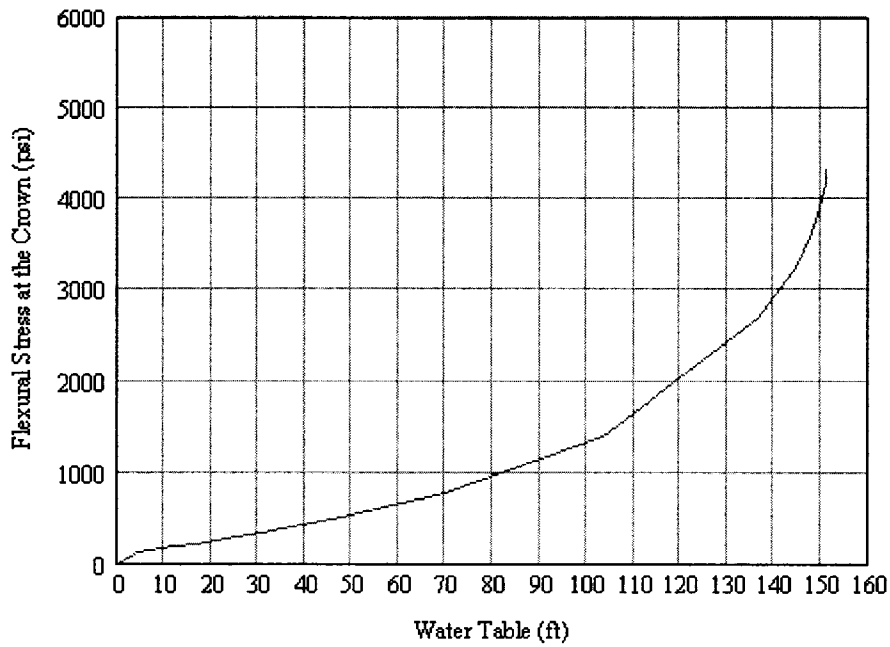

Fig. 4.7 Flexural stress vs. groundwater table

The loading applied to the material characterization specimens was set so that the peak flexural stress (σ_f) at the center of the specimens was approximately equal to 5% and 10% of the flexural strength. For a flexural strength of 4,100 psi for the higher compliance material, 5% and 10% corresponds to 205 psi and 410 psi, respectively. From Fig. 4.7, the corresponding water table heights for these stress levels are 15 and 38 feet, respectively. Although the 38-foot water table would be a very deep installation, the 15

Reproduced with permission of the copyright owner. Further reproduction prohibited without permission.

and 38 feet are within the range of depths that could be encountered in field applications. Thus, the 205 psi and 410 psi target stresses for the higher compliance material characterization specimens are on the high side of the stresses that could be experienced by liners in the field.

After the stress levels were selected, the loads applied to the test specimens can be determined according to ASTM D790 [47]. The peak flexural stress is given as:

$$\sigma_f = 3PL/2bd^2 \tag{4.1}$$

where σ_f is the peak stress in the outer fibers at the midpoint of the specimen, P is the load applied on the specimen, L is the support span, b is the width of the specimen, and d is the depth of the specimen.

For example, for a specimen with L=4 inches (support span), b=1.084 inches (width), and d=0.253 inches (depth), when the peak flexural stress (σ_f) at the center of the specimen for the higher compliance PVC material was set to 205 psi (5% of the flexural strength), then the total load that will be applied to the specimen can be determined as follows:

$$P = \frac{\sigma_f \cdot (2bd^2)}{3L} = \frac{205 \times (2 \times 1.084 \times 0.253^2)}{3 \times 4} = 2.371\, lb \tag{4.2}$$

Thus, applying a load of 2.371 lbs will induce a stress of 205 psi.

Repeating the above calculations for all specimens of the higher compliance and higher stiffness materials and considering the loading and unloading of the specimens results in Table 4.2. Notice that eight specimens were tested for each of the two materials. The table lists the following quantities:

Dia (in) – nominal diameter of the pipe liner

Reproduced with permission of the copyright owner. Further reproduction prohibited without permission.

Spec Thick (in) – thickness of the specimen

Spec Width (in) – width of the specimen

Spec Length (in) – length of the specimen

Yield Strength (psi) – yield strength of the material from manufacturer's data

Percent of Yield Strength – target stress percentage for each flexural specimen

Stress (psi) – the target peak stress in a test specimen

Water Table (ft) – groundwater loading that would produce the peak specimen stress

Weight of Stirrup and Cable (lb) – combined weight of the stirrup and cable

Indicator Force (lb) – force exerted by the dial indicator plunger on the specimen

Total Load (lb) – sum of all applied loads when 100% of loading is applied

Load Removed (%) – the percentage of load removed for recovery testing

Load Remain (lb) – the load remaining during recovery testing (not including stirrup, cable and indicator loads)

Load Removed (lb) – the load removed during recovery testing (50% of Total Load)

Reproduced with permission of the copyright owner. Further reproduction prohibited without permission.

Reproduced with permission of the copyright owner. Further reproduction prohibited without permission.

Table 4.2 Loading table for creep and recovery testing

Spec	Dia (in)	Spec Thick (in)	Spec Width (in)	Spec Length (in)	Yield Strength (psi)	Percent of Yield Strength	Stress (psi)	Water Table (ft)	Weight of Stirrup and Cable (lb)	Indicator Force (lb)	Total Load (lb)	Load Removed (%)	Load Remain (lb)	Load Removed (lb)
LBHC801	8	0.253	1.084	4.000	4100	5%	205.00	15	0.015	0.127	2.371	50	1.043	1.185
LBHC802	8	0.253	1.044	4.000	4100	5%	205.00	15	0.015	0.127	2.283	50	1.000	1.142
LBHC803	8	0.239	1.030	4.000	4100	5%	205.00	15	0.015	0.127	2.010	50	0.863	1.005
LBHC804	8	0.255	1.066	4.000	4100	5%	205.00	15	0.015	0.127	2.368	50	1.042	1.184
LBHC805	8	0.255	0.947	4.000	4100	10%	410.00	38	0.015	0.047	4.208	50	2.042	2.104
LBHC806	8	0.235	1.054	4.000	4100	10%	410.00	38	0.015	0.047	3.977	50	1.927	1.989
LBHC807	8	0.235	0.986	4.000	4100	10%	410.00	38	0.015	0.047	3.721	50	1.798	1.860
LBHC808	8	0.237	0.978	4.000	4100	10%	410.00	38	0.015	0.047	3.754	50	1.815	1.877
LBHS801	8	0.256	1.036	4.000	5000	5%	250.00	18	0.015	0.127	2.829	50	1.272	1.414
LBHS802	8	0.242	1.142	4.000	5000	5%	250.00	18	0.015	0.127	2.787	50	1.251	1.393
LBHS803	8	0.235	1.120	4.000	5000	5%	250.00	18	0.015	0.127	2.577	50	1.147	1.289
LBHS804	8	0.243	1.064	4.000	5000	5%	250.00	18	0.015	0.103	2.618	50	1.167	1.309
LBHS805	8	0.244	1.038	4.000	5000	10%	500.00	41	0.015	0.047	5.150	50	2.513	2.575
LBHS806	8	0.256	1.056	4.000	5000	10%	500.00	41	0.015	0.047	5.767	50	2.822	2.884
LBHS807	8	0.243	1.060	4.000	5000	10%	500.00	41	0.015	0.047	5.216	50	2.546	2.608
LBHS808	8	0.247	1.048	4.000	5000	10%	500.00	41	0.015	0.047	5.328	50	2.602	2.664

- LBHC stands for long term bending test for higher compliance PVC
- LBHS stands for long term bending test for higher stiffness PVC

4.6 Testing Procedure

Fig. 4.8 shows the experimental setup with the 16 loaded specimens. To simulate the seasonal fluctuations in groundwater over one year, the loading on the specimens was divided into four loading periods for a total test time of 8,640 hours. All tests were conducted in an environmental chamber at a temperature of $71 \pm 2^{0}F$ and a relative humidity of 50%.

Fig. 4.8 Creep test on PVC pipe liner materials

4.6.1 Testing Procedure for Loading (Creep)

The loading tests were first performed on the specimens for 2,160 hours. Creep deformation was measured to the nearest 0.0001 inches for the specimens subjected to the lower stress level (5% of the flexural strength) and to the nearest 0.001 inches for the specimens subjected to the higher stress level (10% of the flexural strength. Test readings were taken after approximately 1, 6, 12, 30 minutes and 1, 2, 3, 5, 10, 20, 50, 100, 200,

Reproduced with permission of the copyright owner. Further reproduction prohibited without permission.

500, 700, and 1,000 hours. The actual time of measurement varied somewhat from these values, and additional data was taken in many cases as the tests were monitored; for example, the tests were monitored every few days between 700 and 1,000 hours, and data was taken in-between these times to make sure there were no problems. The measurement was based on ASTM Standard Practice for Testing Stress-Relaxation of Plastics [1].

4.6.2 Testing Procedure for Partial Unloading (Strain Recovery)

After the initial loading, 50% of the loading was removed to allow the specimens to recover from the accumulated deformation, and specimen deformation was observed for the next 2,160 hours. The load was removed from the loading system carefully to avoid disturbing the specimen. Recovery measurement was approximately taken after 1, 6, 12, 30 minutes; 1, 2, 3, 5, 10, 20, 50, 100, 200, 500, 700, and 1,000 hours. These measurements were also based on ASTM D2990 [1].

4.6.3 Testing Procedure for Reloading

When the recovery tests were completed, the loading removed in the previous recovery loading cycle was reapplied to the specimen for another 2,160 hour period. The load was added carefully when reloading (smoothly to prevent specimen movement and bounce). The same reading schedules were taken for the creep deformation after reloading, and the measurement was also based on ASTM D2990 [1].

4.6.4 Testing Procedure for Reunloading

Finally, 50% of the loading was again removed for 2,160 hours to complete the annual load-unload-load-unload cycle associated with seasonal changes in groundwater

Reproduced with permission of the copyright owner. Further reproduction prohibited without permission.

levels. The same reading schedules were taken for the recovery deformation after reunloading, and the measurement was also based on ASTM D2990 [1].

4.7 Summary

The specimens, apparatus, and the test procedures for the creep and strain recovery tests on the PVC material were discussed in this chapter. Both the higher compliance PVC material and the higher stiffness PVC material were evaluated in the tests; eight specimens were tested for each of the two materials. The specimens were constructed based on the dimensions recommended in ASTM D790 [47]. The loads applied were small to focus on the behavior of the material at stress levels that are anticipated in field applications; even so, the applied loading was still on the high side of what would be expected in the field, since 15 feet of water table would be a significant water table depth in the field (and 38 feet would be a very high depth below the water table). There is a compromise to be made since very low loads (such as 2% of the yield strength) would be more typical of field conditions, but these very low loads are not large enough to produce significant deformations for creep testing using the dial indicators employed in this research. However, it is important to use stress levels that are as small as possible since the materials often show a nonlinear increase in deformation rates with increasing loads (doubling the load more than doubles the strain rate).

Loading and unloading procedures were used to simulate seasonal groundwater variations. The specimens were first tested 2,160 hours at full load followed by partial unloading (50% of the load was removed) for another 2,160 hours. Another two similar load and partial unload procedures were carried out to complete the annual load-unload-load-unload cycle associated with seasonal changes in groundwater levels.

Reproduced with permission of the copyright owner. Further reproduction prohibited without permission.

CHAPTER FIVE

ANALYSIS OF MATERIAL TESTING RESULTS

5.1 Introduction

In this chapter, the material parameters associated with the constitutive relations presented in Chapter 3 are determined for the two PVC materials. The data obtained from the creep and recovery tests described in Chapter 4 were fit using a linear viscoelastic material model, and the retardation times and the compliance constants were determined. Since the ABAQUS© finite element software package represents viscoelastic behavior using relaxation terms, an efficient and accurate numerical method of interconversion from a retardation function to a relaxation function was employed based on the integral relationship between these two functions.

5.2 Fitting of Experimental Data

Data fitting is a useful method to determine the numerical values of parameters that best characterize the relationship between the test data points and an underlying mathematical model. Several fitting methods including Procedure X [48], collocation [49], and the Multidata Method [50] were developed to quantify the parameters of the viscoelastic models. In this study, the multiple linear regression approach based on the least squares method was used to fit the data.

Reproduced with permission of the copyright owner. Further reproduction prohibited without permission.

5.2.1 Fitting Function

To understand the deformation behavior of PVC liners under seasonal groundwater loading, the strain response of the material under varying loading conditions should be evaluated. Plots of strain versus time for the load variation described in Chapter 4 are given in Appendix A for each of the two PVC materials at each of the two load levels. The linear viscoelastic material model used to fit the data is the generalized Kelvin model, which is useful when the excitation is a stress.

$$D(t) = D_g + \sum_n D_n \left[1 - \exp(-\frac{t}{\tau_n}) \right] + \phi \cdot t \qquad (5.1)$$

where, D_g is glassy compliance

D_n's are retardation compliance constants

τ_n's are retardation times

$\phi = 1/\eta$, and η is coefficient of long-time viscosity

Here, the summation index n varies from 1 to N, where n is the number of units in the generalized Kelvin model.

To simulate the seasonal groundwater changes in one year, there are four test periods: loading, unloading, reloading, re-unloading. A step function generated is shown in Fig. 5.1 for a 50% variation in load and a 3 month time variation.

Reproduced with permission of the copyright owner. Further reproduction prohibited without permission.

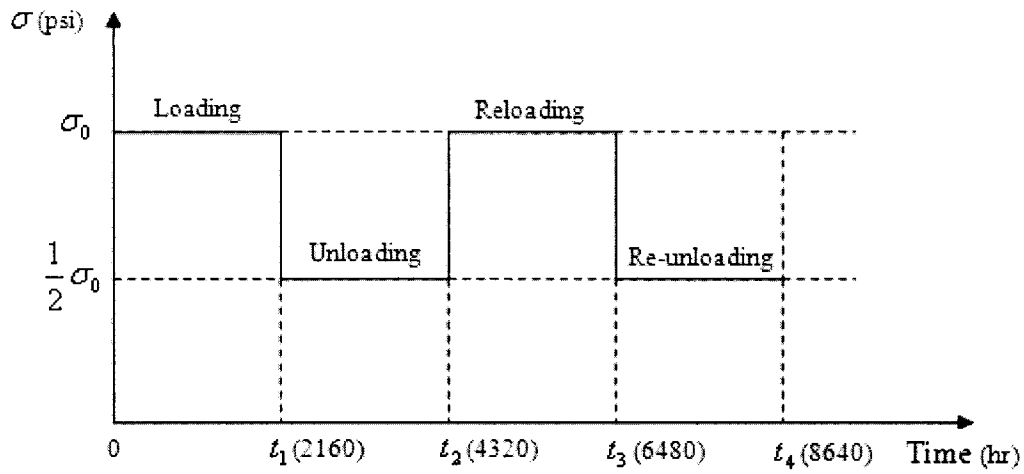

Fig. 5.1 Loading history on material test specimens

For the first time period ($0 \le t \le t_1$), the loading period, a constant stress level σ_0 was applied on a specimen and the strain response at this period can be obtained directly from (5.1) as

$$\varepsilon_1(t) = \sigma_0 \cdot D(t) \quad (0 \le t \le t_1) \tag{5.2}$$

For the second time period ($t_1 \le t \le t_2$), the unloading period, half of the original stress was removed from the specimen at time t_1, and the recovery strain of the generalized Kelvin Model can be considered as a negative strain resulting from a negative stress, $-(1/2)\sigma_0$.

$$\varepsilon^r(t) = -\frac{1}{2}\sigma_0 \cdot D(t - t_1) \quad (t_1 \le t \le t_2) \tag{5.3}$$

The total strain $\varepsilon_2(t)$ for the unloading period, using the superposition principle, should be the sum of the strain resulting from the original stress σ_1 and the recovery strain resulting from the stress removed.

$$\varepsilon_2(t) = \sigma_0 \cdot D(t) - \frac{1}{2}\sigma_0 \cdot D(t - t_1) \qquad (t_1 \le t \le t_2) \tag{5.4}$$

Reproduced with permission of the copyright owner. Further reproduction prohibited without permission.

For the third time period ($t_2 \le t \le t_3$), the reloading period, the stress level returns back to the original level. Using the superposition principle again, the total strain $\varepsilon_3(t)$ can be given as,

$$\varepsilon_3(t) = \sigma_0 D(t) - \frac{\sigma_0}{2} D(t-t_1) + \frac{\sigma_0}{2} D(t-t_2) \quad (t_2 \le t \le t_3) \tag{5.5}$$

For the last time period ($t_3 \le t \le t_4$), the re-unloading period, half of original stress was removed again from the specimen at time t_3. The total strain $\varepsilon_4(t)$ can be computed as

$$\varepsilon_4(t) = \sigma_0 D(t) - \frac{\sigma_0}{2} D(t-t_1) + \frac{\sigma_0}{2} D(t-t_2) - \frac{\sigma_0}{2} D(t-t_3) \quad (t_3 \le t \le t_4) \tag{5.6}$$

5.2.2 Retardation Times

It is difficult to determine two sets of constants, coefficients (D_n) and retardation times (τ_n), in Eq. 5.1 simultaneously (12 constants in all). By assuming the set of relaxation times (τ_n), the unknowns were reduced to the linear coefficients (D_n) and ϕ, thereby avoiding the difficulty of determining 12 unknowns. A method has been suggested by Schapery [49] to find the relaxation times by relating τ_n to the times (t_n).

$$\tau_n = a \cdot t_n \tag{5.7}$$

where a is a proportionality constant to be determined. Generally, it is satisfactory to choose a=1.443 [45]. Experimental observations on linear viscoelastic materials are usually made at time intervals which are equally spaced on a logarithmic scale. Therefore,

$$t_n = 10^{n+b} \tag{5.8}$$

where the determination of b is described below. So Eq.5.7 now becomes

Reproduced with permission of the copyright owner. Further reproduction prohibited without permission.

$$\tau_n = a \cdot 10^{n+b} \tag{5.9}$$

The readings for the experimental data were taken at regular intervals, immediately after the load was applied, and the first reading was taken at about 0.01 hour. Since b marks the beginning of the time scale in Eq. 5.6, we shall choose b = -2 for n = 0 (since n = 0 when the readings first start), and Eq. 5.8 and Eq. 5.9 now become

$$t_n = 10^{n-2} \tag{5.10}$$

and

$$\tau_n = a \cdot 10^{n-2} \tag{5.11}$$

The value of n can be chosen depending on the available data. The creep tests were conducted up to 8,160 hours ($t_n \approx 10^4$), giving an upper bound of n = 6. Therefore, n can be chosen from 1 to 6 (since n – 2 = 6 – 2 = 4). The accuracy of the model is related to the number of terms in the summation index [45], and here, it was determined that a material model with five Kelvin units in series as shown in Fig. 5.2 is accurate enough to fit the experimental data. Thus, n = 5 for this research.

Reproduced with permission of the copyright owner. Further reproduction prohibited without permission.

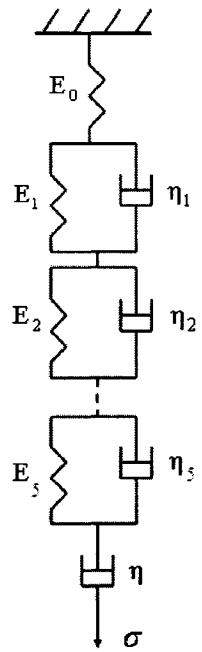

Fig. 5.2 Generalized Kelvin Model (5 Kelvin units)

5.2.3 Multiple Linear Regression Model

After specifying the retardation times, the unknowns in each strain response function can be reduced to the seven unknown parameters $\{D_0, D_1 \cdots D_4, D_5, \phi\}$. And, comparing all of these strain response functions, it was easy to find that each function can be rewritten as a linear function of the unknown parameters. Therefore, a multilinear regression analysis was performed in this study to determine the unknown parameters. The multiple linear regression model is given by

$$y = D_0 + D_1 x_1 + \cdots + D_4 x_4 + D_5 x_5 + \phi \cdot x_6 \tag{5.12}$$

where $y = \varepsilon(t)/\sigma_0$ and x_n is a function of time (for example, $x_n = 1 - \exp(-\frac{t}{\tau_n})$ for the first five items, and $x_6 = t$ when $0 \le t \le t_1$).

Reproduced with permission of the copyright owner. Further reproduction prohibited without permission.

5.2.4 Determination of Retardation Constants

The software package SAS® V8 [51] was used to fit the constants for the material model using the multiple linear regression analysis based on the data given in Appendix A. Deflection values were recorded at a number of times that have not been included in Appendix A for conciseness. However, the average of all of the data collected for each material at each stress and time was utilized for fitting the material parameters. The plots showing material behavior that are included in Appendix A include all of the data points collected. The tabular data in Appendix A was included to preserve a written record of the collected data that describes the overall creep-recovery behavior of the materials.

For each material, four separate fits were completed. For the first loading cycle where $0 \le t \le t_1$, Eq. 5.2 was used to determine the seven unknown parameters $\{D_0, D_1 \cdots D_4, D_5, \phi\}$ using the assumed values for τ_n as described earlier. The fitting process was repeated for the first unloading cycle based on Eq. 5.4 for $t_1 \le t \le t_2$, resulting in another set of seven parameters. The process was repeated for each of the two remaining loading cycles ($t_2 \le t \le t_3$ using Eq. 5.5 and $t_3 \le t \le t_4$ using Eq. 5.6) to determine two more sets of seven constants. At this point, a total of four sets of seven constants had been determined for a single material (such as the higher compliance PVC at 205 psi). The constants were plugged into the material model of Eq. 5.1, and using Eqs. 5.2, 5.4, 5.5 and 5.6, the material model was plotted over the experimental data. The four different constant sets were each used separately and compared to the experimental data, and the constant set which best fit the data was selected by observation to describe

Reproduced with permission of the copyright owner. Further reproduction prohibited without permission.

the material. The constants resulting in the best fit for each material are given in Table 5.1, and the curves for each material are given in Figs. 5.3 – 5.6.

Table 5.1 Compliance constants for generalized Voigt model

Parameter	HC Specimens (at 205 psi)	HC Specimens (at 410 psi)	HS Specimens (at 250 psi)	HS Specimens (at 500 psi)
D_0	6.10E-6	7.73E-6	5.610E-6	5.280E-6
D_1	1.15E-6	1.43E-6	6.310E-7	7.510E-7
D_2	2.03E-6	4.276E-7	4.053E-7	1.020E-7
D_3	4.556E-7	1.59E-6	5.118E-7	6.875E-7
D_4	1.99E-6	1.44E-6	9.426E-7	5.173E-7
D_5	4.65E-6	5.38E-6	2.360E-6	2.500E-6
$\phi = 1/\eta$	1.813E-12	3.622E-12	1.807E-12	1.827E-12
τ_1	0.1443	0.1443	0.1443	0.1443
τ_2	1.443	1.443	1.443	1.443
τ_3	14.43	14.43	14.43	14.43
τ_4	144.3	144.3	144.3	144.3
τ_5	1443	1443	1443	1443

Reproduced with permission of the copyright owner. Further reproduction prohibited without permission.

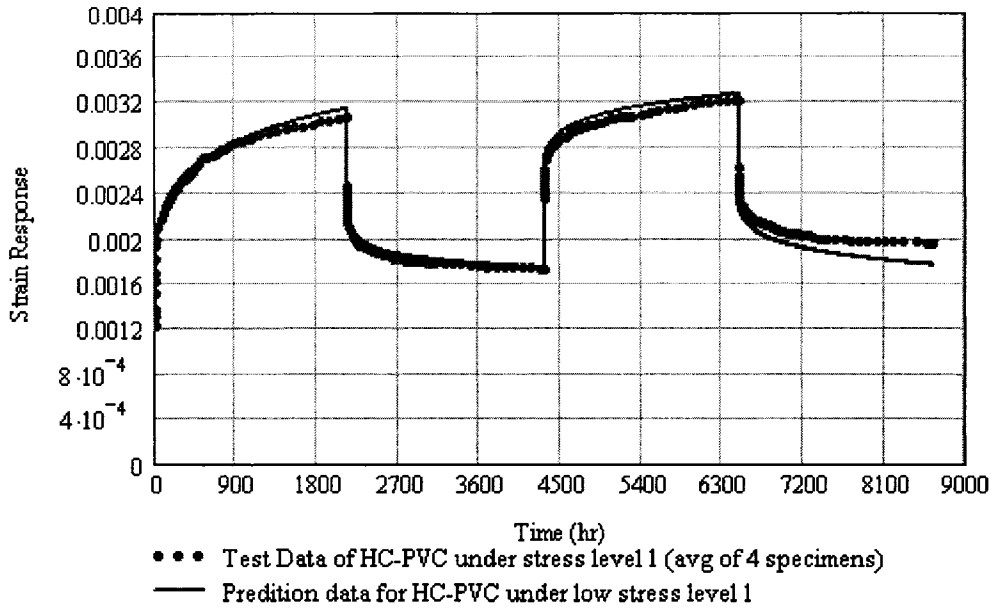

Fig. 5.3 Strain vs. time for HC-PVC under stress level 1 (205 psi), curve fit generated using constants from table 5.1

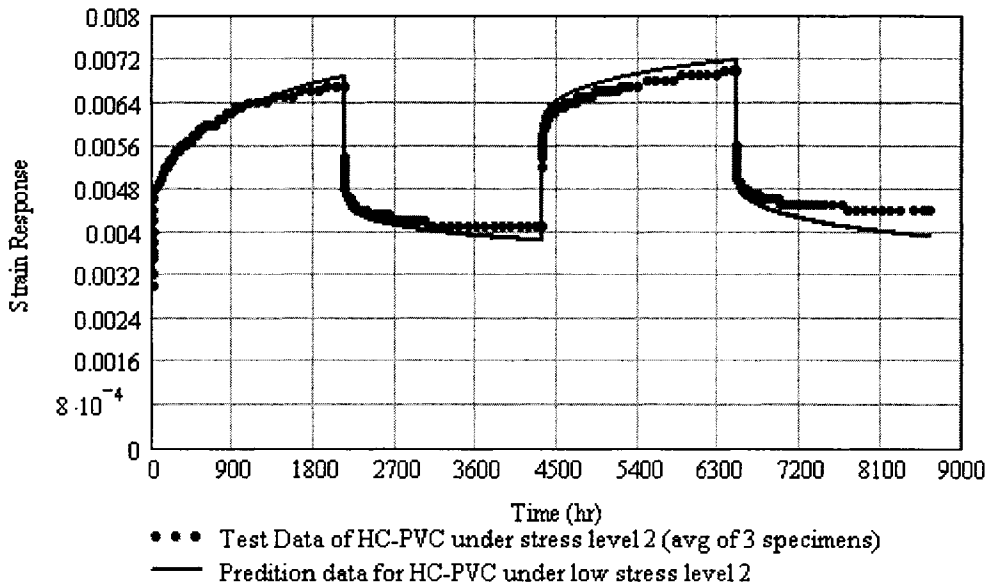

Fig. 5.4 Strain vs. time for HC-PVC under stress level 2 (410 psi), curve fit generated using constants from table 5.1

Reproduced with permission of the copyright owner. Further reproduction prohibited without permission.

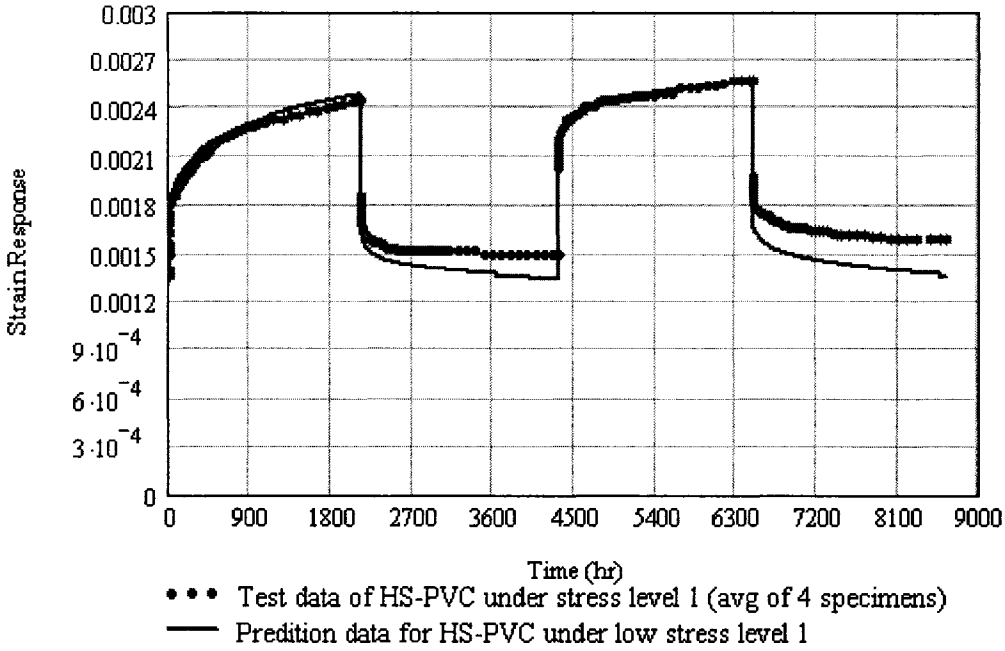

Fig. 5.5 Strain vs. time for HS-PVC under stress level 1 (250 psi), curve fit generated using constants from table 5.1

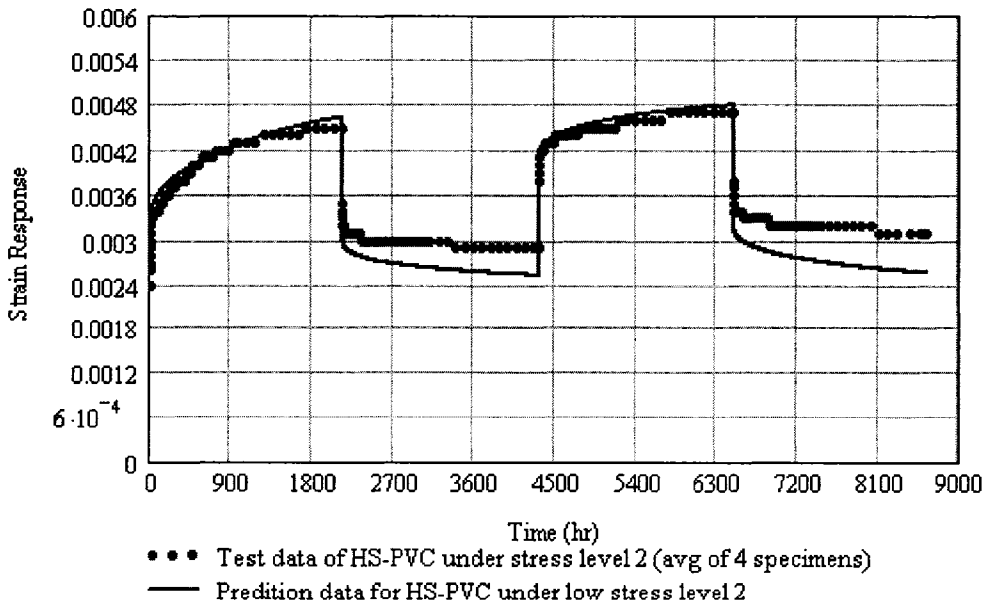

Fig. 5.6 Strain vs. time for HS-PVC under stress level 2 (500 psi), curve fit generated using constants from table 5.1

Reproduced with permission of the copyright owner. Further reproduction prohibited without permission.

From Figs. 5.3-5.6, it may be noted that there is good agreement for the creep and recovery tests. Since the stresses expected in the field will be closer to the stresses experienced at the lower stress levels (5% of the flexural strength), the material constants obtained for these lower stress levels will be utilized throughout the remainder of this work. If the material parameters for the lower stress level are used to model the response of the material at the higher stress level, we obtain the plot shown in Fig. 5.7. Notice that the constants do follow the general trend of the data, but not as well as the constants specifically determined for that stress level (as expected). The material model lies a little below the experimental data, indicating that the material is showing some degree of nonlinear viscoelasticity. This reinforces the need to use material characterization data collected at stress levels that match the conditions that are expected in field applications.

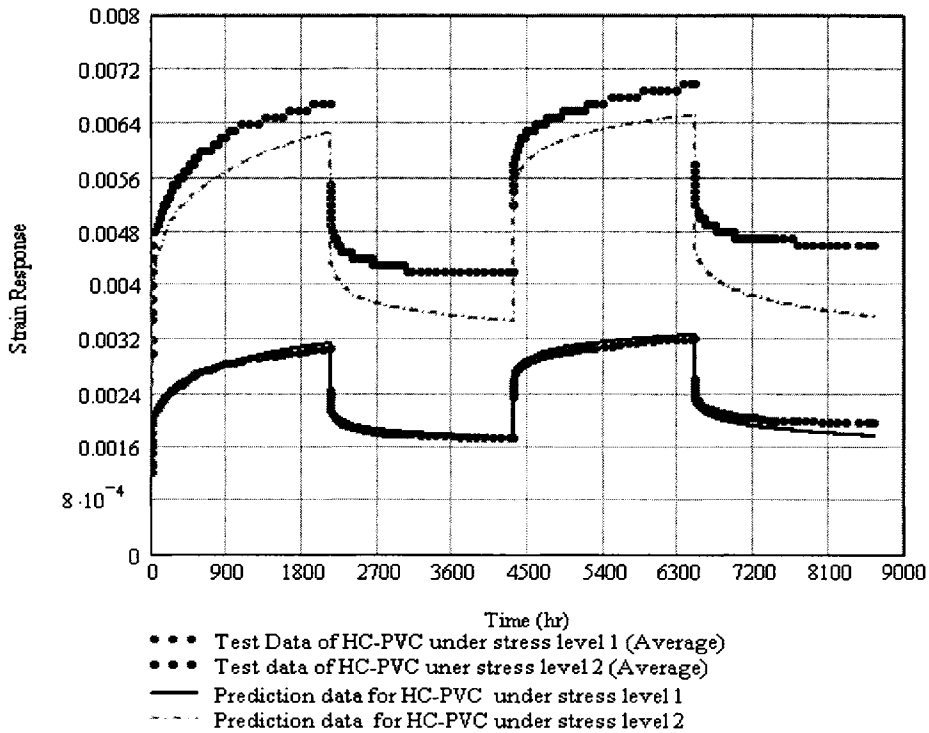

Fig. 5.7 Strain vs. time for HC-PVC under stress level 1 (205 psi) and stress level 2 (410psi), curve fit generated using constants from table 5.1

Reproduced with permission of the copyright owner. Further reproduction prohibited without permission.

5.3 Numerical Interconversion

Interconversion between the relaxation modulus and the creep compliance is sometimes required to allow the results of experimental measurements to be embedded into simulation models. The mathematical interrelationships of the interconversion process have long been studied. Hopkings and Hamming [52] proposed a numerical interconversion method based on the integral relationship, and their method was later improved by Knoff and Hopkings [53]. Baumgaertel and Winter [54] presented an analytical conversion method using the Laplace transform and the PRONY series. To overcome the problem of negative coefficients that may occur during interconversion, Bradshaw and Brinson [55] developed a sign control method for material function fitting and interconversion to force the signs of the PRONY series coefficients to be positive. Schapery and Park [56] proposed a numerical interconversion method also based on the PRONY series.

The ABAQUS© finite element software provides a model where viscoelastic material behavior can be represented by stress relaxation terms (e.g., using a PRONY series). However, the determination of the constants in a PRONY series requires that stress relaxation be monitored over time for constant strain material characterization testing. However, since pipe liners are often subjected to either fixed loading or to loading that changes on a periodic basis, testing of material response through load-controlled tests are more appropriate for the liner design problem. Consequently, creep compliance testing of the liner materials was completed (as summarized earlier and in Appendix A). Thus, it is necessary here to convert the retardation constants of the generalized Kelvin Model to relaxation constants (or PRONY series) that describe the

Reproduced with permission of the copyright owner. Further reproduction prohibited without permission.

generalized Maxwell Model so that the response of pipe liners can be simulated using ABAQUS©.

The generalized Maxwell Model consists of a spring and m Maxwell units connected in parallel, and is given by

$$E(t) = E_e + \sum E_m \exp(-\frac{t}{\rho_m}) \tag{5.13}$$

where E_e - The equilibrium modulus ($E_e = 0$ for viscoelastic liquids)

E_m - Relaxation constants

ρ_m - Relaxation times (all positive constants).

Here, the classic short-term or Young's modulus would be $E = E_e + \sum E_m$.

Having a basic understanding of linear differential and integral equations, the interrelationships between the linear viscoelastic models can be represented in standard mathematical forms which are mathematically equivalent for each mode of loading [56]. So, the generalized Kelvin Model (source function) can be converted to the generalized Maxwell Model (target function).

The uni-axial, non-aging isothermal stress-strain equation for a linear viscoelastic material can be represented by the Boltmann Superposition Integral [57]

$$\sigma(t) = \int_0 E(t-\tau)\frac{d\varepsilon(\tau)}{d\tau}d\tau \tag{5.14}$$

From Eq. 5.14, the relaxation modulus and creep compliance for a viscoelastic material can be represented as [57]

$$\int_0 E(t-\tau)\frac{dD(\tau)}{d\tau}d\tau = 1 \quad (t > 0) \tag{5.15}$$

Reproduced with permission of the copyright owner. Further reproduction prohibited without permission.

This equation can be reconciled intuitively by understanding that for a simple spring the stiffness E is the inverse of the compliance D, such that the product of E times D is 1; this relationship can be extended to time-dependent material behavior using Eq. 5.15. This integral equation can be used to determine the relaxation modulus from the known creep compliances (which were determined in Section 3.5).

While the material functions defined by Eqs. 5.1 and 5.13 are in the time domain, the corresponding functions in the Laplace transform domain can be easily obtained in terms of the constants in Eqs. 5.1 and 5.13 as [57]

$$\widetilde{D}(s) \equiv s\int_0^\infty D(t)\exp(-st)dt = D_g + \sum_{j=1}^{n}\frac{D_j}{s\tau_j + 1} + \frac{1}{\eta s} \tag{5.16}$$

and

$$\widetilde{E}(s) \equiv s\int_0^\infty E(t)\exp(-st)dt = E_e + \sum_{i=1}^{m}\frac{s\rho_i E_i}{s\rho_i + 1} \tag{5.17}$$

The s multiplied Laplace transform is often called Carson transform. From Eq. 5.13 to Eq. 5.15, one can obtain the following relationship between the two Carson transform functions.

$$\widetilde{E}(s)\widetilde{D}(s) = 1 \tag{5.18}$$

When one set of constants, either $\{D_g, D_j(j=1,\ldots,n), \tau_j, and\ \eta\}$ or $\{E_e, E_i(i=1,\ldots,m), and\ \rho_i\}$ is known, the other set of constants can be determined from a mathematical interrelationship between the modulus and compliance functions. In this research, a set of constants $\{D_g, D_j(j=1,\ldots,n), \tau_j, and\ \eta\}$ has already been obtained, and the other set $\{E_e, E_i(i=1,\ldots,m), and\ \rho_i\}$ will be found. It is noted that if $E_e = 0$ for the

Reproduced with permission of the copyright owner. Further reproduction prohibited without permission.

viscoelastic fluid model, then the problem of interconversion reduces to solving the following system of linear algebraic equations for E_m:

$$A_{ki}E_i = B_k \quad (summed\ on\ i;\ i = 1,\ldots,m;\ k = 1,\ldots,p) \tag{5.19}$$

where $$A_{ki} = \left(D_g + \sum_{j=1}^{n} \frac{D_j}{s_k\tau_j + 1} + \frac{1}{\eta s_k} \right)\left(\frac{s_k\rho_i}{s_k\rho_i + 1} \right) \quad (i = 1,\ldots,m;\ k = 1,\ldots,p) \tag{5.20}$$

$$B_k = 1 \tag{5.21}$$

The symbol s_k ($k = 1,\ldots,p$) denotes a discrete value of the transform variable at which the interrelationship is satisfied, and its selection is analogous to that of t_k except that $s_k = 1/t_k$. Relaxation time constants ρ_i ($i = 1,\ldots,m$) were numerically determined by taking the negative reciprocal of the solutions of equation $\tilde{D}(s) = 0$ ($s < 0$).

The values of E_i calculated from Eq. 5.19 for five Kelvin units in series with a Maxwell unit are given in Table 5.2. An expanded analysis of this procedure showing the process of interconversion in detail for the HC specimens at 205 psi is provided in Appendix B.

Reproduced with permission of the copyright owner. Further reproduction prohibited without permission.

Table 5.2 Relaxation modulus for generalized Kelvin model

Parameter	HC Specimens (at 205 psi)	HS Specimens (at 250 psi)
E_1	2.716E+4	1.664E+4
E_2	2.937E+4	1.166E+4
E_3	4.735E+3	8.9165E+3
E_4	1.846E+4	1.889E+4
E_5	2.292E+4	2.518E+4
E_6	6.101E+4	9.606E+4
ρ_1	0.121	0.13
ρ_2	1.131	1.355
ρ_3	13.776	13.453
ρ_4	117.119	127.013
ρ_5	1.038E+3	1.118E+3
ρ_6	9.029E+6	5.71E+6

For convenience, Eq. 5.13 can be written as

$$E(t) = E_0\left[1 - \sum_n g_n(1 - \exp(\frac{-t}{\tau_n}))\right] \tag{5.22}$$

where

$$E_0 = E_e + \sum_n E_n \tag{5.23}$$

and

$$g_n = \frac{G_n}{G_0} \tag{5.24}$$

Reproduced with permission of the copyright owner. Further reproduction prohibited without permission.

The relaxation constants listed in Table 5.2 can be rewritten in terms of g_n and ρ_n, as listed in Table 5.3. This is important since the constants as given in Table 5.3 are required later for the ABAQUS© finite element simulations.

Table 5.3 Relaxation modulus for generalized Kelvin Model in terms of g_n and ρ_n

Parameter	HC Specimens (at 205 psi)	HS Specimens (at 250 psi)
g_1	0.1658	0.0937
g_2	0.1793	0.0657
g_3	0.0289	0.0502
g_4	0.1127	0.1058
g_5	0.1399	0.1418
g_6	0.3724	0.5409
ρ_1	0.121	0.13
ρ_2	1.131	1.355
ρ_3	13.776	13.453
ρ_4	117.119	127.013
ρ_5	1.038E+3	1.118E+3
ρ_6	9.029E+6	5.71E+6

Reproduced with permission of the copyright owner. Further reproduction prohibited without permission.

The constants, g_n and ρ_n, can be input into ABAQUS© as material properties with using keyword "VISCOELASTIC, time=PRONY" when performing the liner buckling simulations.

5.4 Single Element Model Verification

In ABAQUS©, a single continuum plane strain element, "CPE4", was used to simulate the PVC material properties under the test loading conditions. The material properties obtained from the tests were embedded into ABAQUS© as a PRONY series. The command "VISCOELASTIC, time =PRONY" was applied and the material constants were entered into ABAQUS© (see Appendix C for the input file). The displacements at the bottom of the element were simply supported as shown in Fig. 5.8. Time-varying loading was applied using the LOAD OP =AMPLITUDE command and the variation of the loading with time is also shown in Fig. 5.9. The axial strain versus time for the single-element simulation is shown in Fig. 5.10 for a time period of one year. It can be seen that the curves generated in ABAQUS© agree well with the test data; comparing Fig. 5.10 to Fig. 5.3 shows that the ABAQUS© response follows the same trend as the compliance model, indicating that the interconversion of constants was successful.

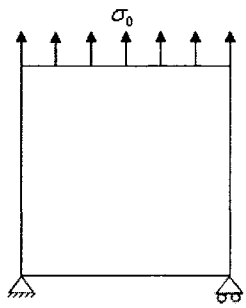

Fig. 5.8 Single element model used for verification

Reproduced with permission of the copyright owner. Further reproduction prohibited without permission.

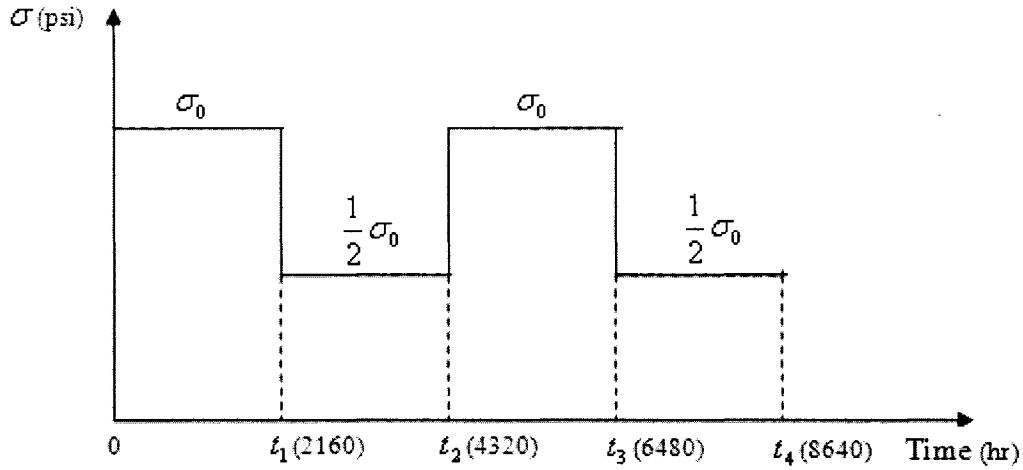

Fig. 5.9 Time dependent loading applied to the single element model

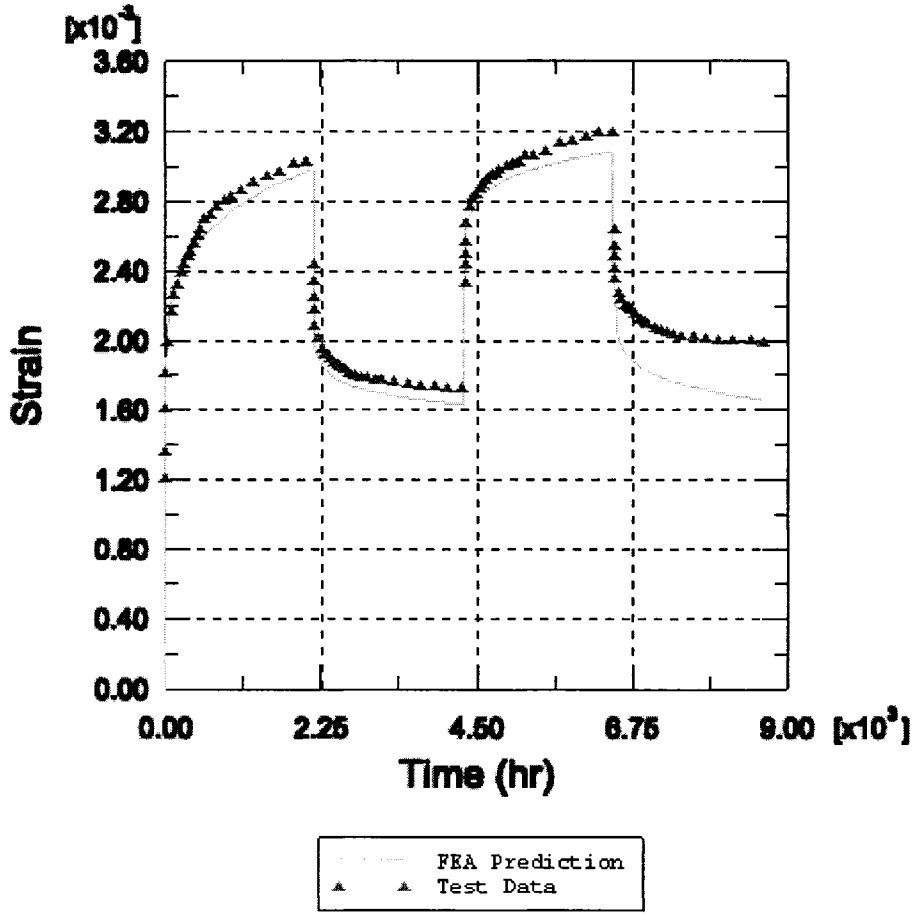

Fig 5.10 Plot of axial strain from single element FEA model for HC PVC material constants from table 5.2 were used

Reproduced with permission of the copyright owner. Further reproduction prohibited without permission.

5.5 Summary

Material constants for the generalized Kelvin and generalized Maxwell Models were determined for the material characterization data presented in Appendix A. The retardation constants determined for the Kelvin Model were subjected to an interconversion procedure to determine relaxation terms that could be embedded into the PRONY series material model in the ABAQUS© finite element package. A single element ABAQUS© model confirmed that the PRONY series material model which will be utilized in Chapter 6 to simulate liner collapse can be used to accurately model the behavior of the linear viscoelastic PVC materials studied in this work.

Reproduced with permission of the copyright owner. Further reproduction prohibited without permission.

CHAPTER SIX

FINITE ELEMENT MODELING

6.1 Introduction

It is expensive and very time consuming to evaluate the long-term behavior of constrained liners using laboratory testing. Moreover, the wide scatter inherent in the buckling times determined from long-term liner buckling experiments often hinders the identification of relationships between structural behavior and systematic changes in liner geometry or loading patterns ([58], [59], and [60]). Consequently, finite element analysis (FEA) provides an attractive tool for simulating the response of liner-host pipe systems. In particular, the influence of small changes in system geometry or loading history can be systematically studied so that the relationships between geometry, loading and material properties can understood and incorporated into liner design models. In this work, the ABAQUS© finite element software is employed to study the creep recovery behavior of higher compliance and higher stiffness PVC pipe liners subjected to seasonal variations in groundwater loading. The ABAQUS© model developed accounts for material nonlinearity, geometric nonlinearity, and the boundary condition nonlinearity associated with the evolving contact conditions between the liner and the host pipe and the variable groundwater loading.

Reproduced with permission of the copyright owner. Further reproduction prohibited without permission.

6.2 Assumptions

Several assumptions were made when constructing the finite element model:

1. The host pipe is taken as a rigid body since it is much stiffer than the liner materials and will incur very limited deflections as a result of contact with the liner.
2. The liner materials are homogeneous and isotropic.
3. The problem can be simplified as a plane strain problem such that a 2-D ring of plane strain elements are used to model entire liner length. This assumption is appropriate because of the interlocking of the liner with the host pipe during installation, which limits significant deflections along the axis of the pipe.
4. The original soil and pipe system is strong enough to carry all ground and traffic loading, and hence, the only load acting on the liner is the external groundwater pressure.

6.3 Finite Element Model

A clear understanding of the geometric configuration of the liner and host-pipe system is essential for liner buckling analyses. Folded PVC pipe liners are inserted into partially deteriorated sewer-pipe systems and then be heated along with internal pressure to cause the liner to conform to the shape of the host pipe. During the cooling phase of the PVC liner inversion process, a small radial gap usually develops between the liner and the host pipe. The gap g between the liner and the host pipe was assumed to be uniform for this research. A schematic representation of the liner geometry is shown as Fig. 6.1.

Reproduced with permission of the copyright owner. Further reproduction prohibited without permission.

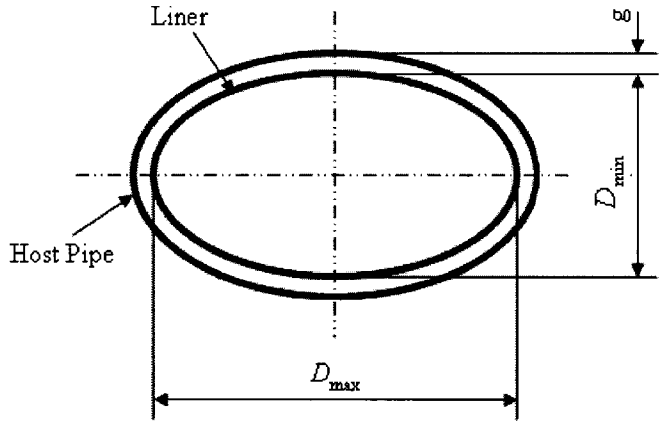

Fig. 6.1 Schematic of the two-lobe model with even gap

6.3.1 Basic Liner Geometrical Parameters

Dimension ratio (DR), ovality, and annular gap between the liner and host pipe are the main three geometrical parameters that will influence liner behavior.

Dimension Ratio (DR) is the ratio defined as the mean liner diameter D to the liner thickness t,

$$DR = \frac{D}{t} \tag{6.1}$$

Notice that in some studies, the standard dimension ratio (SDR) was used.

$$SDR = DR + 1 \tag{6.2}$$

Ovality The liner and the host pipe are assumed to have the same initial ovality, which can be defined as:

$$OV\% = \frac{D_{max} - D_{min}}{D_{max} + D_{min}} \cdot 100\% \tag{6.3}$$

where

OV = ovality of the liner

Reproduced with permission of the copyright owner. Further reproduction prohibited without permission.

D_{max} = major outer diameter of the liner

D_{min} = minor outer diameter of the liner

Gap The two-lobe liner deflection model with a uniformly distributed gap was developed for simulating long term creep and recovery effects. The gap between the liner and the host pipe in the evenly distributed mode can be defined as

$$G\% = \frac{g}{D} \cdot 100 \tag{6.4}$$

where

$$g = \frac{\Delta}{2} \tag{6.5}$$

where Δ is the difference of the inner diameter of the host pipe and outer diameter of the liner.

Based on the recommendation from manufacturer, single liner geometry was studied in this research: a liner with a dimension ratio of 32.5, a gap of 0.4% and an ovality of 5%. Typical values of these parameters are summarized in Table 6.1.

Table 6.1 Geometric parameters for the 2-D models

Geometrical Parameter	Value
DR	32.5
Ovality	5%
Gap	0.4%

6.3.2 Model Setup

The PVC liner buckling problem can be simplified to a 2-D plane strain model since the length of the liner segment is very long compared to the thickness of the liner.

Reproduced with permission of the copyright owner. Further reproduction prohibited without permission.

The liner is modeled using standard four-node, two-dimensional plane strain (CPE4) elements, and the host pipe is modeled with a set of two-node, two-dimensional, rigid body (R2D2) elements.

Structural symmetry is used in computational analyses when possible to reduce model size and the computational time. A quarter-symmetry model was employed to generate a two-lobe liner model with even gap between the host pipe and the liner. And, symmetric boundary conditions were applied at the ends of the model, as listed in Table 6.2. The displacement boundary conditions are shown in Fig. 6.2.

Table 6.2 Boundary conditions for the two-lobe buckling model

	U_x	U_y	UR_z
Top	Fixed	Free	Fixed
Bottom	Free	Fixed	Fixed

Reproduced with permission of the copyright owner. Further reproduction prohibited without permission.

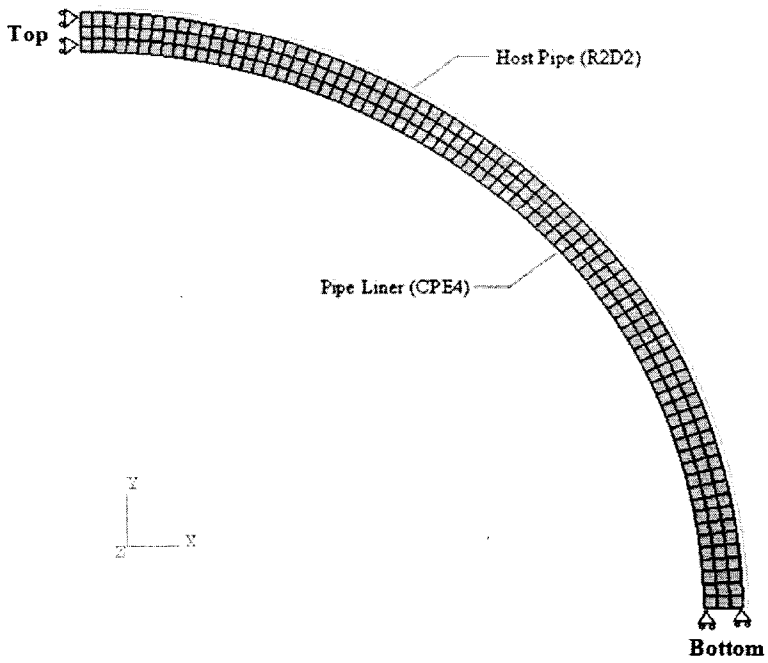

Fig. 6.2 Two-lobe finite element model (External pressure is applied to the liner in the gap between the liner and the host pipe)

6.3.3 Nonlinear Features

Two basic nonlinear features have to be considered when setting up the model: material nonlinearities and geometrical nonlinearity.

Material Nonlinearity Long-term buckling of PVC liners is a time-dependent process involving evolving stresses and deformations as a result of time-dependent material behavior. The viscoelastic material model described in Chapters 3 and 5 was embedded into ABAQUS© to simulate creep and recovery of the material. The *VISCOELASTIC, time =PRONY command was used to indicate viscoelastic behavior. The relaxation modulus constants (g_n^P) and the relaxation time constants (ρ_n) which were listed for the PVC materials in Table 5.3 were entered below the keyword *VISCOELASTIC, time =PRONY . See the ABAQUS© input file given in Appendix C to see an example input file.

Reproduced with permission of the copyright owner. Further reproduction prohibited without permission.

Geometrical Nonlinearity Geometric nonlinearity must be included in the model due to the large deflections of the liner (especially as buckling is approached) and because of the evolving contact conditions between the liner and the host pipe. Including geometric nonlinearities requires that ABAQUS© utilize the instantaneous liner-host pipe configuration to compute the current stresses and increments in displacement, as opposed to referring back to the original underformed body throughout the analysis. Nonlinear effects are included through the ABAQUS© option *STEP, NLGEOM. When the NLGEOM option is specified, elements are formulated in the current configuration using the current nodal position.

6.3.4 Loading Conditions

As described earlier, the loads applied to the liner can be divided into groundwater pressure and contact forces from host pipe. Groundwater loading is an external load that is applied directly to the liner surface (between the liner and the host pipe), and contact forces are computed by ABAQUS© during the analysis.

Groundwater Loading Before the liner contacts with the host pipe, the only significant load applied on the liner is external pressure caused by the groundwater leaking through cracks in the host pipe. This load can be modeled with the *DLOAD command in ABAQUS©. When used together with the *LOAD, AMPLITUDE command, *DLOAD can effectively simulate variations in groundwater pressure.

Contact Conditions Under external pressure, surface to surface interaction of the liner and host pipe will occur, and this interaction will strongly influence the behavior of the encased liner. The constraint provided by the host pipe to the liner will increase the buckling resistance and slow the deformation of the liner.

Reproduced with permission of the copyright owner. Further reproduction prohibited without permission.

In ABAQUS©, the *SURFACE DEFINITION and *CONTACT PAIR commands are used together to define the contact surfaces. The liner is a deformable body, and its outer surface is defined as a slave surface. The host pipe is a rigid body, and its inner surface is defined as a master, a rigid surface.

A finite-sliding formulation is applied in the contact analysis to simulate smooth contact surface between the deformable liner and the rigid host pipe. When applying this formulation, ABAQUS© *"automatically smoothes the surface normals of element-based master surfaces"* [61]

6.3.5 Viscoelastic Modeling

Long-term buckling was modeled using time-dependent, viscoelastic material behavior. In ABAQUS©, viscoelastic behavior of a liner can be modeled using the *STATIC command followed by the *VISCO command. The *STATIC command allows for time-independent pressure loading and assumes that the loading increases monotonically from zero to the liner buckling pressure. This procedure does not allow viscous material behavior. The command *VISCO is a software switch for ABAQUS© to activate time-dependent features; this command is required when simulating creep-induced buckling. ABAQUS© automatically adjusts the time increments based on the error tolerance of creep strain that was specified by the user and will stop the solution when the liner collapses.

6.3.6 Simulation of Groundwater Level Variation

Groundwater levels will vary from place to place and from time to time based on a complex combination of both natural and human-induced factors. As discussed in Chapter 2, the groundwater is likely to be recharged during the wet season, and the water

Reproduced with permission of the copyright owner. Further reproduction prohibited without permission.

table will be at its highest at this time; during the dry season, the groundwater level will typically decline, and the water table will be at its lowest.

Step variation and sinusoidal variation in groundwater pressures were used by Kini [27] to simulate the long-term buckling of CIPP liner due to seasonal groundwater variations. Step variation assumes that the groundwater height varies instantaneously from highest to lowest with no transition, as shown in Fig. 6.3.

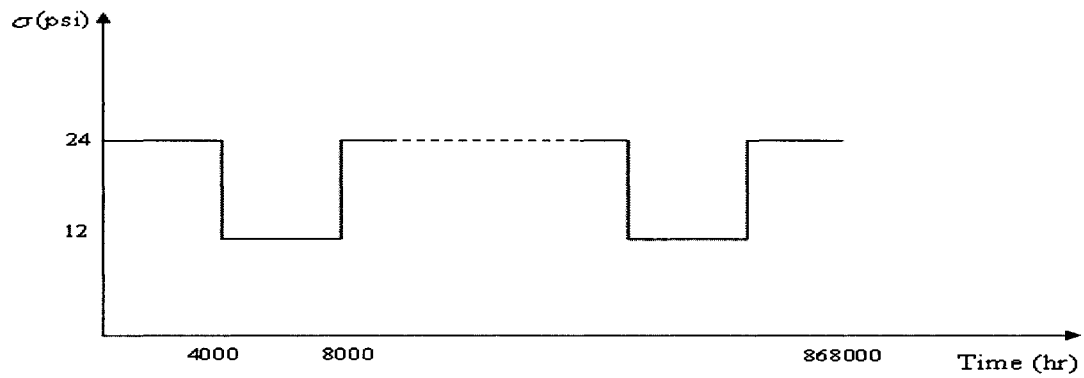

Fig. 6.3 Step variation of groundwater pressure [27]

A sinusoidal variation in groundwater pressures, which avoids sudden changes in water levels, is more realistic as shown in Fig. 6.4.

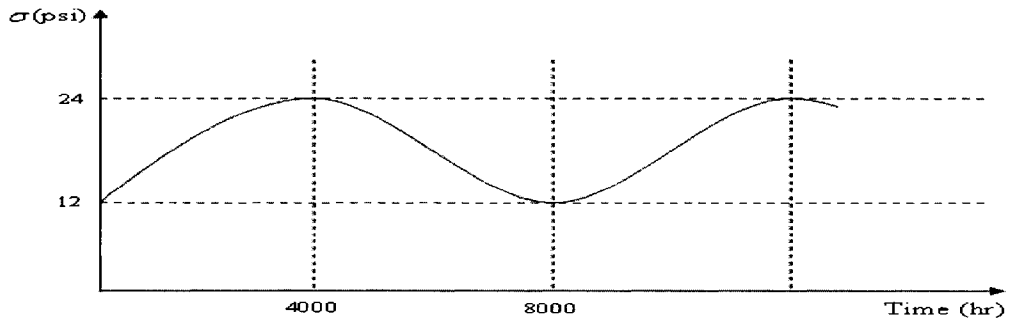

Fig. 6.4 Sinusoidal variation simulating variations in groundwater pressure [27]

Reproduced with permission of the copyright owner. Further reproduction prohibited without permission.

In many geographic regions, the dry season is much longer than the wet season, and the reverse is true on other regions. To accommodate the ability to vary the relative lengths of the wet and dry seasons, a trapezoidal loading pattern can be considered as shown in Fig. 6.5. This loading pattern was adopted for this research. This loading pattern can represent three distinct groundwater histories: longer peak pressure with shorter low pressure ($t_{high} > t_{low}$), equal peak and low pressure periods ($t_{high} = t_{low}$), and shorter peak pressure with longer low pressure ($t_{low} > t_{high}$).

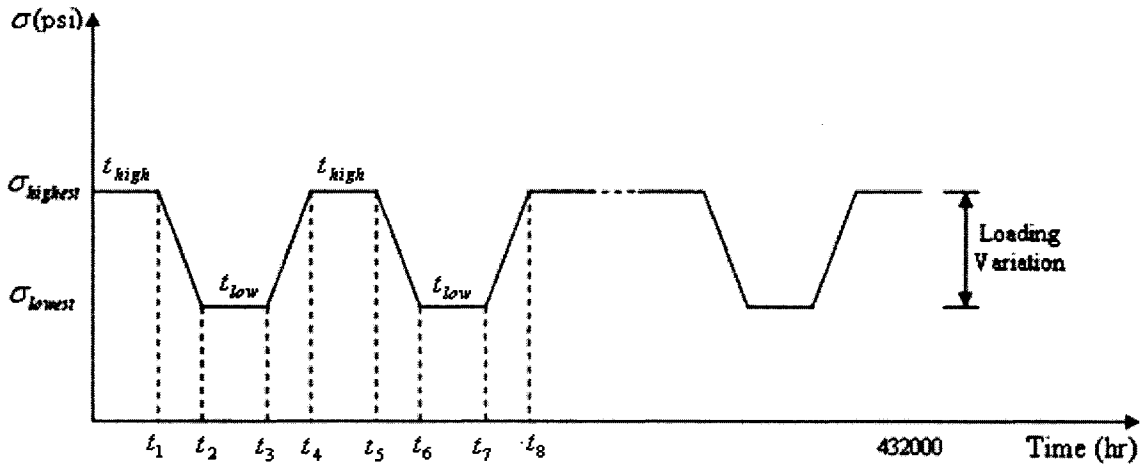

Fig. 6.5 Trapezoidal groundwater loading pattern adopted for this research

6.4 Model Verification

6.4.1 Mesh Refinement

When using the finite element model, the accuracy of the computational analysis generally increases as the number of elements increases. An analysis may not converge or may converge to an inaccurate solution if the mesh is too coarse, and the computation may take excessive time if the mesh is too fine. So, the number of elements should be chosen to balance computational accuracy and cost. A "mesh refinement" study is

Reproduced with permission of the copyright owner. Further reproduction prohibited without permission.

required to determine how many elements is "enough" and to determine the suitability of a given mesh, based on the element size distribution and aspect ratios, for the analysis. When designing a mesh, a general rule is to keep the aspect ratio of elements (the element length divided by the width) as close to one as possible.

A mesh refinement study involves progressively increasing the number of elements until the quantity of interest; the buckling pressure in this case, shows an acceptable level of change between successive runs. The mesh refinement study conducted here is summarized in Tables 6.3 and 6.4. The 3*78 mesh is selected for both liner materials, where 3 is the number of elements through the thickness of the liner and 78 is the number of elements in the circumferential direction. The mesh refinement study revealed that mesh refinement beyond the 3*78 level resulted in buckling pressure changes less than 2%.

Table 6.3 Mesh refinement for the higher compliance PVC

Mesh	Buckling Pressure (psi)	Difference
1*26	53.55	N/A
2*52	71.71	25.3%
3*78	74.72	4.0%
4*104	75.87	1.5%
5*128	76.30	0.6%

Reproduced with permission of the copyright owner. Further reproduction prohibited without permission.

Table 6.4 Mesh refinement for the higher stiffness PVC

Mesh	Buckling Pressure (psi)	Difference
1*26	55.79	N/A
2*52	77.65	28.2%
3*78	81.07	4.2%
4*104	82.09	1.2%
5*128	82.63	0.7%

6.4.2 Verification with Glock's Model

Glock's analytical model was used to evaluate the accuracy of the finite element model for an encased perfectly circular pipe without gap. The two-lobe buckling model, which was initially presented in Chapter 2, is shown again in Eq. 6.6.

$$P_{cr} = 1.323 \cdot \left(\frac{1}{SDR-1}\right)^{2.2} \cdot \frac{E}{1-v^2} \tag{6.6}$$

Because the liner is perfectly circular in the computational analysis, some small perturbation is required to initiate buckling – this will happen naturally in the field due to material and geometrical imperfections. In this case, a very small ovality of 0.17% (instead of 0%) was assumed when generating the mesh geometry – this small ovality will not significantly influence the buckling pressure.

Setting the dimension ratio to $SDR-1 = DR = 32.5$, the elastic modulus E to 164,000 psi (for the higher compliance PVC liner material), and Possion's ratio v to 0.35, the calculated critical buckling pressure P_{cr} from Glock's model is 124.99 psi. The corresponding result for this geometry and material properties using ABAQUS© is

Reproduced with permission of the copyright owner. Further reproduction prohibited without permission.

125.18 psi. For the higher stiffness PVC liner material (E = 179,900 psi), the critical buckling pressure from ABAQUS© is 137.23 psi which is also close to Glock's prediction of 137.11 psi.

6.5 Summary

"A two-dimensional, plane strain, finite element model was set up to evaluate the short- and long-term behavior of a constrained liner. Short-term buckling was modeled using the *STATIC command, while the long-term, viscoelastic response of the liner was modeled using a combination of the *STATIC and *VISCO commands. A standard four-node, two-dimensional plane strain (CPE4) element was chosen to represent the liner. Surface to surface contact was modeled to simulate the interaction between the liner and the host pipe. The adequacy of the mesh to appropriately model the short-term problem was verified through mesh refinement, and the finite element results for an encased perfectly circular pipe without gap was compared with the Glock's analytical model resulting in excellent agreement.

Reproduced with permission of the copyright owner. Further reproduction prohibited without permission.

CHAPTER SEVEN

STRUCTURAL BEHAVIOR OF PVC PIPE LINERS

7.1 Introduction

Most research dealing with the structural behavior and design of pipe liners focuses on the influence of geometric parameters and imperfections on the accurate prediction of short- and long-term buckling resistance based on the assumption of a constant groundwater level. However, the service life of a liner may be extended if the groundwater level drops significantly below the "design groundwater level" for a significant period of time each year. The aim of this research is to study the structural behavior of PVC pipe liners subjected to seasonal groundwater variations and to account for the influence of these variations in liner design. The results and conclusions drawn from the finite element analysis and from the material characterization work are brought together in this chapter to develop a modified design model for pipe liners.

7.2 Essential Factors

The ABAQUS© finite element model presented in Chapter 6 was employed for different seasonal groundwater loading patterns. To simplify the problem, however, single liner geometry was studied: the results given here assume a dimension ratio of 32.5, a gap of 0.4% and an ovality of 5%.

Reproduced with permission of the copyright owner. Further reproduction prohibited without permission.

7.2.1 The 50-Year Pressure

The design lifetime typically applied in the trenchless industry for pipe liner design is 50 years (or 432,000 hours). The pressure that will cause a liner to fail at exactly 50 years is denoted here as the 50-year pressure (P_{50}). The 50-year pressures for the higher compliance and higher stiffness PVC materials can be determined from Figs. 7.1 and 7.2, respectively. These plots are developed by varying the pressure applied to the liner in the ABAQUS© model and observing the simulated buckling time. Fitting the buckling time versus the applied pressure curve provides a method to accurate quantify the 50-year pressures from the plots. Fitting the curves in Figs. 7.1 and 7.2 results in 50-year pressures for the higher compliance and higher stiffness PVC materials of 31.3 psi and 46.4 psi, respectively. Of course, these results apply for a DR of 32.5, a gap of 0.4%, and an ovality of 5%.

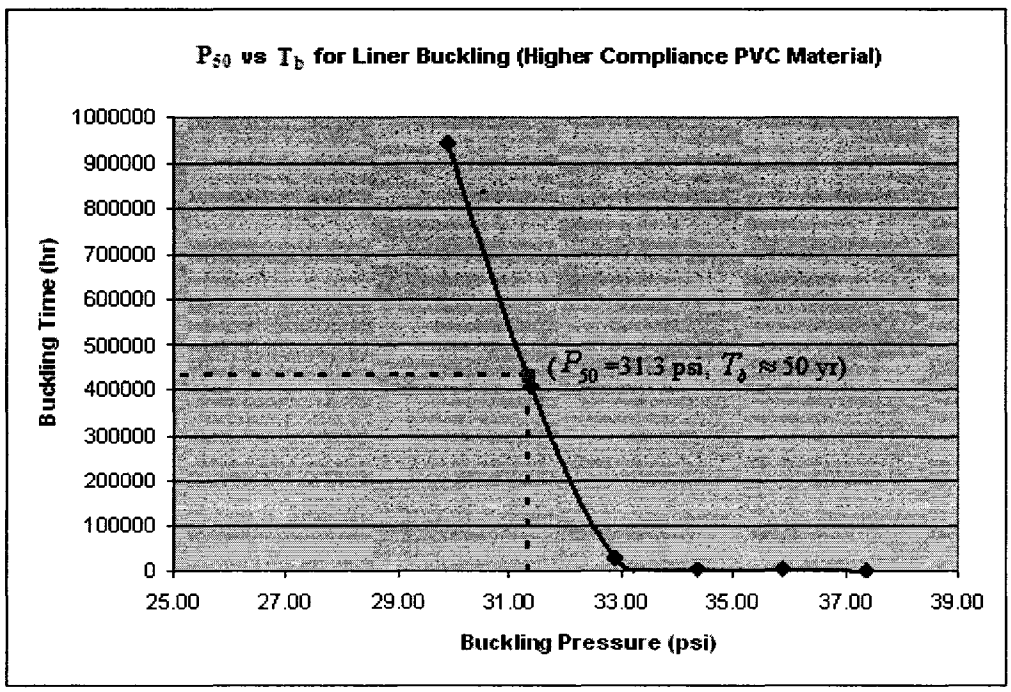

Fig. 7.1 Fifty-year pressure for higher compliance PVC material

Reproduced with permission of the copyright owner. Further reproduction prohibited without permission.

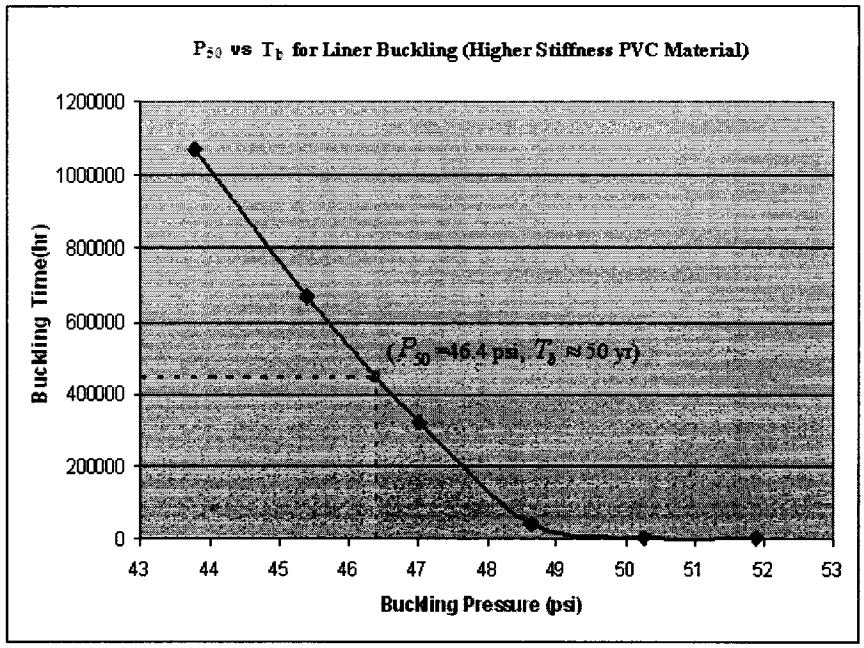

Fig. 7.2 Fifty-year pressure for higher stiffness PVC material

7.2.2 Variations in Groundwater Level

The groundwater was assumed to vary as depicted earlier in Fig. 6.5. The groundwater variation depends on the geographic region and on human induced factors. The water table in some locations may remain at its peak level for most of the year ($t_{high} > t_{low}$), while the water table may remain at a low level for most of the year in other locations ($t_{low} > t_{high}$).

To study how the groundwater variation will affect liner buckling times, two groups of variables were considered in this study: the time variation ratio (TVR) and the depth variation ratio (DVR). TVR or t_{low} / t_{high} values of 0.33, 1.00 and 3.00 were simulated. DVR or H_{low} / H_{high} values of 0.75, 0.50 and 0.25 were also simulated. Both 3-month and 6-month loading cycles were simulated; the 3-month analysis simulates a

Reproduced with permission of the copyright owner. Further reproduction prohibited without permission.

high-low-high-low water level pattern each year while the 6-month analysis simulates a high-low water level pattern (a single wet season followed by a single dry season) each year.

7.3 Effects of Groundwater Variation

7.3.1 Effects on 50-Year Pressure

The 50-year pressure resulting from a finite element simulation will depend on how the groundwater varies. For example, increasing TVR will result in higher pressures since the groundwater stays at a lower pressure for a longer period of time. Likewise, increasing DVR will decrease the 50-year pressure since the lower pressure will be closer to the higher pressure (which is the reference pressure).

To determine the 50-year pressure, the value of P_{high} was varied for set TVR and DVR values resulting in a particular liner lifetime, T_b. The first step in determining the 50-year pressure was to make an initial guess for the value of P_{high} that would result in a T_b of approximately 50 years. If the initial value of P_{high} guess resulted in a T_b that was less than 50 years, then P_{high} would be increased until T_b values both above and below 50 years had been determined (continue to guess until the 50-year mark is bracketed by P_{high}, T_b pairs). At this point, the bisection method was used to systematically hone in on the value of P_{high} corresponding to 50-years. The bisection iteration procedure was continued until the difference between successive P_{high} trials was less than 0.3%.

Table 7.1 shows the bisection iteration procedure used to determine the P_{high} value that resulted in a 50-year liner lifetime for a TVR of 0.33 and a DVR of 0.75. In

Reproduced with permission of the copyright owner. Further reproduction prohibited without permission.

this case, the first guess for P_{high} was 33.5 psi and the second guess was 33 psi. The bisection procedure was then invoked, resulting in a P_{high} value of 33.25 (the average of 33.5 and 33). Since T_b for 33.25 was less than 50 years, the next P_{high} value evaluated as 33.13 psi (the average of 33.25 and 33). Finally, the last value evaluated was 33.19 psi which resulted in a T_b of 414,605 hours (50 years is 432,000 hours). The change in subsequent P_{high} values for the last two simulations was 0.18% ((33.19-33.13)/33.19 = 0.0018). Thus, the 50-year buckling pressure for the higher compliance PVE material is 33.1 psi, and this value is denoted as P_{50v} where the v indicates pressure variation during the simulation.

Table 7.1 Buckling time for PVC-HC under the variation: TVR=0.33 and DVR=0.75

Load Cycle: 3 months		Load Cycle: 6 months	
P_{high} (psi)	T_b (hour)	P_{high} (psi)	T_b (hour)
33.50	226706	33.25	90692
33.25	377948	32.88	298354
33.19	414605	32.69	402278
33.13	451440	32.60	453484
33.00	533428	32.50	505395

Recall from Fig. 7.1 that the 50-year pressure (P_{50}) is equal to 31.30 psi for constant groundwater loading. Comparing the P_{50v} of 33.10 psi for the varying groundwater levels with P_{50} reveals that the liner can withstand higher pressures and still

Reproduced with permission of the copyright owner. Further reproduction prohibited without permission.

last for 50 years when groundwater levels vary seasonally. Notice that the difference between the 50 year pressures is 5.8% which is a significant change. It is important that factors with this level of influence be appropriately included in liner design models.

Table 7.1 included an analysis for both three- and six-month loading cycles. For the 6-month loading cycle, P_{50v} is 32.60 psi. Table 7.2 presents similar results for the higher stiffness PVC material. Here, P_{50v} is 48.8 psi for a 3-month loading cycle, and P_{50v} is 48.0 psi for a 6-month loading cycle. All of these results apply only for a TVR of 0.33 and a DVR of 0.75. The 50-year pressures for all TVR and DVR combinations are provided in Appendix D.

Table 7.2 Buckling time for PVC-HS under the variation: TVR=0.33 and DVR=0.75

Load Cycle: 3 months		Load Cycle: 6 months	
P_{high} (psi)	T_b (hour)	P_{high} (psi)	T_b (hour)
49.50	252708	48.50	332614
49.00	387078	48.13	427554
48.88	421197	48.04	462094
48.75	460040	47.94	505725
48.50	539930	47.75	603858

7.3.2 Effects on Liner Deformation

The long-term deflection of a liner at the critical point depends on depends both TVR and DVR. Fig. 7.3 shows a schematic of a pipe liner experiencing the typical two-lobe deformation pattern; the peak inward radial deflection occurs at the center of the

Reproduced with permission of the copyright owner. Further reproduction prohibited without permission.

lobe as shown. Plotting this displacement versus time provides insight into the structural response of the liner as loading is applied and removed due to seasonal groundwater changes.`

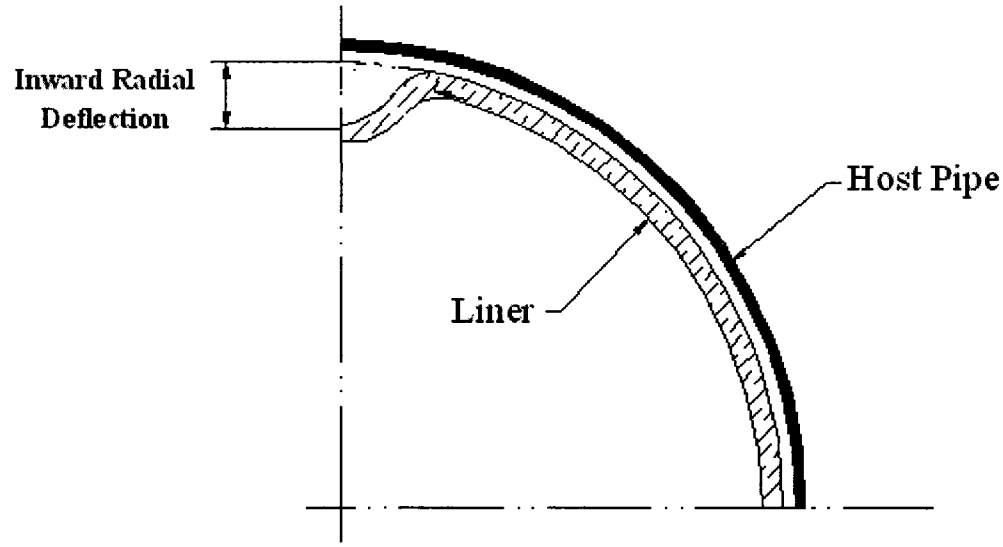

Fig. 7.3 Schematic of a pipe liner experiencing the two-lobe deformation pattern

Figs. 7.4-7.6 show plots of the displacement versus time for liners subjected to the 50-year pressure P_{50v} under variable loading. For these plots, TVR is held to a constant value of 1/3, and DVR values of 3/4, 1/2 and 1/4 are simulated using a 3-month loading cycle in Figs. 7.3-7.5, respectively. Notice that the displacement of the lobe moves inward and outward as pressure is applied and the difference between the minimum and maximum deflection for each cycle increases as DVR decreases, as expected (a lower value of DVR means that a larger portion of the pressure is removed during unloading). Also notice that the peak deflection increases over the life of the liner; however, this peak deflection has a much steeper increase for higher values of DVR since less recovery occurs when less pressure is removed. That is, the slope of the deflection versus time

Reproduced with permission of the copyright owner. Further reproduction prohibited without permission.

curve is much steeper for the higher DVR values. It is clear that recovery has a significant impact on the structural response of the liner when groundwater levels have large fluctuations.

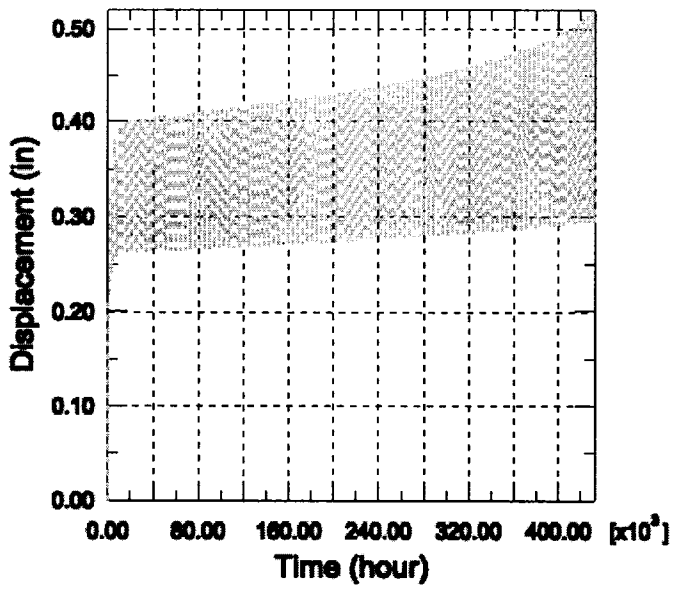

Fig. 7.4 Displacement vs. time for the PVC HC liner (3-month cycle, load= P_{50v} , TVR=1/3, DVR=3/4)

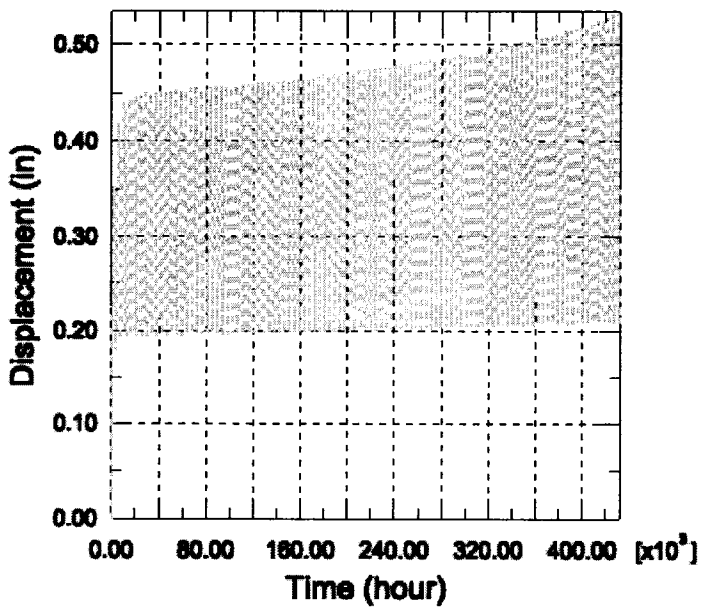

Reproduced with permission of the copyright owner. Further reproduction prohibited without permission.

Fig. 7.5 Displacement vs. time for the PVC HC liner (3-month cycle, load= P_{50v}, TVR=1/3, DVR=1/2)

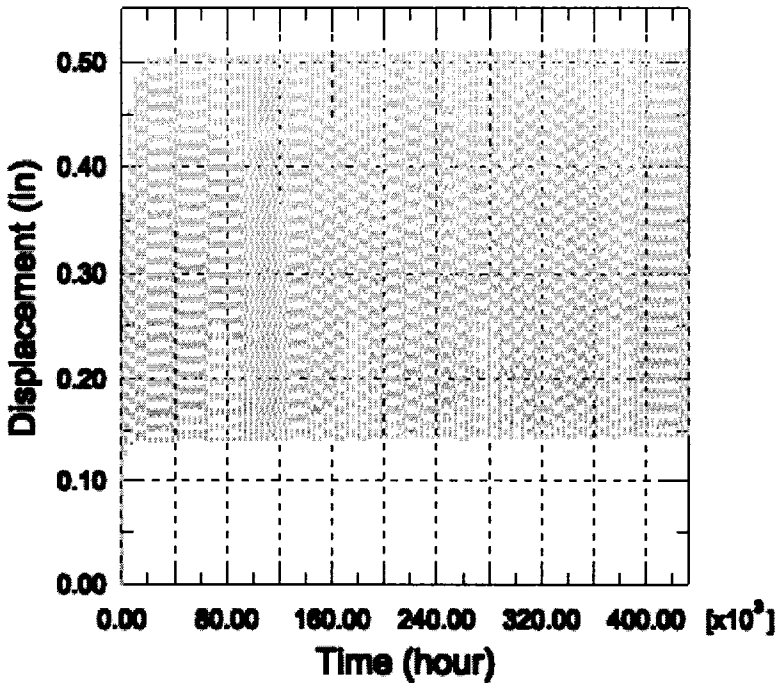

Fig. 7.6 Displacement vs. time for the PVC HC liner (3-month cycle, load= P_{50v}, TVR=1/3, DVR=1/4)

Fig. 7.7 shows a comparison between a model with constant groundwater loading (creep with no recovery) and a model with variable groundwater loading (creep with recovery). The same peak pressure, in this case P_{50}, was applied to all models to illustrate the influence on the deflection due to variable loading. Only a small part of the overall life is shown in Fig. 7.7 so that the results for individual cycles could be seen; the actual 50-year displacement curve consists of many more data points. It is clear that the displacement for a model not incorporating recovery is higher than the displacements for models that incorporate recovery and that the displacement levels increase as DVR is increased. Therefore, a decrease in DVR leads to more recovery and lower displacements.

Reproduced with permission of the copyright owner. Further reproduction prohibited without permission.

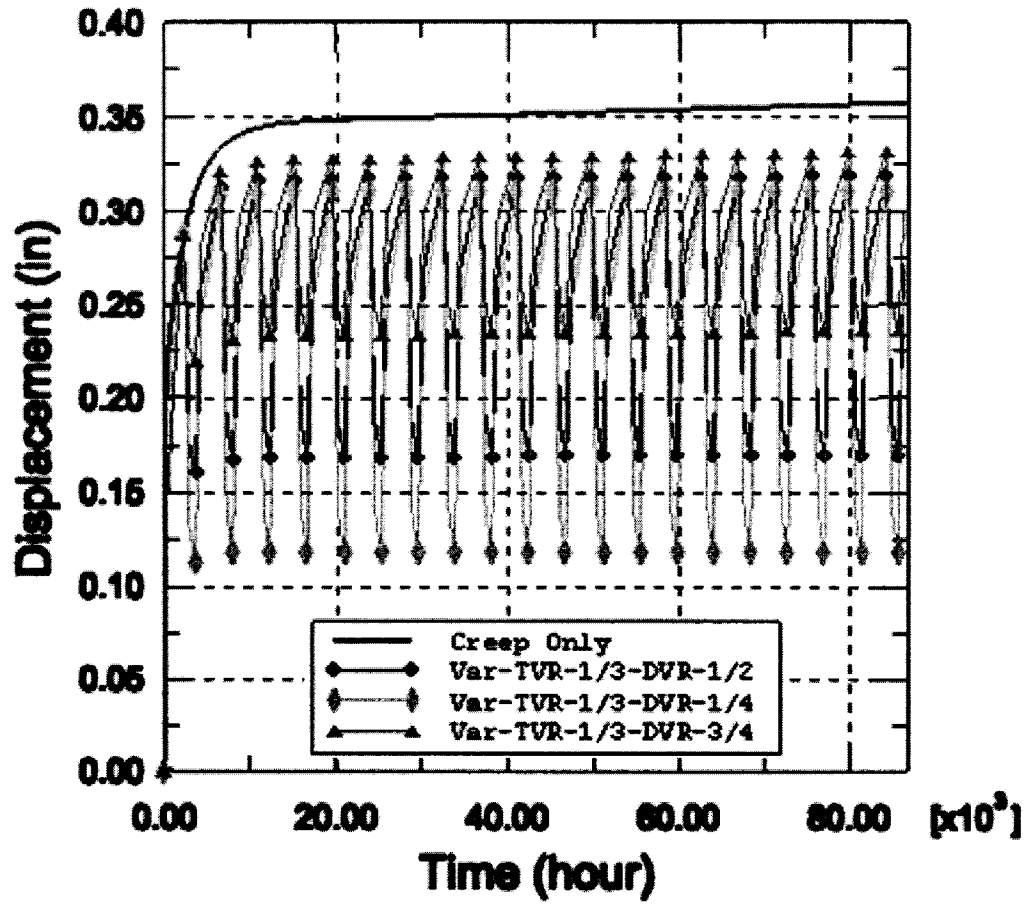

Fig. 7.7 Comparison with liner response for constant groundwater loading and variable groundwater loading at short times (3-month cycle, load= P_{50})

Figs. 7.8-7.9 essentially repeat the plots shown earlier in Figs. 7.3-7.5 for variations in TVR with a fixed DVR value. TVR values of 1/3, 1 and 3 were simulated for a fixed DVR value of 3/4 (the plot for a TVR of 1/3 and a DVR of 3/4 was presented earlier in Fig. 7.3). These three plots all have very similar trends; however, it is important to recognize that the applied pressure P_{50v} is higher for lower values of TVR as expected (recall that TVR is defined as t_{low} / t_{high}).

Reproduced with permission of the copyright owner. Further reproduction prohibited without permission.

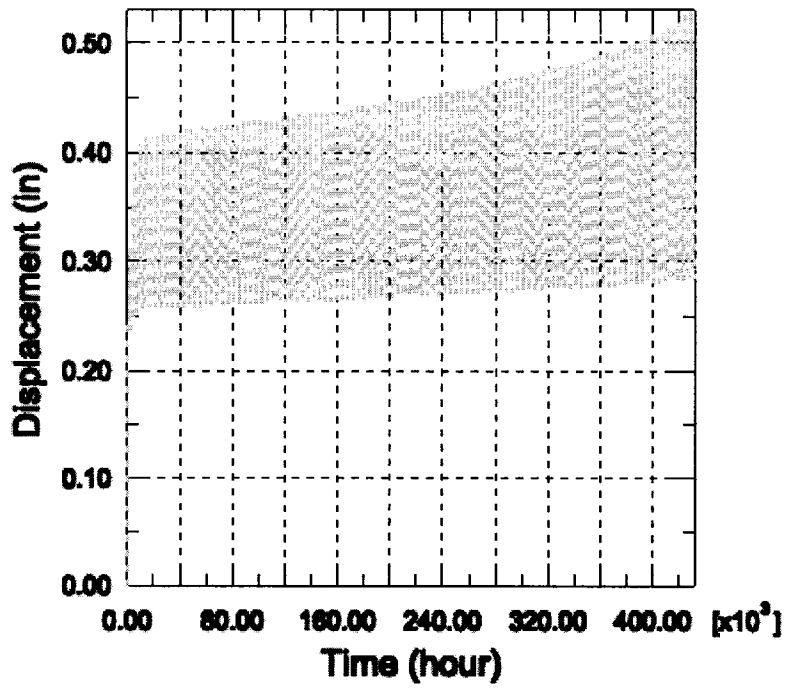

Fig. 7.8 Displacement vs. time for the PVC HC liner (3-month cycle, load=P_{50v}, TVR=1, DVR=3/4)

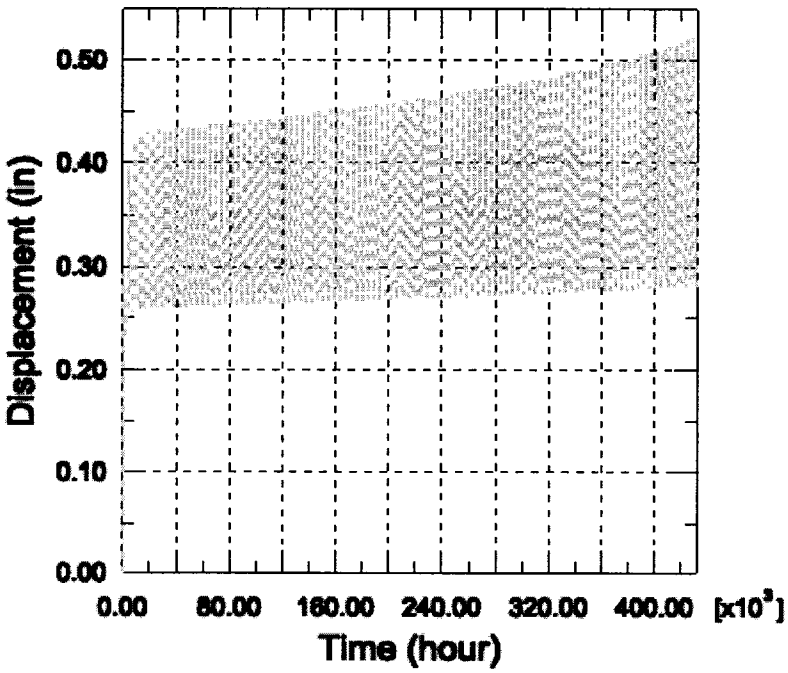

Fig. 7.9 Displacement vs. time for the PVC HC liner (3-month cycle, load=P_{50v}, TVR=3, DVR=3/4)

Reproduced with permission of the copyright owner. Further reproduction prohibited without permission.

Fig. 7.10 illustrates the differences in the deflection for these three TVR cases when the same loading is applied, P_{50}. Notice that when t_{low} is a larger portion of the overall loading time (as in the case for TVR = 3), more recovery should occur resulting in lower overall deflections for a given applied pressure. Also notice that any amount of recovery time significantly lowers the deflection compared to the constant loading case. Therefore, increasing TVR results in lower deflections and longer life.

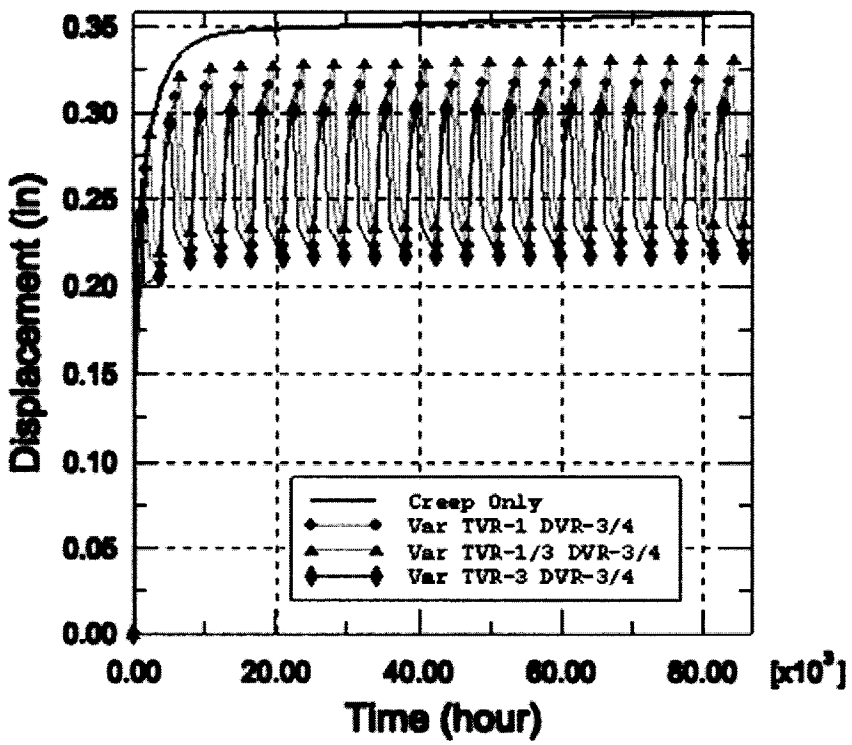

Fig. 7.10 Comparison with liner response for constant groundwater loading and variable groundwater loading at short times (3-month cycle, load=P_{50})

Fig 7.11 compares displacement histories for three-month and six-month loading cycles when the same pressure P_{50} is applied to the liners. As the number of loading cycles increase, recovery occurred at more frequent intervals and resulted in a lower displacement.

Reproduced with permission of the copyright owner. Further reproduction prohibited without permission.

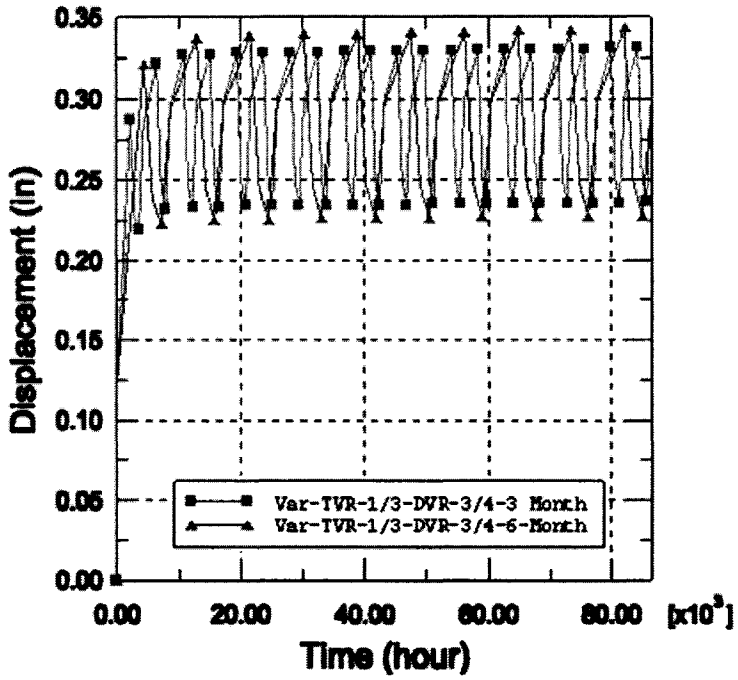

Fig. 7.11 Effect of time variation frequency for a liner subjected to loading of 50-year pressure with TVR=1/3 and DVR=3/4

7.3.3 Effects on Liner Design

A major aim of this work is to evaluate the influence of groundwater variation on liner design. The finite element results presented earlier clearly show that the 50-year pressure for variable loading is higher than that for constant loading. A correction factor (CF) is defined here as the ratio of the 50-year pressure with groundwater variation (P_{50v}) to the 50-year pressure without groundwater variation (P_{50})

$$CF = \frac{P_{50v}}{P_{50}} \tag{7.1}$$

where P_{50v} depends on the time variation ratio (TVR) and the depth variation ratio (DVR).

Correction factors corresponding to different TVR and DVR combinations are listed in Table 7.3-7.6 and plotted in Fig. 7.12-7.15.

Reproduced with permission of the copyright owner. Further reproduction prohibited without permission.

Table 7.3 Correction factors for HC PVC, 3-month cycle

	TVR=1/3	TVR=1	TVR=3
DVR=1	1	1	1
DVR=3/4	1.058	1.086	1.122
DVR=1/2	1.092	1.136	1.192
DVR=1/4	1.115	1.160	1.224

Table 7.4 Correction factors for HS PVC, 3-month cycle

	TVR=1/3	TVR=1	TVR=3
DVR=1	1	1	1
DVR=3/4	1.051	1.074	1.105
DVR=1/2	1.082	1.115	1.163
DVR=1/4	1.104	1.141	1.184

Table 7.5 Correction factors for HC PVC, 6-month cycle

	TVR=1/3	TVR=1	TVR=3
DVR=1	1	1	1
DVR=3/4	1.042	1.064	1.096
DVR=1/2	1.060	1.092	1.141
DVR=1/4	1.073	1.108	1.170

Reproduced with permission of the copyright owner. Further reproduction prohibited without permission.

Table 7.6 Correction factors for HS PVC, 6-month cycle

	TVR=1/3	TVR=1	TVR=3
DVR=1	1	1	1
DVR=3/4	1.036	1.055	1.080
DVR=1/2	1.054	1.078	1.118
DVR=1/4	1.065	1.094	1.142

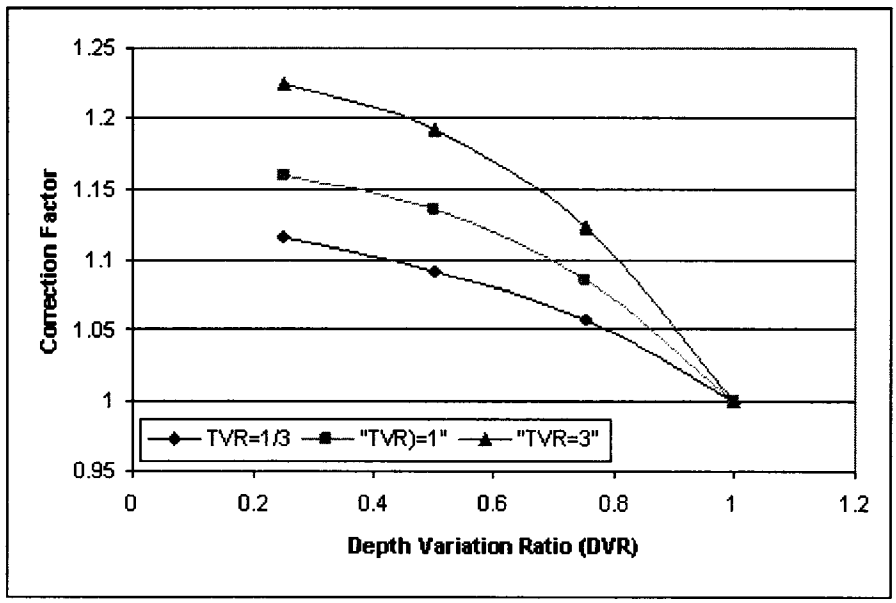

Fig. 7.12 Correction factor curves (HC, 3-month cycle)

Reproduced with permission of the copyright owner. Further reproduction prohibited without permission.

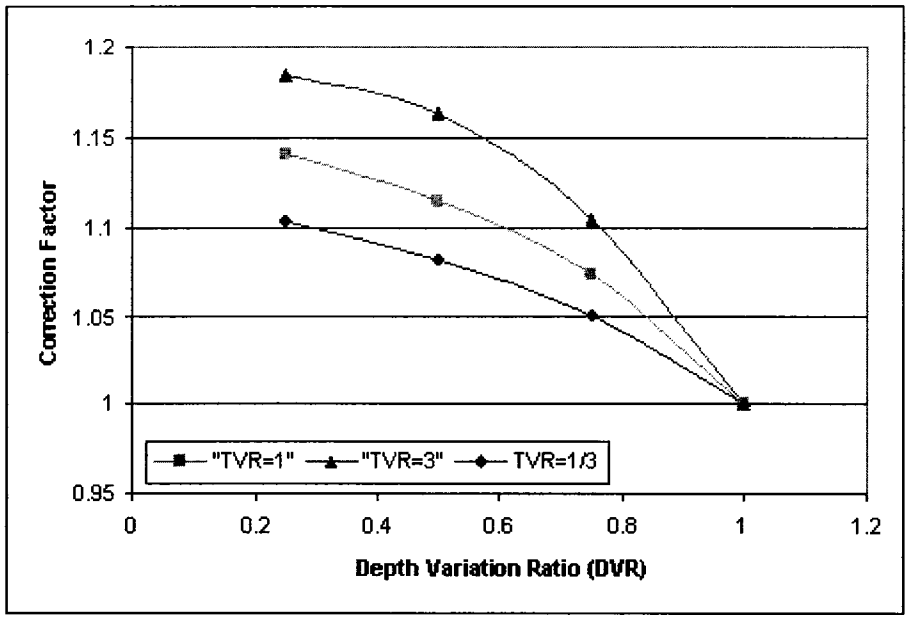

Fig. 7.13 Correction factor curves (HS, 3-month cycle)

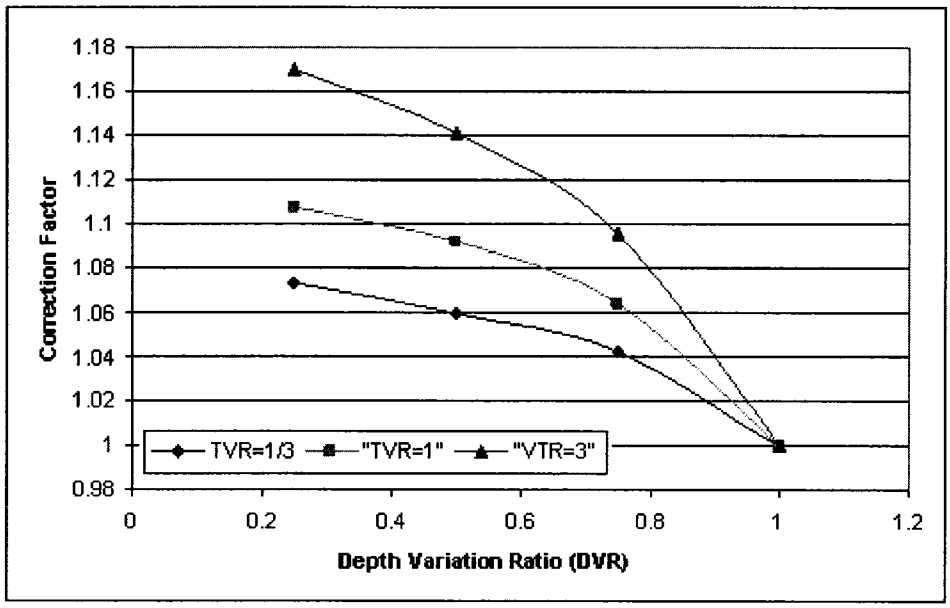

Fig. 7.14 Correction factor curves (HC, 6-month cycle)

Reproduced with permission of the copyright owner. Further reproduction prohibited without permission.

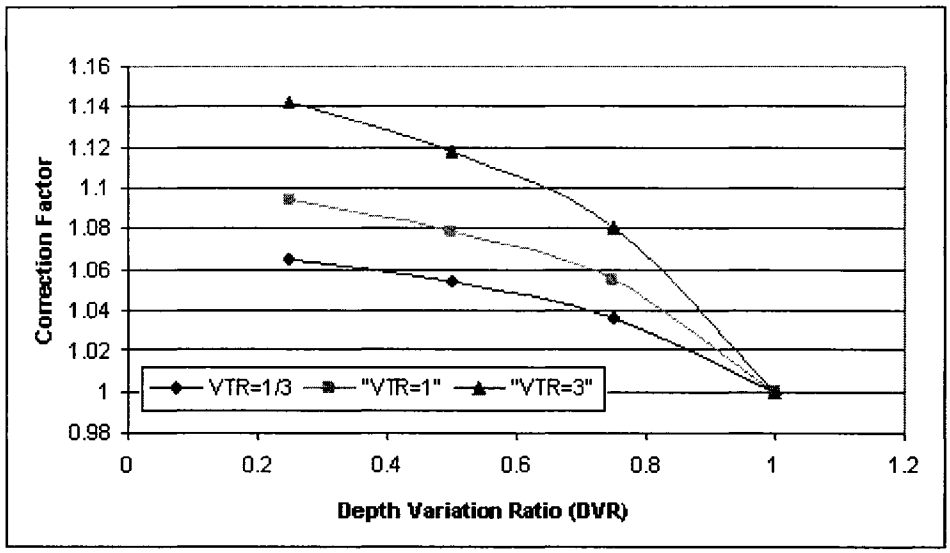

Fig. 7.15 Correction factor curves (HS, 6-month cycle)

The finite element results show that liners which experience groundwater variations can withstand a 50-year pressure that is higher than liners exposed to a constant groundwater level. Referring back to the ASTM F1216-05 [29] design equation for liners installed in partially deteriorated pipes, we see that the design pressure, P_{cr}, for long-term liner design is the pressure level that will cause the liner to fail at 50 years. From Eq. 7.1, P_{50v} is equal to CF times P_{50}. Thus, multiplying the 50-year pressure computed in the ASTM design model by CF allows the model to incorporate the influence of variable groundwater loading. The revised ASTM model can be written as

$$P_{cr} = \frac{2 \cdot K \cdot E_L}{1-\nu^2} \cdot \frac{1}{(SDR-1)^3} \cdot \frac{C}{N} \cdot CF \tag{7.2}$$

where P_{cr} is the groundwater pressure exerted on the liner during the wet season (P_{high}).

For a given wet-season groundwater level, which will be input into Eq. 7.2 as P_{cr}, a CF greater than 1.0 will also cause an increase in DR (DR=SDR-1) and a decrease in thickness. In other words, allowing the liner time to recover during the dry season will

Reproduced with permission of the copyright owner. Further reproduction prohibited without permission.

make the liner deform less over time and last longer. Or, for a fixed wet-season groundwater level, a thinner liner subjected to variable loading will have the same life as a thicker liner subjected to constant loading.

Notice from Figs. 7.11 through 7.14 that the correction factors do not depend on liner geometry parameters. This means that it may be possible to extend these same correction factors to liners with different geometries (although geometry parameters will likely have some level of influence on CF values). The correction factors will likely show significant dependence on the creep and recovery properties of the liner materials. That is, liner materials that exhibit more recovery will have higher correction factors than liners that show less recovery (or material memory).

7.3.4 Liner Design Examples

Here, we will consider three PVC liner design examples to illustrate the application of a correction factor in ASTM F1216-05 [29]. Assuming the mean inside diameter of the original host pipe is 8 inch with 5% ovality, the ovality reduction factor C is calculated to be 0.64. If the short-term elastic modulus of the higher compliance PVC liner material, E, is 145,000 psi, then the 50-year corrected elastic modulus, E_L, can be estimated as ½ of E, which is 72,500 psi (this is common industry practice). Poisson's ratio will be taken as 0.35, and the enhancement factor, K, is set to 7 as recommended in ASTM F1216-05 [29]. A factor of safety, N, is 2 as recommended in ASTM F1216-05 [29].

When the liner thickness is selected as 0.2462 in for the 8-inch liner, then the dimension ratio of the liner is 32.5 and the 50-year pressure can be calculated by ASTM model (Eq 2.9) as

Reproduced with permission of the copyright owner. Further reproduction prohibited without permission.

$$P_{cr} = \frac{2 \cdot 7 \cdot 72500}{1 - 0.35^2} \cdot \frac{1}{(32.5)^3} \cdot \frac{0.64}{2} \tag{7.3}$$

The resulting P_{cr} is 10.78 psi.

Case 1

Assume the wet-season groundwater loading is 10.78 psi. When the groundwater level varies downward from 10.78 psi according to TVR=1/3 and DVR=3/4 for a 3-month loading cycle, a correction factor of 1.058 from Table 7.3 is applied to the ASTM design equation:

$$10.78 = \frac{2 \cdot 7 \cdot 72500}{1 - 0.35^2} \cdot \frac{1}{(DR_v)^3} \cdot \frac{0.64}{2} \cdot 1.058 \tag{7.4}$$

The resulting DR_v is 33.1 which corresponds to a liner thickness of 0.2417 inches (8/33.1). Thus, the liner thickness is reduced from 0.2462 in to 0.2417 in due to groundwater variations for this case (a 1.8% decrease).

Case 2

If the wet-season groundwater loading is 10.78 psi with TVR=3 and DVR=1/4 for a 3-month loading cycle, a correction factor of 1.224 from Table 7.3 can be applied to the ASTM design equation:

$$10.78 = \frac{2 \cdot 7 \cdot 72500}{1 - 0.35^2} \cdot \frac{1}{(DR_v)^3} \cdot \frac{0.64}{2} \cdot 1.224 \tag{7.5}$$

The resulting DR_v is 34.7 which corresponds to a liner thickness of 0.2305 in. (8/34.7). Thus, the liner thickness is reduced from 0.2462 in to 0.2305 in due to groundwater variations for this case (a 6.4% decrease).

Reproduced with permission of the copyright owner. Further reproduction prohibited without permission.

Case 3

Fig 7.16 shows 1998-2002 groundwater level hydrographs for a well in Dalton Holme, United Kingdom. The actual variation curve can be simplified as a modified step model with TVR=1 and DVR=3/4 (or 15/20) with a 6-month variation cycle.

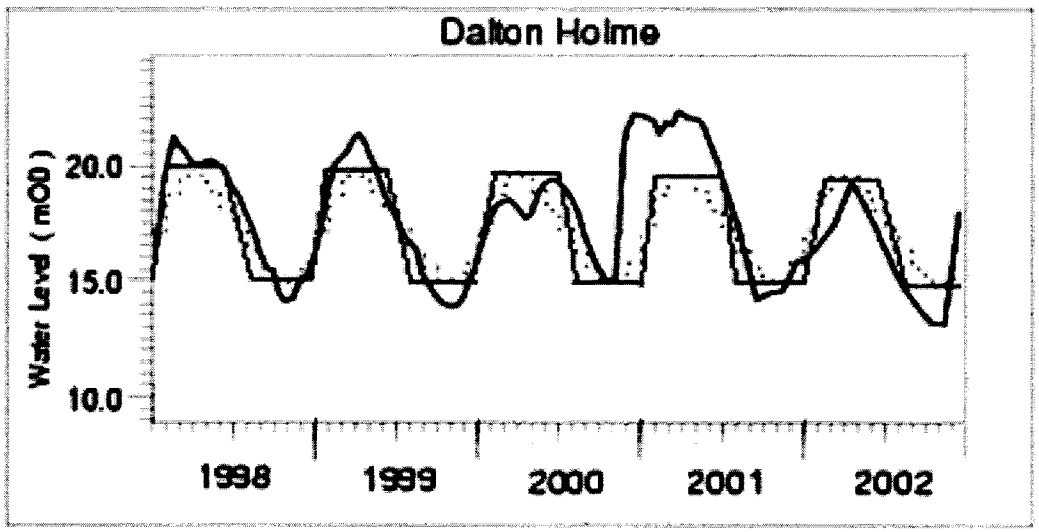

Fig. 7.16 Groundwater level from 1998-2002 for a well in Dalton Holme, UK [62]

Comparing Eq 7.2 with the ASTM design equation, yields

$$\frac{1}{(DR)^3} = \frac{1}{(DR_v)^3} \cdot CF \tag{7.6}$$

Applying a correction factor of 1.064 and assuming an initial DR of 32.5 for a liner thickness of 0.2462 in results in a new DR of 33.2 for a new liner thickness of 0.2410 in.

Variation Trends as a Function of CF

Eq. 7.6 can be rewritten to better understand how thickness varies as a function of the correction factor:

Reproduced with permission of the copyright owner. Further reproduction prohibited without permission.

$$\frac{1}{(D/t)^3} = \frac{1}{(D/t_v)^3} \cdot CF$$

or

$$t_v = \sqrt[3]{CF^{-1}} \cdot t \tag{7.7}$$

Then, the variation in the liner thickness caused by the groundwater variation can be expressed as

$$\frac{t - t_v}{t} = 1 - \sqrt[3]{CF^{-1}} \tag{7.8}$$

Utilizing the CF factors given in Tables 7.3 – 7.6 along with Eq. 7.8, the percent reduction in thickness for the higher compliance and higher stiffness materials for both three- and six-month loading cycles is summarized in Fig. 7.17.

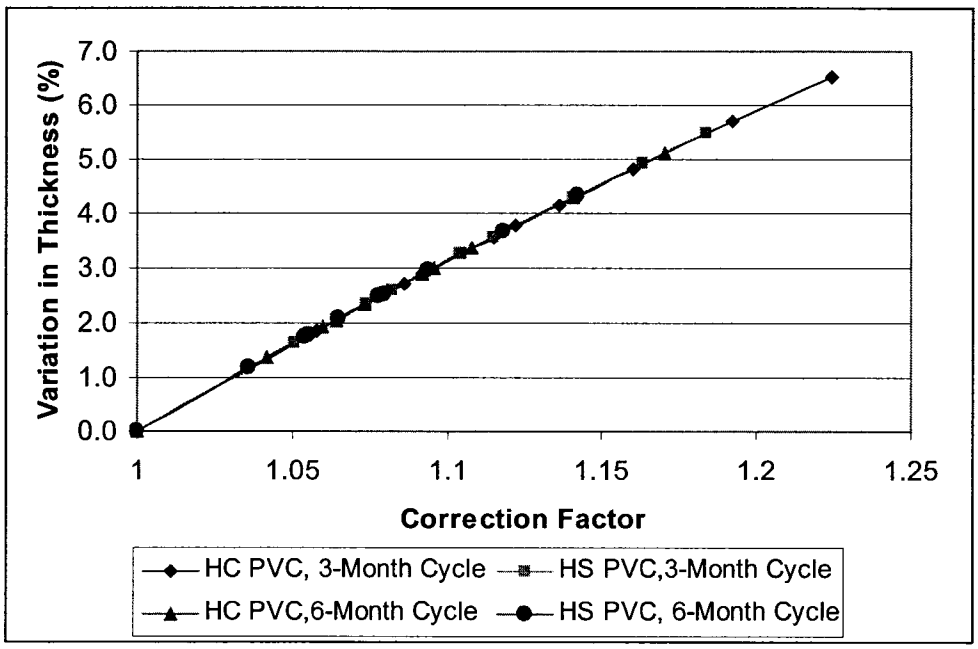

Fig. 7.17 Liner thickness change (%) versus correction factors

Notice that the variation in thickness is greater than 6% for the higher compliance pipe liner subjected to a three-month loading cycle with TVR = 3 and DVR = 1/4.

Reproduced with permission of the copyright owner. Further reproduction prohibited without permission.

7.4 Summary

The following conclusions were obtained based on the finite element results:

1. The service life of liners is extended due to groundwater variation, and the depth of water variation is the most dominant variable in long-term buckling analysis.
2. The displacement for a model not incorporating recovery is higher than the displacements for models which incorporate recovery.
3. When the value for the depth variation ratio (DVR) decreases, the corresponding displacement decreases.
4. The displacement decreases as the time variation ratio (TVR) increases.
5. The displacement decreases as the number of creep and recovery cycles increases.
6. The ASTM design model for partially deteriorated liners was modified to account for variable groundwater loading, and significant changes in liner thickness apply for certain combination of DVR and TVR.

Reproduced with permission of the copyright owner. Further reproduction prohibited without permission.

CHAPTER EIGHT

CONCLUSIONS AND RECOMMENDATIONS

8.1 Conclusions

8.1.1 Material Characterization Testing

In this study, creep and recovery tests were conducted on higher compliance and higher stiffness PVC liner specimens to evaluate time-dependent liner material properties under variable loading. Three-point flexural testing was conducted on 16 specimens whose axes were aligned with the circumferential direction of the liner. The specimens were tested at 5% and 10% of the yield strength of the material as listed by the manufacturer. The tests for the lower stress level are more applicable to field conditions and were employed throughout this work.

The tests on the specimens lasted for one year and included two loading and unloading cycles, where 50% of the load was removed during unloading. The strain versus time curves developed followed the expected trends, with creep deformation accumulating during loading and recovery of some of the creep deformation occurring during unloading.

8.1.2 Material Modeling

The experimental data obtained from material characterization testing were fit using viscoelastic material models to determine material constants that were later

Reproduced with permission of the copyright owner. Further reproduction prohibited without permission.

embedded into the ABAQUS© finite element code to simulate liner response. Both generalized Kelvin and Maxwell Models were required. Specific conclusions are given below:

- The creep and recovery data was initially fit using a five-unit Kelvin Model that described the compliance of the material as a function of time and stress. A total of 12 fitting constants were required to describe material response
- Because viscoelastic response is modeled in ABAQUS© using a PRONY series which describes the time-dependent stiffness or modulus of the material, the 12 fitting constants (or retardation constants) associated with the generalized Kelvin Model were converted to 12 relaxation constants (or to a PRONY series) as governed by the generalized Maxwell Model.
- The resulting PRONY series constants were embedded into a single element ABAQUS© model under variable loading to simulate material response. The ABAQUS© strain versus time results closely matched the material characterization data, thus confirming the effectiveness of the ABAQUS© model in simulating the response of the liner material.

8.1.3 Finite Element Modeling

To address the need for a liner design model that includes the influence of groundwater variation, finite element simulations of pipe liners subjected seasonal groundwater variation were completed using ABAQUS©. A 2-D liner buckling model was constructed for a liner having 5% ovality, 0.4% gap and a DR of 32.5. A standard four-node, two-dimensional plane-strain element, CPE4, was chosen to represent the liner. A large number of finite element simulations were completed to simulate the response of

Reproduced with permission of the copyright owner. Further reproduction prohibited without permission.

the higher compliance and higher stiffness PVC materials under variable loading conditions. The key findings are given below:

- Variations in groundwater levels are influenced by both natural conditions and human factors and often vary significantly due to wet and dry seasons. A trapezoidal groundwater loading pattern was adopted to simulate three distinct groundwater histories: longer peak pressure with shorter low pressure ($t_{high} > t_{low}$), equal peak and low pressure periods ($t_{high} = t_{low}$), and shorter peak pressure with longer low pressure ($t_{low} > t_{high}$).
- Two factors were defined to define the groundwater loading history. The time variation ratio TVR is defined as t_{low} / t_{high}, and the depth variation ratio DVR is defined as H_{low} / H_{high} where H is the depth of the liner below the water table surface.
- The simulations indicate that liners designed for a 50-year life can withstand higher peak pressures when groundwater levels vary seasonally.
- The long-term deflection of a liner at the critical point depends on both TVR and DVR. When TVR is held to a constant, a decrease in DVR leads to more recovery and lower displacements. And, when DVR is held to a constant, increasing TVR results in lower deflections and longer life.
- As the number of loading cycles increase, recovery occurred at more frequent intervals and resulted in displacements. Pipe liners last longer when they are subjected to frequent recovery periods.

Reproduced with permission of the copyright owner. Further reproduction prohibited without permission.

- The recovery of the liner induced by the dry season will make the liner deform less over time and last longer. Also, for a fixed wet-season groundwater level, a thinner liner subjected to variable loading will have the same life as a thicker liner subjected to constant loading.

8.1.4 Modified ASTM Liner Design Approach

The liner design model given by ASTM F1216-05 was modified to account for variable groundwater loading by introducing a correction factor. The correction factor was defined as the 50-year pressure due to variable groundwater loading divided by the 50-year pressure due to constant loading (P_{50v}/P_{50}). Conclusions relating to the new design model are given below:

- The correction factor will always have a value greater than or equal to 1.
- The correction factor depends on DVR and TVR. Tables listing correction factors for DVR and TVR combinations were presented for 3-month and 6-month loading cycles for the higher compliance and higher stiffness PVC liner materials. DVR values of 1/4, 1/2 and 3/4 were considered along with TVR values of 1/3, 1 and 3.
- The correction factor increases as DVR decreases and as TVR increases, indicating that significantly thinner liners can be used for low DVR and high TVR combinations. Example calculations for three liner design cases were presented.
- The correction factors were determined based on ABAQUS© simulations for a given set of liner geometry parameters and for two different PVC materials. The correction factors do not explicitly depend on liner geometry, indicating that the correction factors could be used with caution for other liner geometries (different

Reproduced with permission of the copyright owner. Further reproduction prohibited without permission.

gaps and ovalities). However, the correction factors will likely show significant dependence on the creep and recovery properties of the liner materials; liner materials that exhibit more recovery will have higher correction factors than liners that show less recovery (or material memory). Also, for the two materials studied, the higher compliance (the material that creeps the most) benefits more from the reduced load during the variable loading period than the higher stiffness material. That is, the correction factors are higher for the higher compliance material.

- While the correction factor was applied to the ASTM liner design model for partially deteriorated pipe liners, the same factors can be applied to any other long-term liner design model where the groundwater level is a design variable. In this case, the groundwater pressure should be divided by the correction factor. In other words, the finite element simulations on which the correction factors are based in no way depend on the ASTM F1216 design model.

8.2 Recommendations

- The long-term behavior of the PVC liners material studied here was based on the assumption that there is no physical aging of the material over its 50-year life. However, for polymer materials, the short-term stiffness of the material often increases slowly with time. Further research should consider the effect of aging on the structural behavior of the PVC liners.
- Future studies should study the impact of variable loading on other materials such as CIPP (Cured-In-Place-Pipe) materials. This will allow the extension of the correction factors to include other materials that are commonly used in pipeline rehabilitation applications.

Reproduced with permission of the copyright owner. Further reproduction prohibited without permission.

- The finite element simulations of liner behavior were performed for a liner having 5% ovality and 0.4% gap with a DR of 32.5. Future studies should study the influence of these geometric parameters on liners subjected to variable loading.
- A trapezoidal loading pattern was chosen to simulate seasonal groundwater loading. However, the variation can be much more complex in actual field conditions. Future studies should simulate more loading conditions.
- In some situations, the water level may have significant fluctuation over a short period of time (several days) and then recede. Further studies should study the loading pattern for short peaks with long low periods. These studies would be valuable to engineers designing liners for creek crossings, where the water level can rapidly rise over a short period of time and then recede within hours or days.

Reproduced with permission of the copyright owner. Further reproduction prohibited without permission.

APPENDIX A

MATERIAL CHARACTERIZATION DATA

Reproduced with permission of the copyright owner. Further reproduction prohibited without permission.

Table A.1 Experimental data for higher compliance PVC specimen - HC01

SAMPLE : LBHC01
Test Type : Three-point Bending
Yield strength = 4100 psi
Stress Level: 205 psi (5% of yield strength)
Specimen Thickness: 0.253 in.
Specimen Width: 1.084 in.
Length of Specimen: 4 in.
Total Load: 2.371 lb

1. Stress = 205 psi (Initial Loading)

Time (hr)	Deformation (in)	Strain
0	0.01295	0.00123
0.017	0.01365	0.00130
0.1	0.01465	0.00139
0.2	0.01598	0.00152
0.5	0.01675	0.00159
1	0.01770	0.00168
2	0.01915	0.00182
5	0.02055	0.00195
20	0.02135	0.00203
44	0.02255	0.00214
92	0.02383	0.00226
212	0.02566	0.00243
500	0.02810	0.00267
692	0.02933	0.00278
980	0.03027	0.00287
2136	0.03300	0.00313

2. Stress = 102.5 psi (First Recovery)

Time (hr)	Deformation (in)	Strain
0	0.02600	0.00247
0.017	0.02562	0.00243
0.1	0.02500	0.00237
0.2	0.02470	0.00234
0.5	0.02402	0.00228
1	0.02370	0.00225
2	0.02321	0.00220
5	0.02273	0.00216
20	0.02218	0.00210
44	0.02180	0.00207
92	0.02127	0.00202
212	0.02060	0.00195
500	0.01959	0.00186
692	0.01942	0.00184
980	0.01921	0.00182
2184	0.01858	0.00176

3. Stress = 205 psi (Second Loading)

Time (hr)	Deformation (in)	Strain
0	0.02470	0.00234
0.017	0.02520	0.00239
0.1	0.02580	0.00245
0.2	0.02587	0.00245
0.5	0.02628	0.00249
1	0.02660	0.00252
2	0.02702	0.00256
5	0.02706	0.00257
20	0.02865	0.00272
44	0.02915	0.00277
92	0.02989	0.00284
212	0.03080	0.00292
500	0.03180	0.00302
692	0.02933	0.00278
980	0.03222	0.00306
2160	0.03430	0.00325

4. Stress = 102.5 psi (Second Recovery)

Time (hr)	Deformation (in)	Strain
0	0.02790	0.00265
0.017	0.02770	0.00263
0.1	0.02727	0.00259
0.2	0.02671	0.00253
0.5	0.02610	0.00248
1	0.02580	0.00245
2	0.02559	0.00243
5	0.02530	0.00240
20	0.02470	0.00234
44	0.02420	0.00230
92	0.02360	0.00224
212	0.02300	0.00218
500	0.02186	0.00207
692	0.02160	0.00205
980	0.02118	0.00201
2160	0.02070	0.00196

Reproduced with permission of the copyright owner. Further reproduction prohibited without permission.

Table A.2 Experimental data for higher compliance PVC specimen - HC02

SAMPLE : LBHC02
Test Type : Three-point Bending
Yield strength = 4100 psi
Stress Level: 205 psi (5% of yield strength)
Specimen Thickness: 0.253 in.
Specimen Width: 1.044 in.
Length of Specimen: 4 in.
Total Load: 2.283 lb

1. Stress = 205 psi (Initial Loading)

Time (hr)	Deformation (in)	Strain
0	0.01290	0.00122
0.017	0.01390	0.00132
0.1	0.01450	0.00138
0.2	0.01600	0.00152
0.5	0.01760	0.00167
1	0.01820	0.00173
2	0.01951	0.00185
5	0.02076	0.00197
20	0.02160	0.00205
44	0.02265	0.00215
92	0.02383	0.00226
212	0.02564	0.00243
500	0.02851	0.00270
692	0.02955	0.00280
980	0.03043	0.00289
2136	0.03236	0.00307

2. Stress = 102.5 psi (First Recovery)

Time (hr)	Deformation (in)	Strain
0	0.02706	0.00257
0.017	0.02648	0.00251
0.1	0.02606	0.00247
0.2	0.02581	0.00245
0.5	0.02533	0.00240
1	0.02511	0.00238
2	0.02461	0.00233
5	0.02408	0.00228
20	0.02351	0.00223
44	0.02293	0.00218
92	0.02180	0.00207
212	0.02075	0.00197
500	0.01971	0.00187
692	0.01950	0.00185
980	0.01929	0.00183
2184	0.01886	0.00179

3. Stress = 205 psi (Second Loading)

Time (hr)	Deformation (in)	Strain
0	0.02616	0.00248
0.017	0.02656	0.00252
0.1	0.02700	0.00256
0.2	0.02716	0.00258
0.5	0.02734	0.00259
1	0.02774	0.00263
2	0.02811	0.00267
5	0.02855	0.00271
20	0.02944	0.00279
44	0.02990	0.00284
92	0.03045	0.00289
212	0.03073	0.00292
500	0.03214	0.00305
692	0.03266	0.00310
980	0.03325	0.00315
2160	0.03449	0.00327

4. Stress = 102.5 psi (Second Recovery)

Time (hr)	Deformation (in)	Strain
0	0.02936	0.00279
0.017	0.02856	0.00271
0.1	0.02819	0.00267
0.2	0.02801	0.00266
0.5	0.02795	0.00265
1	0.02771	0.00263
2	0.02710	0.00257
5	0.02698	0.00256
20	0.02646	0.00251
44	0.02606	0.00247
92	0.02528	0.00240
212	0.02486	0.00236
500	0.02390	0.00227
692	0.02374	0.00225
980	0.02332	0.00221
2160	0.02310	0.00219

Reproduced with permission of the copyright owner. Further reproduction prohibited without permission.

Table A.3 Experimental data for higher compliance PVC specimen - HC03

SAMPLE : LBHC03
Test Type : Three-point Bending
Yield strength = 4100 psi
Stress Level: 205 psi (5% of yield strength)
Specimen Thickness: 0.239 in.
Specimen Width: 1.030 in.
Length of Specimen: 4 in.
Total Load: 2.010 lb

1. Stress = 205 psi (Initial Loading)

Time (hr)	Deformation (in)	Strain
0	0.01341	0.00120
0.017	0.01439	0.00129
0.1	0.01484	0.00133
0.2	0.01579	0.00142
0.5	0.01741	0.00156
1	0.01821	0.00163
2	0.01963	0.00176
5	0.02106	0.00189
20	0.02179	0.00195
44	0.02296	0.00206
92	0.02436	0.00218
212	0.02638	0.00236
500	0.02959	0.00265
692	0.03065	0.00275
980	0.03208	0.00288
2136	0.03405	0.00305

2. Stress = 102.5 psi (First Recovery)

Time (hr)	Deformation (in)	Strain
0	0.02754	0.00247
0.017	0.02692	0.00241
0.1	0.02645	0.00237
0.2	0.02619	0.00235
0.5	0.02557	0.00229
1	0.02474	0.00222
2	0.02454	0.00220
5	0.02422	0.00217
20	0.02344	0.00210
44	0.02304	0.00206
92	0.02229	0.00200
212	0.02183	0.00196
500	0.02059	0.00185
692	0.02028	0.00182
980	0.02000	0.00179
2184	0.01968	0.00176

3. Stress = 205 psi (Second Loading)

Time (hr)	Deformation (in)	Strain
0	0.02640	0.00237
0.017	0.02720	0.00244
0.1	0.02780	0.00249
0.2	0.02802	0.00251
0.5	0.02860	0.00256
1	0.02898	0.00260
2	0.02918	0.00262
5	0.02955	0.00265
20	0.03032	0.00272
44	0.03100	0.00278
92	0.03161	0.00283
212	0.03272	0.00293
500	0.03390	0.00304
692	0.03427	0.00307
980	0.03488	0.00313
2160	0.03650	0.00327

4. Stress = 102.5 psi (Second Recovery)

Time (hr)	Deformation (in)	Strain
0	0.03040	0.00272
0.017	0.02940	0.00263
0.1	0.02898	0.00260
0.2	0.02857	0.00256
0.5	0.02802	0.00251
1	0.02759	0.00247
2	0.02753	0.00247
5	0.02740	0.00246
20	0.02680	0.00240
44	0.02660	0.00238
92	0.02584	0.00232
212	0.02512	0.00225
500	0.02398	0.00215
692	0.02368	0.00212
980	0.02325	0.00208
2160	0.02275	0.00204

Reproduced with permission of the copyright owner. Further reproduction prohibited without permission.

Table A.4 Experimental data for higher compliance PVC specimen - HC04

SAMPLE : LBHC04
Test Type : Three-point Bending
Yield strength = 4100 psi
Stress Level: 205 psi (5% of yield strength)
Specimen Thickness: 0.255 in.
Specimen Width: 1.066 in.
Length of Specimen: 4 in.
Total Load: 2.368 lb

1. Stress = 205 psi (Initial Loading)

Time (hr)	Deformation (in)	Strain
0	0.01292	0.00124
0.017	0.01421	0.00136
0.1	0.01461	0.00140
0.2	0.01659	0.00159
0.5	0.01727	0.00165
1	0.01780	0.00170
2	0.01920	0.00184
5	0.01994	0.00191
20	0.02077	0.00199
44	0.02162	0.00207
92	0.02292	0.00219
212	0.02459	0.00235
500	0.02695	0.00258
692	0.02781	0.00266
980	0.02894	0.00277
2136	0.03115	0.00298

2. Stress = 102.5 psi (First Recovery)

Time (hr)	Deformation (in)	Strain
0	0.02399	0.00229
0.017	0.02329	0.00223
0.1	0.02278	0.00218
0.2	0.02237	0.00214
0.5	0.02174	0.00208
1	0.02114	0.00202
2	0.02069	0.00198
5	0.02041	0.00195
20	0.02029	0.00194
44	0.02001	0.00191
92	0.01957	0.00187
212	0.01866	0.00178
500	0.01785	0.00171
692	0.01764	0.00169
980	0.01748	0.00167
2184	0.01694	0.00162

3. Stress = 205 psi (Second Loading)

Time (hr)	Deformation (in)	Strain
0	0.02266	0.00217
0.017	0.02324	0.00222
0.1	0.02380	0.00228
0.2	0.02417	0.00231
0.5	0.02464	0.00236
1	0.02496	0.00239
2	0.02534	0.00242
5	0.02547	0.00244
20	0.02626	0.00251
44	0.02679	0.00256
92	0.02746	0.00263
212	0.02845	0.00272
500	0.02966	0.00284
692	0.03001	0.00287
980	0.03036	0.00290
2160	0.03168	0.00303

4. Stress = 102.5 psi (Second Recovery)

Time (hr)	Deformation (in)	Strain
0	0.02566	0.00245
0.017	0.02509	0.00240
0.1	0.02451	0.00234
0.2	0.02425	0.00232
0.5	0.02408	0.00230
1	0.02344	0.00224
2	0.02321	0.00222
5	0.02316	0.00221
20	0.02274	0.00217
44	0.02240	0.00214
92	0.02173	0.00208
212	0.02086	0.00199
500	0.01983	0.00190
692	0.01954	0.00187
980	0.01918	0.00183
2160	0.01898	0.00181

Reproduced with permission of the copyright owner. Further reproduction prohibited without permission.

Table A.5 Experimental data for higher compliance PVC specimen - HC05

SAMPLE : LBHC05
Test Type : Three-point Bending
Yield strength = 4100 psi
Stress Level: 410 psi (10% of yield strength)
Specimen Thickness: 0.255 in.
Specimen Width: 0.947 in.
Length of Specimen: 4 in.
Total Load: 4.208 lb

1. Stress = 410 psi (Initial Loading)

Time (hr)	Deformation (in)	Strain
0	0.0310	0.0030
0.017	0.0324	0.0031
0.1	0.0345	0.0033
0.2	0.0360	0.0034
0.5	0.0375	0.0036
1	0.0399	0.0038
2	0.0420	0.0040
5	0.0443	0.0042
20	0.0455	0.0044
44	0.0475	0.0045
92	0.0503	0.0048
212	0.0535	0.0051
500	0.0583	0.0056
692	0.0602	0.0058
980	0.0631	0.0060
2136	0.0675	0.0065

2. Stress = 205 psi (First Recovery)

Time (hr)	Deformation (in)	Strain
0	0.0559	0.0053
0.017	0.0539	0.0052
0.1	0.0527	0.0050
0.2	0.0521	0.0050
0.5	0.0511	0.0049
1	0.0506	0.0048
2	0.0499	0.0048
5	0.0489	0.0047
20	0.0478	0.0046
44	0.0469	0.0045
92	0.0459	0.0044
212	0.0446	0.0043
500	0.0434	0.0042
692	0.0428	0.0041
980	0.0421	0.0040
2184	0.0414	0.0040

3. Stress = 410 psi (Second Loading)

Time (hr)	Deformation (in)	Strain
0	0.0519	0.0050
0.017	0.0537	0.0051
0.1	0.0546	0.0052
0.2	0.0549	0.0052
0.5	0.0555	0.0053
1	0.0559	0.0053
2	0.0567	0.0054
5	0.0589	0.0056
20	0.0591	0.0057
44	0.0602	0.0058
92	0.0615	0.0059
212	0.0631	0.0060
500	0.0649	0.0062
692	0.0658	0.0063
980	0.0669	0.0064
2160	0.0698	0.0067

4. Stress = 205 psi (Second Recovery)

Time (hr)	Deformation (in)	Strain
0	0.0579	0.0055
0.017	0.0569	0.0054
0.1	0.0557	0.0053
0.2	0.0549	0.0052
0.5	0.0540	0.0052
1	0.0534	0.0051
2	0.0531	0.0051
5	0.0527	0.0050
20	0.0517	0.0049
44	0.0508	0.0049
92	0.0496	0.0047
212	0.0474	0.0045
500	0.0469	0.0045
692	0.0467	0.0045
980	0.0462	0.0044
2160	0.0454	0.0043

Reproduced with permission of the copyright owner. Further reproduction prohibited without permission.

Table A.6 Experimental data for higher compliance PVC specimen - HC06

SAMPLE : LBHC06
Test Type : Three-point Bending
Yield strength = 4100 psi
Stress Level: 410 psi (10% of the yield strength)
Specimen Thickness: 0.235 in.
Specimen Width: 1.054 in.
Length of Specimen: 4 in.
Total Load: 3.977 lb

1. Stress = 410 psi (Initial Loading)

Time (hr)	Deformation (in)	Strain
0	0.0341	0.0030
0.017	0.0370	0.0033
0.1	0.0410	0.0036
0.2	0.0419	0.0037
0.5	0.0441	0.0039
1	0.0466	0.0041
2	0.0491	0.0043
5	0.0519	0.0046
20	0.0539	0.0047
44	0.0563	0.0050
92	0.0591	0.0052
212	0.0631	0.0056
500	0.0689	0.0061
692	0.0714	0.0063
980	0.0738	0.0065
2136	0.0789	0.0070

2. Stress = 205 psi (First Recovery)

Time (hr)	Deformation (in)	Strain
0	0.0641	0.0056
0.017	0.0623	0.0055
0.1	0.0611	0.0054
0.2	0.0606	0.0053
0.5	0.0593	0.0052
1	0.0584	0.0051
2	0.0576	0.0051
5	0.0566	0.0050
20	0.0555	0.0049
44	0.0545	0.0048
92	0.0536	0.0047
212	0.0518	0.0046
500	0.0501	0.0044
692	0.0496	0.0044
980	0.0487	0.0043
2184	0.0478	0.0042

3. Stress = 410 psi (Second Loading)

Time (hr)	Deformation (in)	Strain
0	0.0608	0.0054
0.017	0.0624	0.0055
0.1	0.0636	0.0056
0.2	0.0641	0.0056
0.5	0.0649	0.0057
1	0.0654	0.0058
2	0.0661	0.0058
5	0.0671	0.0059
20	0.0689	0.0061
44	0.0701	0.0062
92	0.0719	0.0063
212	0.0737	0.0065
500	0.0759	0.0067
692	0.0768	0.0068
980	0.0783	0.0069
2160	0.0816	0.0072

4. Stress = 205 psi (Second Recovery)

Time (hr)	Deformation (in)	Strain
0	0.0681	0.0060
0.017	0.0661	0.0058
0.1	0.0649	0.0057
0.2	0.0641	0.0056
0.5	0.0631	0.0056
1	0.0621	0.0055
2	0.0617	0.0054
5	0.0612	0.0054
20	0.0601	0.0053
44	0.0591	0.0052
92	0.0579	0.0051
212	0.0564	0.0050
500	0.0549	0.0048
692	0.0547	0.0048
980	0.0537	0.0047
2160	0.0530	0.0047

Reproduced with permission of the copyright owner. Further reproduction prohibited without permission.

Table A.7 Experimental data for higher compliance PVC specimen - HC08

SAMPLE : LBHC08
Test Type : Three-point Bending
Yield strength = 4100 psi
Stress Level: 410 psi (10% of yield strength)
Specimen Thickness: 0.237 in.
Specimen Width: 0.978 in.
Length of Specimen: 4 in.
Total Load: 3.754 lb

1. Stress = 410 psi (Initial Loading)

Time (hr)	Deformation (in)	Strain
0	0.0332	0.0030
0.017	0.0366	0.0033
0.1	0.0392	0.0035
0.2	0.0407	0.0036
0.5	0.0432	0.0038
1	0.0451	0.0040
2	0.0473	0.0042
5	0.0501	0.0045
20	0.0517	0.0046
44	0.0542	0.0048
92	0.0567	0.0050
212	0.0604	0.0054
500	0.0660	0.0059
692	0.0686	0.0061
980	0.0711	0.0063
2136	0.0762	0.0068

2. Stress = 205 psi (First Recovery)

Time (hr)	Deformation (in)	Strain
0	0.0621	0.0055
0.017	0.0611	0.0054
0.1	0.0601	0.0053
0.2	0.0594	0.0053
0.5	0.0583	0.0052
1	0.0576	0.0051
2	0.0569	0.0051
5	0.0559	0.0050
20	0.0549	0.0049
44	0.0539	0.0048
92	0.0530	0.0047
212	0.0515	0.0046
500	0.0503	0.0045
692	0.0499	0.0044
980	0.0493	0.0044
2184	0.0489	0.0043

3. Stress = 410 psi (Second Loading)

Time (hr)	Deformation (in)	Strain
0	0.0604	0.0054
0.017	0.0621	0.0055
0.1	0.0632	0.0056
0.2	0.0639	0.0057
0.5	0.0645	0.0057
1	0.0651	0.0058
2	0.0659	0.0059
5	0.0667	0.0059
20	0.0682	0.0061
44	0.0695	0.0062
92	0.0709	0.0063
212	0.0724	0.0064
500	0.0745	0.0066
692	0.0753	0.0067
980	0.0766	0.0068
2160	0.0801	0.0071

4. Stress = 205 psi (Second Recovery)

Time (hr)	Deformation (in)	Strain
0	0.0671	0.0060
0.017	0.0652	0.0058
0.1	0.0642	0.0057
0.2	0.0639	0.0057
0.5	0.0629	0.0056
1	0.0621	0.0055
2	0.0616	0.0055
5	0.0611	0.0054
20	0.0601	0.0053
44	0.0591	0.0053
92	0.0580	0.0052
212	0.0567	0.0050
500	0.0554	0.0049
692	0.0551	0.0049
980	0.0543	0.0048
2160	0.0536	0.0048

Reproduced with permission of the copyright owner. Further reproduction prohibited without permission.

Table A.8 Experimental data for higher stiffness PVC specimen - HS01

SAMPLE : LBHS01
Test Type : Three-point Bending
Yield strength = 5000 psi
Stress Level: 250 psi (5% of yield strength)
Specimen Thickness: 0.256 in.
Specimen Width: 1.036 in.
Length of Specimen: 4 in.
Total Load: 2.829 lb

1. Stress = 250 psi (Initial Loading)

Time (hr)	Deformation (in)	Strain
0	0.01319	0.00127
0.017	0.01379	0.00132
0.1	0.01437	0.00138
0.2	0.01475	0.00142
0.5	0.01516	0.00146
1	0.01584	0.00152
2	0.01619	0.00155
5	0.01658	0.00159
20	0.01695	0.00163
44	0.01732	0.00166
92	0.01812	0.00174
212	0.01915	0.00184
500	0.02105	0.00202
692	0.02187	0.00210
980	0.02272	0.00218
2136	0.02372	0.00228

2. Stress = 125 psi (First Recovery)

Time (hr)	Deformation (in)	Strain
0	0.01872	0.00180
0.017	0.01852	0.00178
0.1	0.01832	0.00176
0.2	0.01803	0.00173
0.5	0.01794	0.00172
1	0.01771	0.00170
2	0.01762	0.00169
5	0.01747	0.00168
20	0.01717	0.00165
44	0.01711	0.00164
92	0.01673	0.00161
212	0.01656	0.00159
500	0.01625	0.00156
692	0.01624	0.00156
980	0.01622	0.00156
2184	0.01602	0.00154

3. Stress = 250 psi (Second Loading)

Time (hr)	Deformation (in)	Strain
0	0.02112	0.00203
0.017	0.02137	0.00205
0.1	0.02140	0.00205
0.2	0.02167	0.00208
0.5	0.02170	0.00208
1	0.02172	0.00209
2	0.02180	0.00209
5	0.02193	0.00211
20	0.02214	0.00213
44	0.02245	0.00216
92	0.02310	0.00222
212	0.02335	0.00224
500	0.02401	0.00230
692	0.02428	0.00233
980	0.02461	0.00236
2160	0.02480	0.00238

4. Stress = 125 psi (Second Recovery)

Time (hr)	Deformation (in)	Strain
0	0.02072	0.00199
0.017	0.02012	0.00193
0.1	0.01987	0.00191
0.2	0.01970	0.00189
0.5	0.01966	0.00189
1	0.01964	0.00189
2	0.01949	0.00187
5	0.01938	0.00186
20	0.01912	0.00184
44	0.01890	0.00181
92	0.01862	0.00179
212	0.01812	0.00174
500	0.01768	0.00170
692	0.01767	0.00170
980	0.01749	0.00168
2160	0.01739	0.00167

Reproduced with permission of the copyright owner. Further reproduction prohibited without permission.

Table A.9 Experimental data for higher stiffness PVC specimen - HS02

SAMPLE : LBHS02
Test Type : Three-point Bending
Yield strength = 5000 psi
Stress Level: 250 psi (5% of yield strength)
Specimen Thickness: 0.242 in.
Specimen Width: 1.142 in.
Length of Specimen: 4 in.
Total Load: 2.787 lb

1. Stress = 250 psi (Initial Loading)

Time (hr)	Deformation (in)	Strain
0	0.01495	0.00136
0.017	0.01546	0.00140
0.1	0.01637	0.00149
0.2	0.01678	0.00152
0.5	0.01718	0.00156
1	0.01796	0.00163
2	0.01846	0.00168
5	0.01893	0.00172
20	0.01925	0.00175
44	0.01990	0.00181
92	0.02081	0.00189
212	0.02197	0.00199
500	0.02386	0.00217
692	0.02458	0.00223
980	0.02537	0.00230
2184	0.02696	0.00245

2. Stress = 125 psi (First Recovery)

Time (hr)	Deformation (in)	Strain
0	0.02047	0.00186
0.017	0.02012	0.00183
0.1	0.01986	0.00180
0.2	0.01953	0.00177
0.5	0.01935	0.00176
1	0.01924	0.00175
2	0.01882	0.00171
5	0.01851	0.00168
20	0.01824	0.00166
44	0.01777	0.00161
92	0.01757	0.00159
212	0.01719	0.00156
500	0.01675	0.00152
692	0.01672	0.00152
980	0.01670	0.00152
2184	0.01649	0.00150

3. Stress = 250 psi (Second Loading)

Time (hr)	Deformation (in)	Strain
0	0.02240	0.00203
0.017	0.02278	0.00207
0.1	0.02307	0.00209
0.2	0.02320	0.00211
0.5	0.02360	0.00214
1	0.02370	0.00215
2	0.02390	0.00217
5	0.02420	0.00220
20	0.02470	0.00224
44	0.02500	0.00227
92	0.02567	0.00233
212	0.02592	0.00235
500	0.02688	0.00244
692	0.02706	0.00246
980	0.02720	0.00247
2160	0.02823	0.00256

4. Stress = 125 psi (Second Recovery)

Time (hr)	Deformation (in)	Strain
0	0.02230	0.00202
0.017	0.02172	0.00197
0.1	0.02168	0.00197
0.2	0.02145	0.00195
0.5	0.02120	0.00192
1	0.02105	0.00191
2	0.02092	0.00190
5	0.02080	0.00189
20	0.02040	0.00185
44	0.02010	0.00182
92	0.01977	0.00179
212	0.01930	0.00175
500	0.01868	0.00170
692	0.01855	0.00168
980	0.01825	0.00166
2160	0.01791	0.00163

Reproduced with permission of the copyright owner. Further reproduction prohibited without permission.

Table A.10 Experimental data for higher stiffness PVC specimen - HS03

SAMPLE : LBHS03
Test Type : Three-point Bending
Yield strength = 5000 psi
Stress Level: 250 psi (5% of yield strength)
Specimen Thickness: 0.235 in.
Specimen Width: 1.120 in.
Length of Specimen: 4 in.
Total Load: 2.577 lb

1. Stress = 250 psi (Initial Loading)

Time (hr)	Deformation (in)	Strain
0	0.01496	0.00132
0.017	0.01579	0.00139
0.1	0.01668	0.00147
0.2	0.01710	0.00151
0.5	0.01766	0.00156
1	0.01835	0.00162
2	0.01887	0.00166
5	0.01938	0.00171
20	0.01985	0.00175
44	0.02052	0.00181
92	0.02135	0.00188
212	0.02241	0.00197
500	0.02376	0.00209
692	0.02451	0.00216
980	0.02513	0.00221
2136	0.02623	0.00231

2. Stress = 125 psi (First Recovery)

Time (hr)	Deformation (in)	Strain
0	0.02143	0.00189
0.017	0.02123	0.00187
0.1	0.02092	0.00184
0.2	0.02071	0.00183
0.5	0.02045	0.00180
1	0.02028	0.00179
2	0.02013	0.00177
5	0.01984	0.00175
20	0.01958	0.00173
44	0.01923	0.00169
92	0.01903	0.00168
212	0.01870	0.00165
500	0.01827	0.00161
692	0.01825	0.00161
980	0.01796	0.00158
2184	0.01771	0.00156

3. Stress =250 psi (Second Loading)

Time (hr)	Deformation (in)	Strain
0	0.02273	0.00200
0.017	0.02323	0.00205
0.1	0.02345	0.00207
0.2	0.02368	0.00209
0.5	0.02389	0.00211
1	0.02395	0.00211
2	0.02413	0.00213
5	0.02435	0.00215
20	0.02480	0.00219
44	0.02504	0.00221
92	0.02553	0.00225
212	0.02588	0.00228
500	0.02658	0.00234
692	0.02684	0.00237
980	0.02716	0.00239
2160	0.02813	0.00248

4. Stress = 125 psi (Second Recovery)

Time (hr)	Deformation (in)	Strain
0	0.02353	0.00207
0.017	0.02261	0.00199
0.1	0.02242	0.00198
0.2	0.02223	0.00196
0.5	0.02208	0.00195
1	0.02201	0.00194
2	0.02183	0.00192
5	0.02171	0.00191
20	0.02143	0.00189
44	0.02131	0.00188
92	0.02100	0.00185
212	0.02053	0.00181
500	0.02020	0.00178
692	0.02003	0.00177
980	0.01970	0.00174
2160	0.01965	0.00173

Reproduced with permission of the copyright owner. Further reproduction prohibited without permission.

Table A.11 Experimental data for higher stiffness PVC specimen - HS04

SAMPLE : LBHS04
Test Type : Three-point Bending
Yield strength = 5000 psi
Stress Level: 250 psi (5% of yield strength)
Specimen Thickness: 0.243 in.
Specimen Width: 1.064 in.
Length of Specimen: 4 in.
Total Load: 2.618 lb

1. Stress = 250 psi (Initial Loading)

Time (hr)	Deformation (in)	Strain
0	0.01451	0.00132
0.017	0.01491	0.00136
0.1	0.01559	0.00142
0.2	0.01591	0.00145
0.5	0.01671	0.00152
1	0.01719	0.00157
2	0.01771	0.00161
5	0.01816	0.00165
20	0.01855	0.00169
44	0.01886	0.00172
92	0.01960	0.00179
212	0.02061	0.00188
500	0.02197	0.00200
692	0.02256	0.00206
980	0.02310	0.00210
2136	0.02436	0.00222

2. Stress = 125 psi (First Recovery)

Time (hr)	Deformation (in)	Strain
0	0.01876	0.00171
0.017	0.01866	0.00170
0.1	0.01834	0.00167
0.2	0.01810	0.00165
0.5	0.01781	0.00162
1	0.01746	0.00159
2	0.01726	0.00157
5	0.01704	0.00155
20	0.01661	0.00151
44	0.01636	0.00149
92	0.01606	0.00146
212	0.01558	0.00142
500	0.01519	0.00138
692	0.01505	0.00137
980	0.01483	0.00135
2184	0.01446	0.00132

3. Stress = 250 psi (Second Loading)

Time (hr)	Deformation (in)	Strain
0	0.02016	0.00184
0.017	0.02056	0.00187
0.1	0.02086	0.00190
0.2	0.02093	0.00191
0.5	0.02108	0.00192
1	0.02131	0.00194
2	0.02149	0.00196
5	0.02178	0.00198
20	0.02208	0.00201
44	0.02242	0.00204
92	0.02299	0.00209
212	0.02336	0.00213
500	0.02401	0.00219
692	0.02438	0.00222
980	0.02453	0.00224
2160	0.02546	0.00232

4. Stress = 125 psi (Second Recovery)

Time (hr)	Deformation (in)	Strain
0	0.02026	0.00185
0.017	0.01966	0.00179
0.1	0.01936	0.00176
0.2	0.01916	0.00175
0.5	0.01891	0.00172
1	0.01886	0.00172
2	0.01876	0.00171
5	0.01866	0.00170
20	0.01826	0.00166
44	0.01806	0.00165
92	0.01784	0.00163
212	0.01746	0.00159
500	0.01669	0.00152
692	0.01654	0.00151
980	0.01618	0.00147
2160	0.01606	0.00146

Reproduced with permission of the copyright owner. Further reproduction prohibited without permission.

Table A.12 Experimental data for higher stiffness PVC specimen - HS05

SAMPLE : LBHS05
Test Type : Three-point Bending
Yield strength = 5000 psi
Stress Level: 500 psi (10% of yield strength)
Specimen Thickness: 0.244 in.
Specimen Width: 1.038 in.
Length of Specimen: 4 in.
Total Load: 5.150 lb

1. Stress = 500 psi (Initial Loading)

Time (hr)	Deformation (in)	Strain
0	0.0272	0.0025
0.017	0.0281	0.0026
0.1	0.0287	0.0026
0.2	0.0291	0.0027
0.5	0.0302	0.0028
1	0.0310	0.0028
2	0.0320	0.0029
5	0.0330	0.0030
20	0.0338	0.0031
44	0.0348	0.0032
92	0.0361	0.0033
212	0.0385	0.0035
500	0.0385	0.0035
692	0.0385	0.0035
980	0.0439	0.0040
2136	0.0439	0.0040

2. Stress = 250 psi (First Recovery)

Time (hr)	Deformation (in)	Strain
0	0.0370	0.0034
0.017	0.0362	0.0033
0.1	0.0353	0.0032
0.2	0.0342	0.0031
0.5	0.0335	0.0031
1	0.0333	0.0030
2	0.0329	0.0030
5	0.0325	0.0030
20	0.0320	0.0029
44	0.0315	0.0029
92	0.0311	0.0028
212	0.0304	0.0028
500	0.0296	0.0027
692	0.0295	0.0027
980	0.0294	0.0027
2184	0.0293	0.0027

3. Stress = 500 psi (Second Loading)

Time (hr)	Deformation (in)	Strain
0	0.0385	0.0035
0.017	0.0395	0.0036
0.1	0.0401	0.0037
0.2	0.0405	0.0037
0.5	0.0407	0.0037
1	0.0413	0.0038
2	0.0415	0.0038
5	0.0420	0.0038
20	0.0425	0.0039
44	0.0432	0.0040
92	0.0444	0.0041
212	0.0451	0.0041
500	0.0464	0.0042
692	0.0467	0.0043
980	0.0473	0.0043
2160	0.0487	0.0045

4. Stress = 250 psi (Second Recovery)

Time (hr)	Deformation (in)	Strain
0	0.0395	0.0036
0.017	0.0377	0.0034
0.1	0.0371	0.0034
0.2	0.0367	0.0034
0.5	0.0364	0.0033
1	0.0361	0.0033
2	0.0359	0.0033
5	0.0357	0.0033
20	0.0353	0.0032
44	0.0345	0.0032
92	0.0341	0.0031
212	0.0333	0.0030
500	0.0327	0.0030
692	0.0325	0.0030
980	0.0322	0.0029
2160	0.0317	0.0029

Reproduced with permission of the copyright owner. Further reproduction prohibited without permission.

Table A.13 Experimental data for higher stiffness PVC specimen - HS06

SAMPLE : LBHS06
Test Type : Three-point Bending
Yield strength = 5000 psi
Stress Level: 500 psi (10% of yield strength)
Specimen Thickness: 0.256 in.
Specimen Width: 1.056 in.
Length of Specimen: 4 in.
Total Load: 5.767 lb

1. Stress = 500 psi (Initial Loading)

Time (hr)	Deformation (in)	Strain
0	0.0250	0.0024
0.017	0.0262	0.0025
0.1	0.0273	0.0026
0.2	0.0280	0.0027
0.5	0.0289	0.0028
1	0.0296	0.0028
2	0.0307	0.0029
5	0.0318	0.0031
20	0.0324	0.0031
44	0.0336	0.0032
92	0.0349	0.0034
212	0.0368	0.0035
500	0.0392	0.0038
692	0.0400	0.0038
980	0.0416	0.0040
2136	0.0439	0.0042

2. Stress = 250 psi (First Recovery)

Time (hr)	Deformation (in)	Strain
0	0.0336	0.0032
0.017	0.0328	0.0031
0.1	0.0325	0.0031
0.2	0.0322	0.0031
0.5	0.0318	0.0031
1	0.0316	0.0030
2	0.0313	0.0030
5	0.0309	0.0030
20	0.0305	0.0029
44	0.0302	0.0029
92	0.0296	0.0028
212	0.0289	0.0028
500	0.0285	0.0027
692	0.0284	0.0027
980	0.0282	0.0027
2184	0.0276	0.0026

3. Stress = 500 psi (Second Loading)

Time (hr)	Deformation (in)	Strain
0	0.0366	0.0035
0.017	0.0376	0.0036
0.1	0.0383	0.0037
0.2	0.0386	0.0037
0.5	0.0386	0.0037
1	0.0388	0.0037
2	0.0393	0.0038
5	0.0396	0.0038
20	0.0404	0.0039
44	0.0410	0.0039
92	0.0416	0.0040
212	0.0422	0.0041
500	0.0434	0.0042
692	0.0439	0.0042
980	0.0441	0.0042
2160	0.0449	0.0043

4. Stress = 250 psi (Second Recovery)

Time (hr)	Deformation (in)	Strain
0	0.0366	0.0035
0.017	0.0353	0.0034
0.1	0.0346	0.0033
0.2	0.0344	0.0033
0.5	0.0341	0.0033
1	0.0339	0.0033
2	0.0336	0.0032
5	0.0333	0.0032
20	0.0329	0.0032
44	0.0326	0.0031
92	0.0321	0.0031
212	0.0316	0.0030
500	0.0308	0.0030
692	0.0308	0.0030
980	0.0305	0.0029
2160	0.0303	0.0029

Reproduced with permission of the copyright owner. Further reproduction prohibited without permission.

Table A.14 Experimental data for higher stiffness PVC specimen - HS07

SAMPLE : LBHS07
Test Type : Three-point Bending
Yield strength = 5000 psi
Stress Level: 500 psi (10% of yield strength)
Specimen Thickness: 0.243 in.
Specimen Width: 1.060 in.
Length of Specimen: 4 in.
Total Load: 5.216 lb

1. Stress = 500 psi (Initial Loading)

Time (hr)	Deformation (in)	Strain
0	0.0271	0.0025
0.017	0.0288	0.0026
0.1	0.0300	0.0027
0.2	0.0311	0.0028
0.5	0.0321	0.0029
1	0.0331	0.0030
2	0.0339	0.0031
5	0.0346	0.0032
20	0.0354	0.0032
44	0.0366	0.0033
92	0.0383	0.0035
212	0.0407	0.0037
500	0.0439	0.0040
692	0.0452	0.0041
980	0.0466	0.0042
2136	0.0496	0.0045

2. Stress = 250 psi (First Recovery)

Time (hr)	Deformation (in)	Strain
0	0.0386	0.0035
0.017	0.0375	0.0034
0.1	0.0368	0.0034
0.2	0.0366	0.0033
0.5	0.0364	0.0033
1	0.0360	0.0033
2	0.0357	0.0033
5	0.0353	0.0032
20	0.0349	0.0032
44	0.0346	0.0032
92	0.0340	0.0031
212	0.0331	0.0030
500	0.0324	0.0030
692	0.0321	0.0029
980	0.0318	0.0029
2184	0.0310	0.0028

3. Stress = 500 psi (Second Loading)

Time (hr)	Deformation (in)	Strain
0	0.0406	0.0037
0.017	0.0424	0.0039
0.1	0.0428	0.0039
0.2	0.0432	0.0039
0.5	0.0436	0.0040
1	0.0438	0.0040
2	0.0441	0.0040
5	0.0446	0.0041
20	0.0456	0.0042
44	0.0461	0.0042
92	0.0467	0.0043
212	0.0476	0.0043
500	0.0489	0.0045
692	0.0495	0.0045
980	0.0500	0.0046
2160	0.0518	0.0047

4. Stress = 250 psi (Second Recovery)

Time (hr)	Deformation (in)	Strain
0	0.0416	0.0038
0.017	0.0407	0.0037
0.1	0.0399	0.0036
0.2	0.0396	0.0036
0.5	0.0395	0.0036
1	0.0394	0.0036
2	0.0393	0.0036
5	0.0389	0.0035
20	0.0384	0.0035
44	0.0376	0.0034
92	0.0372	0.0034
212	0.0366	0.0033
500	0.0360	0.0033
692	0.0357	0.0033
980	0.0353	0.0032
2160	0.0348	0.0032

Reproduced with permission of the copyright owner. Further reproduction prohibited without permission.

Table A.15 Experimental data for higher stiffness PVC specimen - HS08

SAMPLE : LBHS08
Test Type : Three-point Bending
Yield strength = 5000 psi
Stress Level: 500 psi (10% of yield strength)
Specimen Thickness: 0.247 in.
Specimen Width: 1.048 in.
Length of Specimen: 4 in.
Total Load: 5.328 lb

1. Stress = 500 psi (Initial Loading)

Time (hr)	Deformation (in)	Strain
0	0.0259	0.0024
0.017	0.0279	0.0026
0.1	0.0292	0.0027
0.2	0.0304	0.0028
0.5	0.0314	0.0029
1	0.0319	0.0030
2	0.0329	0.0030
5	0.0339	0.0031
20	0.0349	0.0032
44	0.0359	0.0033
92	0.0371	0.0034
212	0.0394	0.0036
500	0.0428	0.0040
692	0.0447	0.0041
980	0.0462	0.0043
2136	0.0490	0.0045

2. Stress = 250 psi (First Recovery)

Time (hr)	Deformation (in)	Strain
0	0.0380	0.0035
0.017	0.0370	0.0034
0.1	0.0367	0.0034
0.2	0.0364	0.0034
0.5	0.0360	0.0033
1	0.0358	0.0033
2	0.0355	0.0033
5	0.0350	0.0032
20	0.0344	0.0032
44	0.0340	0.0031
92	0.0335	0.0031
212	0.0329	0.0030
500	0.0325	0.0030
692	0.0322	0.0030
980	0.0320	0.0030
2184	0.0312	0.0029

3. Stress = 500 psi (Second Loading)

Time (hr)	Deformation (in)	Strain
0	0.0410	0.0038
0.017	0.0420	0.0039
0.1	0.0425	0.0039
0.2	0.0428	0.0040
0.5	0.0430	0.0040
1	0.0433	0.0040
2	0.0435	0.0040
5	0.0440	0.0041
20	0.0450	0.0042
44	0.0455	0.0042
92	0.0462	0.0043
212	0.0470	0.0044
500	0.0483	0.0045
692	0.0489	0.0045
980	0.0494	0.0046
2160	0.0512	0.0047

4. Stress = 250 psi (Second Recovery)

Time (hr)	Deformation (in)	Strain
0	0.0410	0.0038
0.017	0.0398	0.0037
0.1	0.0390	0.0036
0.2	0.0390	0.0036
0.5	0.0388	0.0036
1	0.0385	0.0036
2	0.0381	0.0035
5	0.0379	0.0035
20	0.0371	0.0034
44	0.0368	0.0034
92	0.0363	0.0034
212	0.0356	0.0033
500	0.0349	0.0032
692	0.0348	0.0032
980	0.0342	0.0032
2160	0.0338	0.0031

Reproduced with permission of the copyright owner. Further reproduction prohibited without permission.

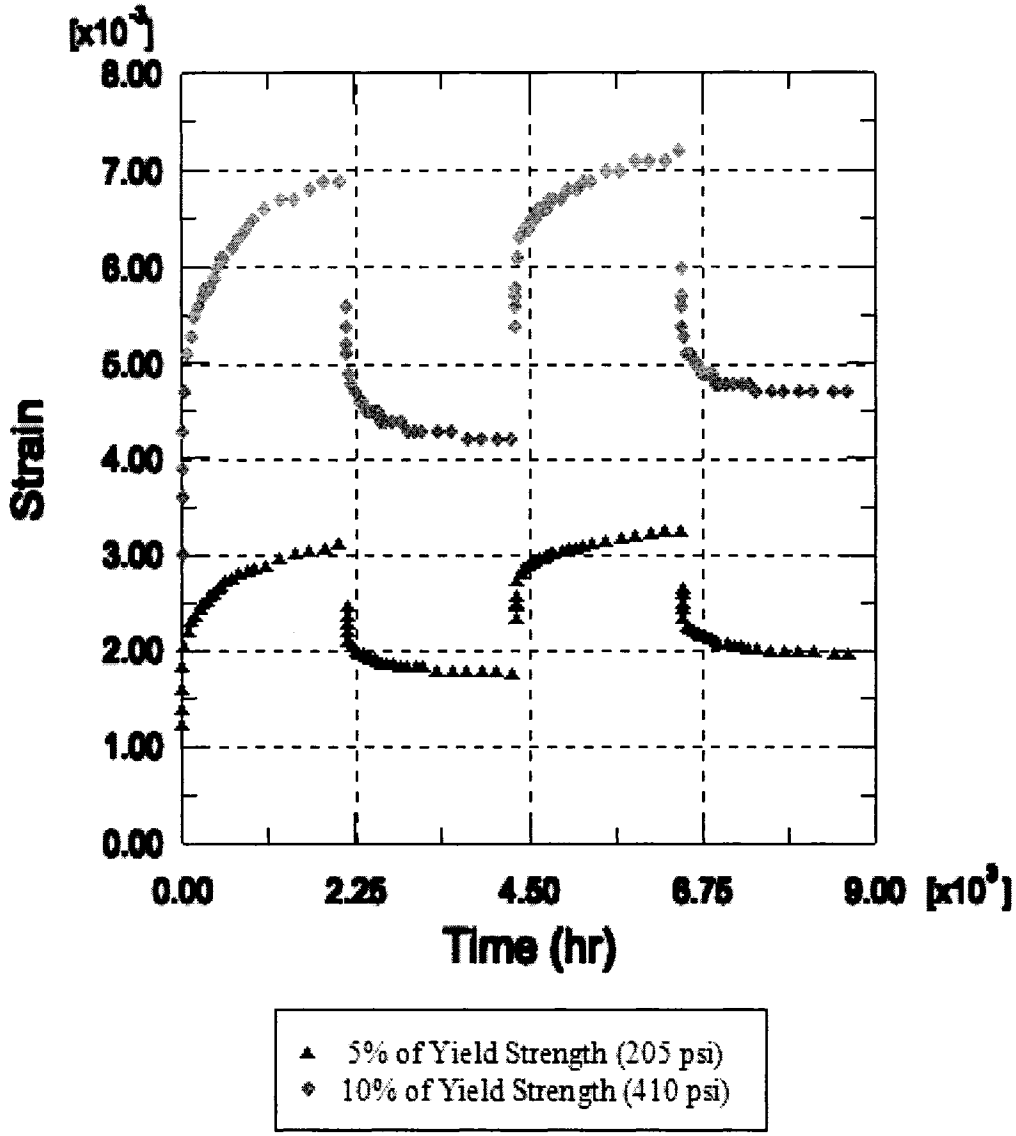

Fig. A.1 Average experimental strain vs. time for higher compliance PVC specimens

Reproduced with permission of the copyright owner. Further reproduction prohibited without permission.

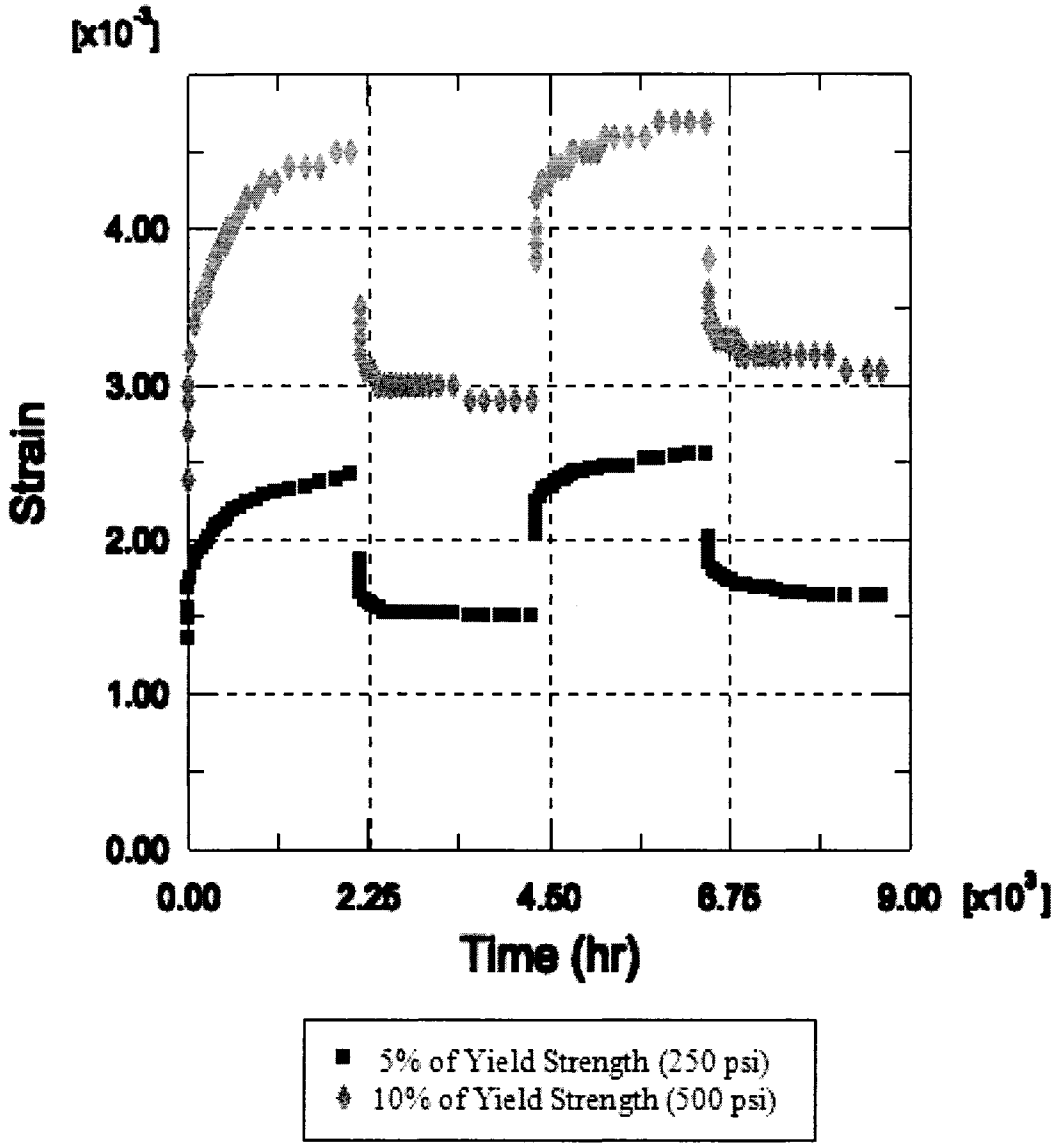

Fig. A.2 Average experimental strain vs. time for higher stiffness PVC specimens

Reproduced with permission of the copyright owner. Further reproduction prohibited without permission.

APPENDIX B

INTERCONVERSION BETWEEN MATERIAL MODELS

Reproduced with permission of the copyright owner. Further reproduction prohibited without permission.

Given:

The retardation constants and retardation times were obtained from the experimental data using the generalized Kelvin Model.

$D_0 := 6.10\times 10^{-6}$ $\tau_1 := 0.144$

$D_1 := 1.15\times 10^{-6}$ $\tau_2 := 1.44$

$D_2 := 2.03\times 10^{-6}$ $\tau_3 := 14.4$

$D_3 := 4.556\times 10^{-7}$ $\tau_4 := 144.$

$D_4 := 1.99\times 10^{-6}$ $\tau_5 := 144$

$D_5 := 4.65\times 10^{-6}$

$\eta := \dfrac{1}{1.813\times 10^{-12}}$

Find:

The relaxation times and relaxation constants represented in the generalized Maxwell Model.

Solution:

1. Determination of time constants for the generalized Maxwell Model (Schapery and Park, 1999)

The Laplace transforms of the compliance function is given as:

$$\tilde{D}(s) \equiv s\int_0^\infty D(t)\exp(-st)dt = D_g + \sum_{j=1}^{n}\frac{D_j}{s\tau_j + 1} + \frac{1}{\eta s} \qquad \text{(B1)}$$

From Eq. B1,

$$\lim_{s\to -(1/\tau_k)} \tilde{D}(s) = \pm\infty \quad (k = 1,\cdots,n) \qquad \text{(B2)}$$

From E.5.18 and Eq. B2,

$$\lim_{s\to -(1/\tau_k)} \tilde{E}(s) = \pm\infty \quad (k = 1,\cdots,n) \qquad \text{(B3)}$$

For given retardation times and retardation constants, the unknown relaxation times can be determined by taking the negative reciprocal of the solutions of Eq. B1 for s<0, yields,

Reproduced with permission of the copyright owner. Further reproduction prohibited without permission.

$\rho_1 := 0.121$

$\rho_2 := 1.131$

$\rho_3 := 13.77($

$\rho_4 := 117.11$

$\rho_5 := 1.038 \times 10^{3}$

$\rho_6 := 9.029 \times 10^{6}$

2. Determination of the relaxation constants

When the relaxation times were obtained, the relaxation constants E_m can be determined based on the Eq. 5.20 by setting symbol $s_k = 1/\rho_k \ (k = 1, \ldots, p)$.
From the retardation times obtained above, s_k are given as,

$s_1 = 8.264$

$s_2 = 0.884$

$s_3 = 0.073$

$s_4 = 8.538 \times 10^{-3}$

$s_5 = 9.634 \times 10^{-4}$

$s_6 = 1.108 \times 10^{-7}$

The matrix A in Eq. 5. 20 can be given as,

$$A := \begin{pmatrix} a_{11} & a_{12} & a_{13} & a_{14} & a_{15} & a_{16} \\ a_{21} & a_{22} & a_{23} & a_{24} & a_{25} & a_{26} \\ a_{31} & a_{32} & a_{33} & a_{34} & a_{35} & a_{36} \\ a_{41} & a_{42} & a_{43} & a_{44} & a_{45} & a_{46} \\ a_{51} & a_{52} & a_{53} & a_{54} & a_{55} & a_{56} \\ a_{61} & a_{62} & a_{63} & a_{64} & a_{65} & a_{66} \end{pmatrix}$$

The elements in the matrix A can be detailed as,

The elements in the first column of matrix A can be written as,

$$a_{11} := \frac{s_1 \cdot \rho_1}{s_1 \cdot \rho_1 + 1} \cdot \left[D_0 + \frac{1}{\eta \cdot s_1} + \sum_{j=1}^{5} \frac{D_j}{\left(s_1 \tau_j + 1 \right)} \right]$$

Reproduced with permission of the copyright owner. Further reproduction prohibited without permission.

$$a_{21} := \frac{s_2 \cdot \rho_1}{s_2 \cdot \rho_1 + 1} \cdot \left[D_0 + \frac{1}{\eta \cdot s_2} + \sum_{j=1}^{5} \frac{D_j}{(s_2 \tau_j + 1)} \right]$$

$$a_{31} := \frac{s_3 \cdot \rho_1}{s_3 \cdot \rho_1 + 1} \cdot \left[D_0 + \frac{1}{\eta \cdot s_3} + \sum_{j=1}^{5} \frac{D_j}{(s_3 \tau_j + 1)} \right]$$

$$a_{41} := \frac{s_4 \cdot \rho_1}{s_4 \cdot \rho_1 + 1} \cdot \left[D_0 + \frac{1}{\eta \cdot s_4} + \sum_{j=1}^{5} \frac{D_j}{(s_4 \tau_j + 1)} \right]$$

$$a_{51} := \frac{s_5 \cdot \rho_1}{s_5 \cdot \rho_1 + 1} \cdot \left[D_0 + \frac{1}{\eta \cdot s_5} + \sum_{j=1}^{5} \frac{D_j}{(s_5 \tau_j + 1)} \right]$$

$$a_{61} := \frac{s_6 \cdot \rho_1}{s_6 \cdot \rho_1 + 1} \cdot \left[D_0 + \frac{1}{\eta \cdot s_6} + \sum_{j=1}^{5} \frac{D_j}{(s_6 \tau_j + 1)} \right]$$

The elements in the second column of matrix A can be written as,

$$a_{12} := \frac{s_1 \cdot \rho_2}{s_1 \cdot \rho_2 + 1} \cdot \left[D_0 + \frac{1}{\eta \cdot s_1} + \sum_{j=1}^{5} \frac{D_j}{(s_1 \tau_j + 1)} \right]$$

$$a_{22} := \frac{s_2 \cdot \rho_2}{s_2 \cdot \rho_2 + 1} \cdot \left[D_0 + \frac{1}{\eta \cdot s_2} + \sum_{j=1}^{5} \frac{D_j}{(s_2 \tau_j + 1)} \right]$$

$$a_{32} := \frac{s_3 \cdot \rho_2}{s_3 \cdot \rho_2 + 1} \cdot \left[D_0 + \frac{1}{\eta \cdot s_3} + \sum_{j=1}^{5} \frac{D_j}{(s_3 \tau_j + 1)} \right]$$

$$a_{42} := \frac{s_4 \cdot \rho_2}{s_4 \cdot \rho_2 + 1} \cdot \left[D_0 + \frac{1}{\eta \cdot s_4} + \sum_{j=1}^{5} \frac{D_j}{(s_4 \tau_j + 1)} \right]$$

$$a_{52} := \frac{s_5 \cdot \rho_2}{s_5 \cdot \rho_2 + 1} \cdot \left[D_0 + \frac{1}{\eta \cdot s_5} + \sum_{j=1}^{5} \frac{D_j}{(s_5 \tau_j + 1)} \right]$$

$$a_{62} := \frac{s_6 \cdot \rho_2}{s_6 \cdot \rho_2 + 1} \cdot \left[D_0 + \frac{1}{\eta \cdot s_6} + \sum_{j=1}^{5} \frac{D_j}{(s_6 \tau_j + 1)} \right]$$

Reproduced with permission of the copyright owner. Further reproduction prohibited without permission.

The elements in the third column of matrix A can be written as,

$$a_{13} := \frac{s_1 \cdot \rho 3}{s_1 \cdot \rho 3 + 1} \cdot \left[D_0 + \frac{1}{\eta \cdot s_1} + \sum_{j=1}^{5} \frac{D_j}{(s_1 \tau_j + 1)} \right]$$

$$a_{23} := \frac{s_2 \cdot \rho 3}{s_2 \cdot \rho 3 + 1} \cdot \left[D_0 + \frac{1}{\eta \cdot s_2} + \sum_{j=1}^{5} \frac{D_j}{(s_2 \tau_j + 1)} \right]$$

$$a_{33} := \frac{s_3 \cdot \rho 3}{s_3 \cdot \rho 3 + 1} \cdot \left[D_0 + \frac{1}{\eta \cdot s_3} + \sum_{j=1}^{5} \frac{D_j}{(s_3 \tau_j + 1)} \right]$$

$$a_{43} := \frac{s_4 \cdot \rho 3}{s_4 \cdot \rho 3 + 1} \cdot \left[D_0 + \frac{1}{\eta \cdot s_4} + \sum_{j=1}^{5} \frac{D_j}{(s_4 \tau_j + 1)} \right]$$

$$a_{53} := \frac{s_5 \cdot \rho 3}{s_5 \cdot \rho 3 + 1} \cdot \left[D_0 + \frac{1}{\eta \cdot s_5} + \sum_{j=1}^{5} \frac{D_j}{(s_5 \tau_j + 1)} \right]$$

$$a_{63} := \frac{s_6 \cdot \rho 3}{s_6 \cdot \rho 3 + 1} \cdot \left[D_0 + \frac{1}{\eta \cdot s_6} + \sum_{j=1}^{5} \frac{D_j}{(s_6 \tau_j + 1)} \right]$$

The elements in the fourth column of matrix A can be written as,

$$a_{14} := \frac{s_1 \cdot \rho 4}{s_1 \cdot \rho 4 + 1} \cdot \left[D_0 + \frac{1}{\eta \cdot s_1} + \sum_{j=1}^{5} \frac{D_j}{(s_1 \tau_j + 1)} \right]$$

$$a_{24} := \frac{s_2 \cdot \rho 4}{s_2 \cdot \rho 4 + 1} \cdot \left[D_0 + \frac{1}{\eta \cdot s_2} + \sum_{j=1}^{5} \frac{D_j}{(s_2 \tau_j + 1)} \right]$$

$$a_{34} := \frac{s_3 \cdot \rho 4}{s_3 \cdot \rho 4 + 1} \cdot \left[D_0 + \frac{1}{\eta \cdot s_3} + \sum_{j=1}^{5} \frac{D_j}{(s_3 \tau_j + 1)} \right]$$

$$a_{44} := \frac{s_4 \cdot \rho 4}{s_4 \cdot \rho 4 + 1} \cdot \left[D_0 + \frac{1}{\eta \cdot s_4} + \sum_{j=1}^{5} \frac{D_j}{(s_4 \tau_j + 1)} \right]$$

Reproduced with permission of the copyright owner. Further reproduction prohibited without permission.

$$a_{54} := \frac{s_5 \cdot \rho 4}{s_5 \cdot \rho 4 + 1} \cdot \left[D_0 + \frac{1}{\eta \cdot s_5} + \sum_{j=1}^{5} \frac{D_j}{(s_5 \tau_j + 1)} \right]$$

$$a_{64} := \frac{s_6 \cdot \rho 4}{s_6 \cdot \rho 4 + 1} \cdot \left[D_0 + \frac{1}{\eta \cdot s_6} + \sum_{j=1}^{5} \frac{D_j}{(s_6 \tau_j + 1)} \right]$$

The elements in the fifth column of matrix A can be written as,

$$a_{15} := \frac{s_1 \cdot \rho 5}{s_1 \cdot \rho 5 + 1} \cdot \left[D_0 + \frac{1}{\eta \cdot s_1} + \sum_{j=1}^{5} \frac{D_j}{(s_1 \tau_j + 1)} \right]$$

$$a_{25} := \frac{s_2 \cdot \rho 5}{s_2 \cdot \rho 5 + 1} \cdot \left[D_0 + \frac{1}{\eta \cdot s_2} + \sum_{j=1}^{5} \frac{D_j}{(s_2 \tau_j + 1)} \right]$$

$$a_{35} := \frac{s_3 \cdot \rho 5}{s_3 \cdot \rho 5 + 1} \cdot \left[D_0 + \frac{1}{\eta \cdot s_3} + \sum_{j=1}^{5} \frac{D_j}{(s_3 \tau_j + 1)} \right]$$

$$a_{45} := \frac{s_4 \cdot \rho 5}{s_4 \cdot \rho 5 + 1} \cdot \left[D_0 + \frac{1}{\eta \cdot s_4} + \sum_{j=1}^{5} \frac{D_j}{(s_4 \tau_j + 1)} \right]$$

$$a_{55} := \frac{s_5 \cdot \rho 5}{s_5 \cdot \rho 5 + 1} \cdot \left[D_0 + \frac{1}{\eta \cdot s_5} + \sum_{j=1}^{5} \frac{D_j}{(s_5 \tau_j + 1)} \right]$$

$$a_{65} := \frac{s_6 \cdot \rho 5}{s_6 \cdot \rho 5 + 1} \cdot \left[D_0 + \frac{1}{\eta \cdot s_6} + \sum_{j=1}^{5} \frac{D_j}{(s_6 \tau_j + 1)} \right]$$

The elements in the six column of matrix A can be written as,

$$a_{16} := \frac{s_1 \cdot \rho 6}{s_1 \cdot \rho 6 + 1} \cdot \left[D_0 + \frac{1}{\eta \cdot s_1} + \sum_{j=1}^{5} \frac{D_j}{(s_1 \tau_j + 1)} \right]$$

$$a_{26} := \frac{s_2 \cdot \rho 6}{s_2 \cdot \rho 6 + 1} \cdot \left[D_0 + \frac{1}{\eta \cdot s_2} + \sum_{j=1}^{5} \frac{D_j}{(s_2 \tau_j + 1)} \right]$$

Reproduced with permission of the copyright owner. Further reproduction prohibited without permission.

$$a_{36} := \frac{s_3 \cdot \rho 6}{s_3 \cdot \rho 6 + 1} \cdot \left[D_0 + \frac{1}{\eta \cdot s_3} + \sum_{j=1}^{5} \frac{D_j}{\left(s_3 \tau_j + 1\right)} \right]$$

$$a_{46} := \frac{s_4 \cdot \rho 6}{s_4 \cdot \rho 6 + 1} \cdot \left[D_0 + \frac{1}{\eta \cdot s_4} + \sum_{j=1}^{5} \frac{D_j}{\left(s_4 \tau_j + 1\right)} \right]$$

$$a_{56} := \frac{s_5 \cdot \rho 6}{s_5 \cdot \rho 6 + 1} \cdot \left[D_0 + \frac{1}{\eta \cdot s_5} + \sum_{j=1}^{5} \frac{D_j}{\left(s_5 \tau_j + 1\right)} \right]$$

$$a_{66} := \frac{s_6 \cdot \rho 6}{s_6 \cdot \rho 6 + 1} \cdot \left[D_0 + \frac{1}{\eta \cdot s_6} + \sum_{j=1}^{5} \frac{D_j}{\left(s_6 \tau_j + 1\right)} \right]$$

Inputting the values of the retardation constants, relaxation times and s_k into the matrix A yields:

$$A = \begin{pmatrix} 3.394\times 10^{-6} & 6.131\times 10^{-6} & 6.728\times 10^{-6} & 6.78\times 10^{-6} & 6.787\times 10^{-6} & 6.787\times 10^{-6} \\ 7.794\times 10^{-7} & 4.032\times 10^{-6} & 7.452\times 10^{-6} & 7.987\times 10^{-6} & 8.055\times 10^{-6} & 8.064\times 10^{-6} \\ 8.285\times 10^{-8} & 7.219\times 10^{-7} & 4.758\times 10^{-6} & 8.514\times 10^{-6} & 9.391\times 10^{-6} & 9.516\times 10^{-6} \\ 1.125\times 10^{-8} & 1.043\times 10^{-7} & 1.147\times 10^{-6} & 5.45\times 10^{-6} & 9.795\times 10^{-6} & 1.09\times 10^{-5} \\ 1.564\times 10^{-9} & 1.461\times 10^{-8} & 1.758\times 10^{-7} & 1.361\times 10^{-6} & 6.71\times 10^{-6} & 1.342\times 10^{-5} \\ 4.388\times 10^{-13} & 4.102\times 10^{-12} & 4.996\times 10^{-11} & 4.247\times 10^{-10} & 3.764\times 10^{-9} & 1.637\times 10^{-5} \end{pmatrix}$$

The matrix B in Eq. 5.20 is given as,

$$B := \begin{pmatrix} 1 \\ 1 \\ 1 \\ 1 \\ 1 \\ 1 \end{pmatrix}$$

Completing the following matrix operations:

Reproduced with permission of the copyright owner. Further reproduction prohibited without permission.

$$A^{-1} \cdot B = \begin{pmatrix} 2.716 \times 10^4 \\ 2.937 \times 10^4 \\ 4.735 \times 10^3 \\ 1.846 \times 10^4 \\ 2.292 \times 10^4 \\ 6.101 \times 10^4 \end{pmatrix}$$

These results are the relaxation constants and they can be rewritten as,

$E_1 := 2.716 \times 10^4$

$E_2 := 2.937 \times 10^4$

$E_3 := 4.735 \times 10^3$

$E_4 := 1.846 \times 10^4$

$E_5 := 2.292 \times 10^4$

$E_6 := 6.101 \times 10^4$

Reproduced with permission of the copyright owner. Further reproduction prohibited without permission.

APPENDIX C

TYPICAL ABAQUS© INPUT FILES

Reproduced with permission of the copyright owner. Further reproduction prohibited without permission.

C.1 Single Element Model Input File

```
*Heading
**
** Single Element Analysis, CPE4, Short-term
**
*Node
     1,       -0.5,       -0.5
     2,        0.5,       -0.5
     3,       -0.5,        0.5
     4,        0.5,        0.5
*Ngen, Nset=Bottom Left
 1,1
*Ngen, Nset=Bottom Right
 2,2
*Element, type=CPE4
1, 1, 2, 4, 3
*Elset, elset=Single
1
*Material, name=Viscoelastic
*Elastic
164000., 0.35
*Viscoelastic, time=PRONY
 0.1658,       0.,    0.121
 0.1793,       0.,    1.131
 0.0289,       0.,   13.776
 0.1127,       0.,  117.119
 0.1399,       0.,    1038.
 0.3724,       0.,  9.029e+06
*Solid Section, elset=Single, material=Viscoelastic
*Surface, name=Top
 Single, S3
*Boundary
 Bottom Left, 1
 Bottom Left, 2
 Bottom Right, 1
*Restart, write, frequency=25
*Preprint, echo=NO
*Preprint, model=NO
*Preprint, history=NO
**
** Loading1
**
*Step, nlgeom, inc=1000
*Static
0.0001, 0.001, 1e-15, 0.001
```

Reproduced with permission of the copyright owner. Further reproduction prohibited without permission.

```
*Dsload
Top, P2, -205.
*Node Output
U,
*End Step
*Step, nlgeom, inc=5000
*Visco, cetol=0.02
1., 2136., 1e-15, 500.
*Node Output
U,
*End Step
**
** Unloading1
**
*Step, nlgeom, inc=1000
*Static
0.0001, 0.001, 1e-15, 0.001
*Dsload
Top, P2, -102.5.
*Node Output
U,
*End Step
*Step, nlgeom, inc=5000
*Visco, cetol=0.02
1., 2184., 1e-15, 500.
*Node Output
U,
*End Step
**
** Loading2
**
*Step, nlgeom, inc=1000
*Static
0.0001, 0.001, 1e-15, 0.001
*Dsload
Top, P2, -205.
*Node Output
U,
*End Step
*Step, nlgeom, inc=5000
*Visco, cetol=0.02
1., 2160., 1e-15, 500.
*Node Output
U,
*End Step
**
```

Reproduced with permission of the copyright owner. Further reproduction prohibited without permission.

```
** Unloading2
**
*Step, nlgeom, inc=1000
*Static
0.0001, 0.001, 1e-15, 0.001
*Dsload
Top, P2, -102.5.
*Node Output
U,
*End Step
*Step, nlgeom, inc=5000
*Visco, cetol=0.02
1., 2160., 1e-15, 500.
*Node Output
U,
*End Step
```

Reproduced with permission of the copyright owner. Further reproduction prohibited without permission.

C.2 General 2-D Model Input File

```
*Heading
(Oval=5%), (Gap=0.4%) Liner Buckling Analysis, CPE4, Long-term
**
** Liner, material definition
**
* Node, input=liner1.inp
* Node, input=liner2.inp
* Node, input=liner3.inp
* Node, input=liner4.inp
*Nset, nset=CROWN
 1,  4,  1
*Nset, nset=MID
 313,  316,   1
*Element, type=CPE4
  1,  1,  2,  6,  5
*Nset, nset=EALL
  1,  3,  1,  1,  313,  4,  3
*Elset,generate, elset=LINER-OUTER-SURF
  1,  232,   3
*Material, name="ELASTIC MATERIAL"
*Elastic, moduli=INSTANTANEOUS
164000., 0.35
*Viscoelastic, time=PRONY
 0.1658,       0.,    0.121
 0.1793,       0.,    1.131
 0.0289,       0.,   13.776
 0.1127,       0.,  117.119
 0.1399,       0.,    1038.
 0.3724,       0., 9.029e+06
**
*Solid Section, elset=EALL, material="ELASTIC MATERIAL"
1.,
**
** Hostpipe, material definition
**
* Node, input=hostpipe.inp
*Element, type=R2D2
 1,  1,  4
*Elset, elset=HOSTPIPE
  1,  60,  1
**Rigid Body, ref node=60, elset=HOSTPIPE
**
** contact analysis
**
```

Reproduced with permission of the copyright owner. Further reproduction prohibited without permission.

```
*Surface Definition, name=Contactsurf1
 LINER-OUTER-SURF, S4
*Surface Definition, name= Contactsurf2
 HOSTPIPE, SPOS
*Contact Pair, interaction=SMOOTH
Contactsurf1, Contactsurf2
*Surface Interaction, name=SMOOTH
1.,
*Friction, slip tolerance=0.005
0.,
*Boundary
CROWN, 1, 1
CROWN, 6, 6
MID, 2, 2
MID, 6, 6
60, ENCASTRE
*Restart, write, frequency=500
*Preprint, echo=NO
*Preprint, model=NO
*Preprint, history=NO
**
** LOADS
**
*Step, nlgeom, inc=1000
*Static
0.0001, 0.001, 1e-15, 0.001
*Dsload
LINER-OUTER-SURF, P2, 31.3
*Node Print, freq=999999, nset=CROWN, SUMMARY=NO
U
*El Print, freq=999999, SUMMARY=NO
S
*End Step
** ----------------------------------------------------------------
The following steps simulate step variation in loading
** ----------------------------------------------------------------
*Amplitude, name=AMP-1
0., 1., 2160., 1.
*Amplitude, name=AMP-2
0., 1., 720., 0.25
*Amplitude, name=AMP-3
0., 0.25, 720., 0.25
*Amplitude, name=AMP-4
0., 0.25, 720., 1.
*Amplitude, name=AMP-5
0., 1., 2160., 1.
```

Reproduced with permission of the copyright owner. Further reproduction prohibited without permission.

```
*Amplitude, name=AMP-6
0., 1., 720., 0.25
*Amplitude, name=AMP-7
0., 0.25, 720., 0.25
*Amplitude, name=AMP-8
0., 0.25, 720., 1.
**
** STEP: loading-1
**
*Step, nlgeom, inc=1000
*Visco, cetol=0.0001
1., 2160., 1e-10, 800.
*Dsload, op=NEW, amplitude=AMP-1
LINER-OUTER-SURF, P, 31.3
*Restart, write, frequency=500
*Output, field, frequency=8888888
*Node Output
U,
*Output, history, frequency=8888888
*Node Output, nset=CROWN
U2,
*End Step
**
** STEP: transition-decrease-a1
**
*Step, nlgeom, inc=1000
*Visco, cetol=0.0001
1., 720., 1e-10, 400.
*Dsload, op=NEW, amplitude=AMP-2
LINER-OUTER-SURF, P, 31.3
*Restart, write, frequency=500

*Output, field, frequency=8888888
*Node Output
U,
*Output, history, frequency=8888888
*Node Output, nset=CROWN
U2,
*End Step
**
** STEP: unloading-1
**
*Step, nlgeom, inc=1000
*Visco, cetol=0.0001
1., 720., 1e-10, 720.
*Dsload, op=NEW, amplitude=AMP-3
```

Reproduced with permission of the copyright owner. Further reproduction prohibited without permission.

```
LINER-OUTER-SURF, P, 31.3
*Restart, write, frequency=500
*Output, field, frequency=8888888
*Node Output
U,
*Output, history, frequency=8888888
*Node Output, nset=CROWN
U2,
*End Step
**
** STEP: transition-increase-b1
**
*Step, nlgeom, inc=1000
*Visco, cetol=0.0001
1., 720., 1e-10, 400.
*Dsload, op=NEW, amplitude=AMP-4
LINER-OUTER-SURF, P, 31.3
*Restart, write, frequency=500
*Output, field, frequency=8888888
*Node Output
U,
*Output, history, frequency=8888888
*Node Output, nset=CROWN
U2,
*End Step
**
** STEP: reloading-1
**
*Step, nlgeom, inc=1000
*Visco, cetol=0.0001
1., 2160., 1e-10, 800.
*Dsload, op=NEW, amplitude=AMP-5
LINER-OUTER-SURF, P, 31.3
*Restart, write, frequency=500
*Output, field, frequency=8888888
*Node Output
U,
*Output, history, frequency=8888888
*Node Output, nset=CROWN
U2,
*End Step
**
** STEP: transition-decrease-c1
**
*Step, nlgeom, inc=1000
*Visco, cetol=0.0001
```

Reproduced with permission of the copyright owner. Further reproduction prohibited without permission.

```
1., 720., 1e-10, 400.
*Dsload, op=NEW, amplitude=AMP-6
LINER-OUTER-SURF, P, 31.3
*Restart, write, frequency=500
*Output, field, frequency=8888888
*Node Output
U,
*Output, history, frequency=8888888
*Node Output, nset=CROWN
U2,
*End Step
**
** STEP: reunloading-1
**
*Step, nlgeom, inc=1000
*Visco, cetol=0.0001
1., 720., 1e-10, 720.
*Dsload, op=NEW, amplitude=AMP-7
LINER-OUTER-SURF, P, 31.3
*Restart, write, frequency=500
*Output, field, frequency=8888888
*Node Output
U,
*Output, history, frequency=8888888
*Node Output, nset=CROWN
U2,
*End Step
**
** STEP: transition-increase-d1
**
*Step, nlgeom
*Visco, cetol=0.0001
1., 720., 1e-10, 400.
*Dsload, op=NEW, amplitude=AMP-8
LINER-OUTER-SURF, P, 31.3
*Restart, write, frequency=500
*Output, field, frequency=8888888
*Node Output
U,
*Output, history, frequency=8888888
*Node Output, nset=CROWN
U2,
*End Step
---------
```

Repeat the loading steps as often as necessary to achieve a total of 50 years. Modifying parameters in the AMPLITUDE command can simulate different loading variations.

Reproduced with permission of the copyright owner. Further reproduction prohibited without permission.

APPENDIX D

DETERMINATION OF 50-YEAR PRESSURES

Reproduced with permission of the copyright owner. Further reproduction prohibited without permission.

Table D.1 Buckling time for PVC-HC for TVR=0.33 (load cycle: 3 months)

DVR=0.75		DVR=0.5		DVR=0.25	
P_{high} (psi)	T_b (hour)	P_{high} (psi)	T_b (hour)	P_{high} (psi)	T_b (hour)
33.50	226706	34.50	71270	35.25	10560.1
33.25	377948	34.30	328738	35.08	12878.9
33.19	414605	34.25	399597	34.99	28073.5
33.13	451440	34.20	473053	34.90	>65yrs
33.00	533428	34.10	>65yrs	34.55	>65yrs

Table D.2 Buckling time for PVC-HC for TVR=1 (load cycle: 3 months)

DVR=0.75		DVR=0.5		DVR=0.25	
P_{high} (psi)	T_b (hour)	P_{high} (psi)	T_b (hour)	P_{high} (psi)	T_b (hour)
34.70	25211.3	35.75	14382.4	36.50	10008.7
34.30	252059	35.63	239050	36.44	10052.2
34.10	385849	35.57	468010	36.38	14388.4
34.00	455044	35.50	>65yrs	36.32	>65yrs
33.90	525773	35.25	>65yrs	36.25	>65yrs

Table D.3 Buckling time for PVC-HC for TVR=3 (load cycle: 3 months)

DVR=0.75		DVR=0.5		DVR=0.25	
P_{high} (psi)	T_b (hour)	P_{high} (psi)	T_b (hour)	P_{high} (psi)	T_b (hour)
35.50	190813	37.50	9331.7	38.50	9326.46
35.25	385202	37.40	13668.9	38.40	9362.94
35.19	431002	37.35	22328.6	38.30	>65yrs
35.13	480247	37.30	>65yrs	38.10	>65yrs
35.00	573859	37.10	>65yrs	37.70	>65yrs

Table D.4 Buckling time for PVC-HS for TVR=0.33 (load cycle: 3 months)

DVR=0.75		DVR=0.5		DVR=0.25	
P_{high} (psi)	T_b (hour)	P_{high} (psi)	T_b (hour)	P_{high} (psi)	T_b (hour)
49.50	252708	50.75	108992	51.70	22750.1
49.00	387078	50.45	269050	51.45	109272
48.88	421197	50.30	395813	51.32	293023
48.75	460040	50.23	464376	51.25	442800
48.50	539930	50.15	550064	51.20	571568

Reproduced with permission of the copyright owner. Further reproduction prohibited without permission.

Table D.5 Buckling time for PVC-HS for TVR=1 (load cycle: 3 months)

DVR=0.75		DVR=0.5		DVR=0.25	
P_{high} (psi)	T_b (hour)	P_{high} (psi)	T_b (hour)	P_{high} (psi)	T_b (hour)
50.75	178551	52.50	10001.5	53.00	10065.4
50.13	359972	52.00	282236	52.94	>65yrs
49.98	403182	51.88	404340	52.88	>65yrs
49.82	450715	51.75	515516	52.75	>65yrs
49.50	544520	51.50	>65yrs	52.50	>65yrs

Table D.6 Buckling time for PVC-HS for TVR=3 (load cycle: 3 months)

DVR=0.75		DVR=0.5		DVR=0.25	
P_{high} (psi)	T_b (hour)	P_{high} (psi)	T_b (hour)	P_{high} (psi)	T_b (hour)
52.00	169703	54.25	9309.63	55.10	9340.62
51.50	354952	54.00	289036	54.94	>65yrs
51.25	437039	53.94	>65yrs	54.88	>65yrs
51.13	487956	53.88	>65yrs	54.75	>65yrs
51.00	536752	53.75	>65yrs	54.50	>65yrs

Table D.7 Buckling time for PVC-HC for TVR=0.33 (load cycle: 6 months)

DVR=0.75		DVR=0.5		DVR=0.25	
P_{high} (psi)	T_b (hour)	P_{high} (psi)	T_b (hour)	P_{high} (psi)	T_b (hour)
33.25	90691.5	33.50	178539	34.00	21575.7
32.88	298354	33.25	424640	33.75	280782
32.69	402278	33.19	470855	33.63	410384
32.60	453484	33.13	528643	33.57	462239
32.50	505395	33.00	706893	33.50	531636

Table D.8 Buckling time for PVC-HC for TVR=1 (load cycle: 6 months)

DVR=0.75		DVR=0.5		DVR=0.25	
P_{high} (psi)	T_b (hour)	P_{high} (psi)	T_b (hour)	P_{high} (psi)	T_b (hour)
33.75	175683	34.50	115203	35.00	11442.9
33.38	382629	34.25	377033	34.75	391683
33.29	434903	34.19	434880	34.69	521284
33.19	495366	34.13	495367	34.63	645221
33.00	612750	34.00	605314	34.50	896885

Reproduced with permission of the copyright owner. Further reproduction prohibited without permission.

Table D.9 Buckling time for PVC-HC for TVR=3 (load cycle: 6 months)

DVR=0.75		DVR=0.5		DVR=0.25	
P_{high} (psi)	T_b (hour)	P_{high} (psi)	T_b (hour)	P_{high} (psi)	T_b (hour)
34.75	165663	36.00	36021	37.50	9268.1
34.38	386104	35.85	249859	37.00	9873.18
34.29	442574	35.78	364337	36.75	10014
34.19	506625	35.70	502572	36.63	>65yrs
34.00	632115	35.40	1.17E+06	36.50	>65yrs

Table D.10 Buckling time for PVC-HS for TVR=0.33 (load cycle: 6 months)

DVR=0.75		DVR=0.75		DVR=0.25	
P_{high} (psi)	T_b (hour)	P_{high} (psi)	T_b (hour)	P_{high} (psi)	T_b (hour)
48.50	332614	49.75	161817	50.00	191566
48.13	427554	49.25	315353	49.50	407212
48.04	462094	49.00	401693	49.38	462201
47.94	505725	48.88	436315	49.25	514150
47.75	603858	48.75	477726	49.00	620500

Table D.11 Buckling time for PVC-HS for TVR=1 (load cycle: 6 months)

DVR=0.75		DVR=0.75		DVR=0.25	
P_{high} (psi)	T_b (hour)	P_{high} (psi)	T_b (hour)	P_{high} (psi)	T_b (hour)
50.00	149722	50.75	144346	51.50	11409.5
49.38	304738	50.25	348143	51.00	278097
49.06	392794	50.13	400302	50.88	365755
48.91	434806	50.00	452153	50.75	469426
48.75	485042	49.75	560159	50.50	699311

Table D.12 Buckling time for PVC-HS for TVR=3 (load cycle: 6 months)

DVR=0.75		DVR=0.75		DVR=0.25	
P_{high} (psi)	T_b (hour)	P_{high} (psi)	T_b (hour)	P_{high} (psi)	T_b (hour)
50.80	215958	52.50	70555.2	53.25	10048.1
50.40	356385	52.13	268512	53.00	390242
50.20	420151	51.94	384864	52.94	493921
50.10	446555	51.84	442080	52.88	796913
50.00	467976	51.75	511189	52.75	1.40E+06

Reproduced with permission of the copyright owner. Further reproduction prohibited without permission.

REFERENCES

[1] *American Society for Testing and Materials D 2990-01*, standard.

[2] Courtney, T.H., *Mechanical Behavior of Materials* (New York: McGraw-Hill, 1990).

[3] Sears, K. J. and Darby, J. R., *Society of Petroleum Engineers Monograph Series* (New York: Wiley, 1982).

[4] Maseeh, F. and Denturia, S.D., "Viscoelasticity and Creep Recovery of Polyimide Thin Films," *Solid-State Sensor and Actuator Workshop, 4th Technical Digest, Institute of Electrical and Electronics Engineers* (1990): 55-60.

[5] Findley, W.N., Lai, J. S., and Onaran, K., *Creep and Relaxation of Nonlinear Viscoelastic Materials* (Amsterdam: North-Holland Publishers, 1989).

[6] Findley, W.N., "Creep Characteristics of Plastics," *Symposium on Plastics, American Society for Testing and Materials* (1944): 118.

[7] Findley, W.N. and Khosla, G., "An Equation for Tension Creep of Three Unfilled Thermoplastics," *Society of Petroleum Engineers Technical Journal* (December, 1956): 20-25.

[8] Findley, W.N. and Peterson, D.B., "Prediction of Long-Time Creep with Ten-Year Creep Data on Four Plastic Laminates," *Proceeding of American Society for Testing and Materials* 58 (1958): 841.

[9] Nutting, P.G., "A Study of Elastic Viscous Deformation," *Proceeding of American Society for Testing and Materials* 21 (1921): 1162.

[10] Blaga, A., "Properties and Behavior of Plastics," *Canadian Building Digest* (1973): 157.

[11] Kung, T.M. and Li, J.C.M., "Recovery Processes in Amorphous Polymers," *Journal of Material Science* 22 (1987): 3620-3630.

[12] Findly, W.N., "26-Year Creep and Recovery of Poly (Vinyl Chloride) and Polyethylene," *Polymer Engineering and Science* 27 (1987): 582-585.

Reproduced with permission of the copyright owner. Further reproduction prohibited without permission.

[13] Ward, I. M. and Onat, E. T., "Non-linear Mechanical Behavior of Oriented Polypropylene," *Journal of the Mechanics and Physics of Solids* 11 (1963): 217-229.

[14] Neis, V.V. and Sackman, J.L., "An Experimental Study of a Nonlinear Material with Memory", *Journal of Rheology* 11 (1967): 307-333.

[15] Lockett, F.J. and Turner, S., "Nonlinear Creep of Plastics," *Journal of the Mechanics and Physics of Solids* 19 (1971): 201-214.

[16] Edward, G.H. and Stachurski, Z.H., "Large Strain Recovery of Polyethylene," *Journal of Physics D: Applied Physics* 7 (1974): 1778-1787.

[17] TTC, "Preliminary Short-Term Buckling Results," (Trenchless Technology Center, Louisiana Tech University, 1998).

[18] Boot, J.C. and Welch, A.J., "Creep Buckling of Thin-Walled Polymeric Pipe Linings Subjected to External Groundwater Pressure," *Thin-Walled Structure* 24 (1996): 191-210.

[19] Welch, A.J., "Creep Buckling of Infinitely Long Constrained Cylinders under Hydrostatic Loading," (Ph.D. dissertation, University of Bradford, 1989).

[20] Lin, H., "Creep Characterization of CIPP Material under Tension, Compression, and Bending," (MS Thesis, Louisiana Tech University, 1995).

[21] Mahalingam, R., "A Viscoelastic Model to Determine the Long-Term Buckling Pressure of CIPP Liners," (MS Thesis, Louisiana Tech University, 1996).

[22] Straughan, W.T., Guice, L.K., and Mal-Duraipandian, C., "Long-Term Structural Behavior of Pipeline Rehabilitation Systems," *Journal of Infrastructure Systems* 1 (1995): 214-220.

[23] Chunduru, S.M., Barber, M.E., and Bakeer, R.M., "Buckling Behavior of Polyethylene Liner Systems," *Journal of Materials in Civil Engineering* 8 (1996): 201-206.

[24] TTC, "Internal Test Data on Long-Term Buckling Tests," (Trenchless Technology Center, Louisiana Tech University, 1998).

[25] Zhao, Q., "Finite Element Simulation of Creep Buckling of CIPP Liners under External Pressure," (Ph.D. Dissertation, Louisiana Tech University, 1999).

[26] Hall, D.E. and Zhu, M., "Recent Findings and Ongoing Liner Buckling Research at the Trenchless Technology Center," *Proceedings of the North American No Dig 2000* (April, 2000): 77-84.

Reproduced with permission of the copyright owner. Further reproduction prohibited without permission.

[27] Kini, Rajgopal R., "Effect of Varying Pressure on Creep-Buckling of CIPP-Liner," (M.S. Thesis, Louisiana Tech University, 2001).

[28] Timoshenko, S.P., and Gere, J.M., *Theory of Elastic Stability, 2nd Edition* (New York: McGraw-Hill1961).

[29] *American Society for Testing and Materials Designation F1216-05*, standard.

[30] Guice, L.K. and Li, J.Y., "Buckling Models and Influencing Factors for Pipe Rehabilitation Design," *Proceedings of the North American No-Dig 1994*, (April, 1994): WS1:1-WS1:15.

[31] Omara, A. M., "Analysis of Cured-In-Place Pipes (CIPP) Installed in Circular and Oval Host Pipes," (Ph.D. Dissertation, Louisiana Tech University, 1997).

[32] Lu, X., "Finite Element Analysis for CIPP encased in Oval Host Pipes," (Master Thesis, Louisiana Tech University, 1999).

[33] Online: http://academic.evergreen.edu/g/grossmaz/KIEPERME/ (last accessed: June 23, 2006).

[34] Legget, R.F., "Groundwater," *Canadian Building Digest* (1966): 82.

[35] Butterworth, J.A., Schulze, R.E., Simmonds, L.P., Moriarty, P., and Mugabe F., "Hydrological Processes and Water Resources Management in a Dryland Environment IV: Long-term Groundwater Level Fluctuations Due to Variation in Rainfall", *Hydrology and Earth System Sciences* 3 (1990): 353-362.

[36] Online: http://www.lbl.gov/ehs/esg/98ser/98serWEBch06.html#1 (last accessed: June 23, 2006).

[37] Online: http://pmep.cce.cornell.edu/facts-slides-self/facts/wat-so-grw85.html (last accessed: January 15, 2007).

[38] Baird, A.J., and Horn, D.P., "Monitoring and Modeling Groundwater Behavior in Sandy Beaches," *Journal of Coastal Research* 12 (1996): 630-640.

[39] Jiao, J.J. and Tang, Z.H., "An Analytical Solution of Groundwater Response to Tidal Fluctuation in Leaky Confined Aquifer," *Water Resources Research* 35 (1999): 747-751.

[40] Li, H., Jiao, J.J., Luk, M., and Cheung, K., "Tide-induced Groundwater Level Fluctuation in Costal Aquifer Bounded by an L-shaped Coastline," *Water Resources Research* 38 (2002): U55-U6Z.

Reproduced with permission of the copyright owner. Further reproduction prohibited without permission.

[41] Lovelace, J.K., Fontenot, J.W., and Frederick, C.P., "Water-Sources Investigations Report 02-4088," *Louisianan Ground-Water Map* (2002): 14.

[42] Pradeep, K.A., Asish, R.B., and Kshitij, M.K., "Comment on "Arsenic Mobility and Groundwater Extraction in Bangladesh" (I)" *Science* 300 (2003): 584.

[43] Online: http://www.stormwaterauthority.org/assets/022Acitrus1.pdf (last accessed: January 15, 2007).

[44] Online: http://pubs.usgs.gov/sir/2005/5168/ (last accessed: January 15, 2007).

[45] Tschoegl, N.W., *The Phenomenological Theory of Linear Viscoelastic Behavior-An Introduction* (Berlin: Springer-Verlag, 1989).

[46] *Engineering Design Guide Inliner Technologies*, (2003)

[47] *American Society for Testing and Materials D790-00*, standard.

[48] Tobolsky, A.V., *Properties and Structure of Polymer* (New York: Wiley and Sons, 1960): 186-195.

[49] Schapery, R.A., "A Simple Collocation Method for Fitting Viscoelastic Models to Experimental Data," *Graduate Aeronautical Laboratories California Institute of Technology* (1961): *SM61-23A*.

[50] Cost, T.L. and Becker, E.B., "A Multidata Method of Approximate Laplace Transform Inversion," *International Journal of Numerical Methods in Engineering* 2 (1970): 207.

[51] SAS® Version 8, SAS Institute, (1999).

[52] Hopkings, I.L. and Hamming, R.W., "On Creep and Relaxation," *Journal of Applied Physics* 28 (1957): 906-909.

[53] Knoff, W.F. and Hopkings, I.L., "An Improved Numerical Interconversion for Creep Compliance and Relaxation Modulus," *Journal of Applied Polymer Science* 16 (1972): 2963-2972.

[54] Baumgaertel, M. and Winter, H.H., "Determination of Discrete Relaxation and Retardation Time Spectra from Dynamic Mechanical Data," *Rheologica Acta* 28 (1989): 511-519.

[55] Bradshaw, R.D. and Brinson, L.C., "A Sign Control Method for Fitting and Interconverting Material Functions for Linearly Viscoelastic Solids," *Mechanics of Time-Dependent Materials* 1 (1997): 85-108.

Reproduced with permission of the copyright owner. Further reproduction prohibited without permission.

[56] Schapery, R.A. and Park, S.W., "Methods of Interconversion between Linear Viscoelastic Material Functions. Part I - A Numerical Method Based on Prony Series," *International Journal of Solid and Structures* 36 (1999): 1653-1675.

[57] Ferry, J.D., *Viscoelastic Properties of Polymers, 3rd Edition* (New York: John Wiley and Sons, 1980).

[58] Zhao, W., "Finite Element Analysis and Statistical Modeling of Pipeline Rehabilitation Liners with Material Imperfections," (Ph.D. Dissertation, Louisiana Tech University, 2003).

[59] Moore, I. D., "Elastic Buckling of Buried Flexible Tubes – A Review of Theory and Experiment," *Journal of Geo-technical Engineering* 115 (1988): 340-357.

[60] McAlpine, G.A., "TTC Report on Long-term Structural Behavior of Pipeline Rehabilitation Systems – A Discussion," *No-Dig Engineering* 3 (1996): 21-24.

[61] Online: http://scv.bu.edu/Graphics/ABAQUS©docs/v6.5/books/usb/default.htm (last accessed: April 05, 2006).

[62] Online: http://www.nerc-wallingford.ac.uk/ih/nrfa/yb/yb2002/grf1.html (last accessed: October 25, 2006).

Reproduced with permission of the copyright owner. Further reproduction prohibited without permission.